

**Potassium Channels and Growth Control:
Identification and Characterisation of
Mutations Affecting Proportional Growth
of the Fin in the Cyprinid *Danio rerio***

Dissertation

der Mathematisch-Naturwissenschaftlichen Fakultät
der Eberhard Karls Universität Tübingen
zur Erlangung des Grades eines Doktors
der Naturwissenschaften
(Dr. rer. nat.)

vorgelegt von
Simon Perathoner
aus Bozen
(Italien)

Tübingen
2012

Tag der mündlichen Qualifikation: 18. 02. 2013

Dekan: Prof. Dr. Wolfgang Rosenstiel

1. Berichterstatter: Prof. Dr. Christiane Nüsslein-Volhard

2. Berichterstatter: Prof. Dr. Gerd Jürgens

A mami y tati

Acknowledgements

Numerous people crossed my path in these five years of doctoral studies and contributed directly or indirectly to the successful outcome of this journey. I would like to express my gratitude to Prof. Dr. Christiane Nüsslein-Volhard for giving me the opportunity to work in her lab, for her unyielding support over the past five years and for valuable advice in the thesis writing process. I am deeply indebted with Dr. Matthew P. Harris for offering me this fascinating project, for his guidance as well as support for all these years. Thanks are also due to the members of my thesis advisory committee, Dr. Dirk Linke, Dr. Christian Söllner and Prof. Dr. Ralf Sommer. Moreover, I gratefully acknowledge my collaborators, Prof. Dr. Guiscard Seeböhm, Dr. Ulrike Henrion and Dr. Katja Steinke, for their contribution to the electrophysiological analysis.

I would like to thank all the members, past and present, of the Nüsslein-Volhard lab for their support. In particular, I gratefully acknowledge Dr. Nicolas Rohner and Iris Koch for initial training in the first months of my PhD, Ines Gehring for her technical expertise in mapping, Hans Martin Maischein for help with injections, and Dr. Ajeet Singh and Andrey Fadeev for assistance in imaging. I am grateful to Dr. Yi-Yen Chen, Christopher M. Dooley and especially Alessandro Mongera for

providing invaluable advice for my project. Thanks also go to the animal caretakers and the non-scientific staff for a lot of help and even more patience.

I would like to address thanks to Tuğba Çolak for all her encouragement and helpful suggestions in the initial steps of the thesis writing, to Daniela Lazzaretti for introducing me to L^AT_EX and to Dr. Dagmar Sigurðardóttir for useful comments on this work. I am deeply grateful to Dr. Jana Krauß for numerous discussions on the project and for critical and meticulous reading of this thesis. Thanks also go to Dr. Uwe Irion for patiently proofreading this work.

Finally, I would like to thank my family and friends, for their continuous support and encouragement throughout my studies. All this would not have been possible without their help.

Contents

List of abbreviations	xiii
Abstract	xvii
Zusammenfassung	xix
1 Introduction	1
1.1 Growth control and size determination	2
1.1.1 Attainment of final size: integrating cell growth and cell proliferation	2
1.1.2 Environmental, systemic and intrinsic factors control growth	6
1.2 Body appendages of the zebrafish as a model for organ growth	9
1.2.1 Fins	10
1.2.2 Barbels	16
1.3 Forward genetics as a means to identify novel factors involved in size determination	21

2	Results	23
2.1	Analysis of mutants showing generalised enlargement of the fins	23
2.1.1	The <i>alf</i> and <i>pfau</i> mutations map to chromosome 20	24
2.1.2	The <i>alf</i> and <i>pfau</i> mutants harbour missense mutations in K ⁺ channel <i>kcnk5b</i>	28
2.1.3	The fins of <i>kcnk5b</i> mutants have elongated segments	33
2.1.4	The <i>pfau</i> mutation acts locally to increase the size of fins and barbels	39
2.1.5	Vascular clones are often, but not always associated with fin overgrowth in transplantations of <i>kcnk5b</i> ^{<i>pfau</i>/+} cells into <i>alb</i> hosts	45
2.1.6	Misexpression of Kcnk5 ^{<i>pfau</i>} leads to local fin overgrowth	50
2.1.7	The amino acids altered in <i>alf</i> and <i>pfau</i> reside within the transmembrane domains of Kcnk5b	55
2.1.8	The <i>alf</i> and <i>pfau</i> mutations lead to an increased conductance of Kcnk5b	58
2.2	Analysis of mutants showing dorsal fin overgrowth	64
2.2.1	The mutants <i>sgl</i> , <i>sllk</i> and <i>fgg</i> harbour missense mutations in the potassium channel <i>kcnh1a</i>	64
2.2.2	The fins of the <i>kcnh1a</i> mutants show an increase in segment number	71
2.2.3	Transplantation experiments suggest a local role for the <i>sllk</i> mutation	74

2.2.4	A revertant of <i>sllk</i> shows a second mutation within <i>kcnh1a</i>	77
2.2.5	The mutations in <i>sgl</i> , <i>sllk</i> and <i>fpg</i> affect the TM domains of Kcnh1a	80
2.2.6	The electrophysiological properties of the mutant Kcnh1a variants are altered . . .	84
2.2.7	The gene <i>kcnh1a</i> might play a role in fin length variation of poeciliid fish	87
3	Discussion	92
3.1	Changes in K ⁺ channel activity underlie the phenotype of several fin overgrowth mutants . .	93
3.2	K ⁺ channels can intrinsically determine fin size	95
3.3	Tissues involved in the overgrowth phenotype of <i>kcnk5b</i> mutants	97
3.4	Fin growth and ray segment formation	100
3.5	Ion channels and growth control	101
3.5.1	Kcnk5b and the role of K ⁺ currents in cell proliferation	101
3.5.2	Kcnh1 and its current-independent role in cell proliferation	104
3.5.3	K ⁺ channels and growth: possible mechanisms	109
3.6	Extrapolating the role of K ⁺ channels in fin growth to natural populations	115
4	Materials & Methods	117
4.1	Fish maintenance	117
4.2	Bleaching of fish eggs	117
4.3	Anaesthesia	118
4.4	Measurements	118

4.5	Generation of <i>fgg</i> mutant fish and <i>sllk</i> revertant	118
4.6	DNA preparation	119
4.7	Mapping	120
4.8	Total RNA isolation	121
4.9	cDNA synthesis	122
4.10	Cloning of <i>kcnk5b</i> and <i>kcnh1a</i> cDNA	122
4.11	Cloning of <i>kcnh1a</i> cDNA from poecilids	126
4.12	Competent cells	126
4.13	Transformation	127
4.14	Plasmid purification	127
4.15	Digestions with restriction enzymes	127
4.16	Sequencing	128
4.17	Genotyping	129
4.18	Transplantations	130
4.19	Injections	130
4.20	Calcein staining	131
4.21	cRNA Preparation	131
4.22	Electrophysiology	133
4.23	Immunohistochemistry	134
4.24	Imaging	135
4.25	Cloning of misexpression constructs	135
4.26	PCR mutagenesis	137
4.27	<i>kcnk5b</i> 6.7 kb reporter construct	141
4.28	<i>kcnk5b</i> BAC reporter construct	142

Contributions 156

Appendix A: Zebrafish *eda* and *edar* mutants reveal conserved and ancestral roles of ectodysplasin signaling in vertebrates. 157

Appendix B: Enhancing the efficiency of N-ethyl-N-nitrosourea-induced mutagenesis in the zebrafish.	173
Appendix C: Supplementary tables and figures.	179
Bibliography	198

List of Figures

1.1	Transplants of the limb rudiment between <i>A. punctatum</i> and <i>A. tirgrinum</i>	5
1.2	Anatomy of the zebrafish fin.	13
1.3	Anatomy of the zebrafish barbel.	18
2.1	Phenotype of <i>alf</i> and <i>pfau</i> mutants.	25
2.2	Mapping of <i>alf</i> and <i>pfau</i> mutations.	27
2.3	Electropherogram of <i>kcnk5b</i> at the <i>pfau</i> and <i>alf</i> locus.	29
2.4	Alignment of vertebrate <i>Kcnk5</i>	32
2.5	Lepidotrichial segment number in mutants with generalised fin overgrowth.	35
2.6	Lepidotrichia of mutants with generalised fin overgrowth.	36
2.7	Segment length of lepidotrichia in mutants with generalised fin overgrowth.	38
2.8	Transplantation of <i>pfau</i> : expected scenarios. . .	41
2.9	Chimaeras resulting from transplantation of <i>pfau</i> /+; Tg(β -actin::GFP)/+ into <i>alb</i>	43
2.10	Locally increased segment length in <i>pfau</i> /+ clones.	44
2.11	GFP positive tissue types found in chimaeric fish.	47
2.12	Analysis of overgrowth in <i>pfau</i> chimaeras.	49

2.13	Mosaic expression of <i>ef1a:DsRed;ef1a:kcnk5b^{pfau}</i> in wild type fish.	52
2.14	Expression of <i>ef1a:DsRed</i> in various tissues. . .	53
2.15	Overgrown clones expressing <i>kcnk5b^{pfau}</i> and DsRed. 55	
2.16	Structure of Kcnk5b	57
2.17	Electrophysiological properties of wild type and mutant Kcnk5b	61
2.18	Effects of wild type and mutant Kcnk5b on mem- brane potential	62
2.19	Phenotype of <i>sgl</i> , <i>fgg</i> and <i>sllk</i> mutants.	65
2.20	Mapping of <i>sgl</i> and <i>sllk</i> mutations.	67
2.21	Electropherogram of <i>kcnh1a</i> at the <i>sllk</i> , <i>fgg</i> and <i>sgl</i> locus	67
2.22	Alignment of Kcnh1 in metazoans	70
2.23	Lepidotrichia of dorsal fin mutants.	71
2.24	Segment length and segment number in het- erozygous dorsal fin mutants compared to their siblings.	73
2.25	Chimaeras resulting from transplantation of <i>sllk</i> /+ cells into <i>alb</i> blastulas.	77
2.26	Reversion screen for <i>sllk</i>	80
2.27	Amino acid substitution in Kcnh1a in a potential revertant of <i>sllk</i>	81
2.28	Structure of Kcnh1a.	84
2.29	Electrophysiological properties of wild type and mutant Kcnh1a	86
2.30	Sexually dimorphic growth of the dorsal fin in sailfin mollies.	90
2.31	<i>kcnh1a</i> sequence from poecilids.	91

3.1	Current–voltage relationships of rat KCNH1 upon progesterone treatment.	105
3.2	A conformational switch in eag1 stimulates cell proliferation.	108
4.1	Map of <i>ef1a:DsRed; ef1a:kcnk5b^{pfau}</i> plasmid . .	138
4.2	Map of 6.7 kb <i>kcnk5b</i> : Gal4VP16; UAS:GFP . .	140
4.3	Phenotype of homozygous <i>alf</i> and <i>pfau</i> mutants.	180
4.4	Expression of <i>ef1a:DsRed;ef1a:kcnk5b^{pfau}</i> in various tissues.	181
4.5	Effects of mutated selectivity pore P2 on Kcnk5b conductance.	195
4.6	Current-voltage relationship of Kcnh1a ^{S396A} . .	196
4.7	<i>kcnk5</i> reporter line	197

List of Tables

2.1	GFP positive clones associated with fin overgrowth in <i>pfau/alb</i> chimaeras	46
2.2	Overgrowth observed in adult wild type fish expressing <i>Kcnk5b^{pfau}</i>	51
2.3	GFP positive tissue types found in <i>sllk/alb</i> chimaeras	75
2.4	Mutagenesis of <i>sllk</i> fish	78
3.1	Fin mutants affecting ion homeostasis	96
4.1	G4 primer set	143
4.1	G4 primer set (continued)	144
4.1	G4 primer set (continued)	145
4.2	List of OSP primers	146
4.2	List of OSP primers (continued)	147
4.2	List of OSP primers (continued)	148
4.2	List of OSP primers (continued)	149
4.2	List of OSP primers (continued)	150
4.2	List of OSP primers (continued)	151
4.2	List of OSP primers (continued)	152
4.3	List of plasmids	153
4.3	List of plasmids (continued)	154
4.3	List of plasmids (continued)	155

4.4	Genes in the <i>pfau</i> mapping interval	182
4.4	Genes in the <i>pfau</i> mapping interval (continued)	183
4.5	Genes in the <i>segel</i> mapping interval	184
4.5	Genes in the <i>segel</i> mapping interval (continued)	185
4.5	Genes in the <i>segel</i> mapping interval (continued)	186
4.5	Genes in the <i>segel</i> mapping interval (continued)	187
4.6	Alignment of cDNA from <i>P. velifera</i> and <i>P. latipinna</i>	194

List of Abbreviations

4-AP	4 aminopyridine
ACFP	adult caudal fin primordium
AEC	apical epidermal cap
AER	apical epithelial ridge
AF	apical fold
<i>alb</i>	<i>albino</i> mutant of <i>Danio rerio</i>
<i>alf</i>	<i>another longfin</i> mutant of <i>Danio rerio</i>
BAC	bacterial artificial chromosome
Bmp	bone morphogenetic protein
bp	basepair(s)
BrdU	bromodeoxyuridine
Ca ²⁺	calcium (ion)
CaM	calmodulin
CaMK	CaM-dependent protein kinase
cDNA	complementary deoxyribonucleic acid
°C	degree Celsius
Cdk	cyclin-dependent kinase
CDS	coding DNA sequence
<i>chi</i>	<i>chihuahua</i> mutant of <i>Danio rerio</i>
cM	centiMorgan
c-Myc	cellular myelocytomatosis oncogene
DNA	deoxyribonucleic acid

DsRed	red fluorescent protein from <i>Discosoma</i> species
dpf	days post-fertilisation
Eag	ether-à-go-go K ⁺ channel of <i>Drosophila melanogaster</i>
Egl2	egg laying defective-2 K ⁺ channel of <i>Caenorhabditis elegans</i>
<i>ef1a</i>	elongation factor 1 alpha
ENU	N-ethyl-N-nitrosourea
ER α	œstrogen receptor α
EtOH	ethanol
<i>evx</i>	even skipped homeotic gene 1 homologue
Fgf(s)	fibroblast growth factor(s)
<i>fgfr1</i>	<i>fibroblast growth factor receptor 1</i> gene
<i>fgg</i>	<i>flagge</i> mutant of <i>Danio rerio</i>
<i>fls</i>	<i>finless</i> mutant of <i>Danio rerio</i>
GFP	green fluorescent protein from <i>Aequorea victoria</i>
GH	growth hormone
h	hour(s)
HEK293	human embryonic kidney 293 cells
HMM	hidden Markov model
hpf	hours post-fertilisation
IGF-1	insulin-like growth factor 1
JAK/STAT	Janus kinase / signal transducer and activator of transcription pathway
K ⁺	potassium (ion)
K ₂ P	2-pore domain K ⁺ channel
K _{Ca}	Ca ²⁺ -dependent K ⁺ channel
<i>kcnh1a</i>	potassium voltage-gated channel, subfamily H (eag-related), member 1a

<i>kcnh2a</i>	potassium voltage-gated channel, subfamily H (eag-related), member 2a
<i>kcnk5b</i>	potassium channel, subfamily K, member 5b
K _V	voltage-dependent K ⁺ channel
LB	Luria-Bertani broth
LG	Linkage group
<i>lof</i>	<i>longfin</i> mutant of <i>Danio rerio</i>
<i>M</i>	<i>Minute</i> mutant of <i>Drosophila melanogaster</i>
Mb	megabase(s) = 10 ⁶ bp
MetOH	methanol
MFF	median fin fold
<i>mhk</i>	<i>mohawk</i> mutant of <i>Danio rerio</i>
MOPS	3-(N-morpholino)propanesulfonic acid
MPF	mitosis-promoting factor
mRNA	messenger ribonucleic acid
NGS	normal goat serum
OD	optical density
P	pore-forming
PCR	polymerase chain reaction
PFA	paraformaldehyde
Rb	retinoblastoma-associated protein
RVD	regulatory volume decrease
s	second(s)
<i>sgl</i>	<i>segel</i> mutant of <i>Danio rerio</i>
Shh	Sonic hedgehog
SL	standard length
<i>sllk</i>	<i>segel-like</i> mutant of <i>Danio rerio</i>
SNP	single nucleotide polymorphism
SSLP	simple sequence length polymorphism
<i>ssz</i>	<i>schleierschwanz</i> mutant of <i>Danio rerio</i>

T ₃	triiodothyronine
T ₄	thyroxine
TEA	tetraethylammonium
Tg	transgene
TLF	tüpfel longfin strain of <i>Danio rerio</i>
TM	transmembrane
TOR	target of rapamycin
TÜ	wild type Tübingen strain of <i>Danio rerio</i>
V	Volt
WIK	wildtype India Kolkata strain of <i>Danio rerio</i>
ZPA	zone of polarising activity

Abstract

Growth plays an essential role during development, as it provides the raw material upon which morphogenesis and cell differentiation can act. For an organism to achieve final shape and right proportions between its body parts, such process has to be highly coordinated. However, to date, only very little is known about how growth and organ size are regulated. In this study, I used a forward genetic approach in the zebrafish *Danio rerio* to identify genes that can affect organ size and alter proportional growth. I analysed several N-ethyl-N-nitrosourea (ENU) induced adult viable mutants that develop enlarged fins. Through positional cloning I show that two of these, *another longfin* (*alf*) and *pfau*, bear a missense mutation in *kcnk5b*, a gene encoding for a 2-pore domain potassium (K^+) channel. The altered protein residues affect transmembrane domains of the channel and electrophysiological assays in *Xenopus* oocytes indicate that these mutations cause an increase in K^+ conductance, which leads to hyperpolarisation of the membrane potential (V_m) *in ovo*. Transplantation experiments suggest that the mutations in *kcnk5b* act within the fin tissues. By misexpression in somatic clones, I prove that the mutant channel is sufficient to promote local growth of the fin. A second class of mutations, which cause a specific overgrowth of the dorsal fin in the mutants *segel* (*sgl*),

segel-like (sllk) and *flagge (fgg)*, was identified as harbouring defects in another K^+ channel encoding gene, *kcnh1a*. The independent isolation of several fin overgrowth mutants that all alter the function of K^+ channels suggests that ion channels play an important role in organ growth and fin size determination in the zebrafish. In this context, it will be interesting to consider whether K^+ channels play a major role in size regulation also in fish species where exaggerated fin growth is occurring naturally. Preliminary data from poeciliid species displaying sex-specific fin enlargement presented in this work support this notion.

Zusammenfassung

Wachstum spielt während der Entwicklung eine zentrale Rolle, da es die Grundlage für Morphogenese und Zelldifferentierung schafft. Um die endgültige Form eines Organismus zu erreichen und die richtigen Proportionen zwischen dessen Körperteilen zu gewährleisten, muss dieser Vorgang bis ins Detail koordiniert werden. Bis heute weiß man nur sehr wenig darüber, wie die Größe eines Organs bestimmt wird. In der vorliegenden Arbeit habe ich anhand klassischer Mutagenese im Zebraquarienfisch *Danio rerio* Gene identifiziert, welche die Dimension eines Organs beeinflussen und zu wachstumsbedingten Veränderungen der Proportionen führen. Ich analysiere hier unterschiedliche N-Ethyl-N-nitrosourea (ENU) induzierte, adult-lebensfähige Mutanten, welche vergrößerte Flossen zeigen. Durch positionelle Klonierung, konnte ich für zwei dieser Mutanten, *another longfin* (*alf*) und *pfau*, die eine Vergrößerung von Flossen und Barteln vorweisen, zeigen, dass diese eine nicht-synonyme Mutation in *kcnk5b* tragen, einem Gen, welches für einen 2-Porendomänen Kaliumkanal codiert. Die betroffenen Aminosäuren befinden sich in den Transmembrandomänen des Kanals. Elektrophysiologische Analysen in *Xenopus* Oozyten zeigen, dass dies zu einer Zunahme des elektrischen Leitwerts für Kaliumionen führt. Dies führt zu einer Hyperpolarisierung des Membranpotentials (V_m)

der Oocyte. Transplantationsexperimente weisen darauf hin, dass diese Mutationen in der Flosse selbst agieren. Durch Missexpression der mutanten Version des Kanals in somatischen Klonen, zeige ich dass die Mutation in *kcnk5b* ausreichend ist, um lokales Flossenwachstum zu verursachen. Ferner wurden die drei Mutanten *segel* (*sgl*), *segel-like* (*sllk*) and *flagge* (*fgg*) untersucht, welche vergrößerte Rückenflossen entwickeln. Die hier vorgelegten Indizien, deuten darauf hin, dass diese Mutanten Defekte im spannungsabhängigen Kaliumkanal *Kcnh1a* haben. Die unabhängige Isolierung mehrerer Flossenmutanten, die alle Defekte in Kaliumkanälen vorweisen, weist darauf hin, dass Ionenkanäle eine wichtige Rolle in der Kontrolle des Flossenwachstums des Zebrafisches spielen. In diesem Zusammenhang wird es interessant sein zu prüfen, ob Kaliumkanäle an der Größensteuerung von jenen Fischarten beteiligt sind, die sich durch ausgeprägtes Flossenwachstum auszeichnen. Vorläufige Befunde aus lebendgebärenden Zahnkarpfen mit geschlechtsspezifischem Flossenwachstum, die in dieser Arbeit vorgestellt werden, weisen in diese Richtung.

Introduction

Growth plays a central role during development as it determines both final shape and size of an organism. In vertebrates, a conspicuous part of growth occurs during postembryonic development. An extreme example is the red kangaroo (*Macropus rufus*), whose neonates have a body weight of only 0.6 g, while adults reach more than 20 kg [Munn and Dawson, 2003]. Here, postembryonic growth accounts for a mass increase of almost four orders of magnitude. However, what determines the final size of a kangaroo? Or why does it grow such a long tail? Which factors are involved in organ growth and its regulation? In the last decades, developmental biologists have only started to identify the genes and molecular mechanisms involved in growth control and many questions remain open. The following introductory pages give a general overview of growth control and size determination in animal development. Additionally, the basic biology of fins and barbels, which are used here as a model for organ growth, and the general approach taken in this study will be presented briefly.

1.1 Growth control and size determination

Growth is defined as an increase in the physical size of a tissue, organ or animal. In some cases, organs grow through accumulation of fluids or extracellular matrix. This process is referred to as accretion. In most cases, growth occurs through an increase in cell number, through cell proliferation, or cell volume, i.e. cell growth. In fact, cell growth and cell proliferation are often connected events, since a cell usually engages in cell growth before dividing. It is important, though, to keep in mind that these two processes are independent. In early embryogenesis for example, during cleavage, cell proliferation occurs without cell growth resulting in a reduction of cell volume with every mitotic event. In contrast, in muscle hypertrophy, a cell increases in size even if it has withdrawn from the cell cycle.

1.1.1 Attainment of final size: integrating cell growth and cell proliferation

Organ size in invertebrates is often determined by cell growth. In the nematode *Caenorhabditis elegans*, body size continues to increase even when somatic cells do not divide any longer [Flemming et al., 2000]. In fact, during the larval development of both nematodes and insects, several tissues undergo polyploidisation resulting in an increase of cell size and organ growth [Trager, 1935; Abercrombie, 1936; Lambie, 2002]. Variation of organ size in various populations of fruit flies of the *Drosophila* genus was also shown to depend on differences in cell volume [Robertson, 1959; Stevenson et al., 1995]. Cell growth in both

ecdysozoans and vertebrates appears to be orchestrated via the TOR kinase pathway by genes involved in ribosome biogenesis and protein synthesis [Tumaneng et al., 2012]. Mutation of the ribosomal protein p70 S6 kinase (DSK6) in *Drosophila melanogaster* results in smaller flies that have cells reduced in size but not in number [Montagne et al., 1999] and overexpression of c-Myc, a transcription factor that induces ribosomal genes, results in mice with increased liver size due to an enlargement of hepatocyte volume [Kim et al., 2000].

However, cell size has an upper limit dictated by factors such as diffusion rate and surface to volume ratio. In 1930, Alpatov noticed that flies raised at 18°C develop larger wings compared to flies reared at 28°C [Alpatov, 1930]. Since he found that bristle density was reduced in the former group he concluded that cell size plays a major role in wing size determination; however, he also recognised that cell growth alone could not account for the entire increase in organ size and postulated a certain role for cell proliferation. In mammals, the contribution of cell proliferation to growth is often substantial. An adult human individual of 70 kg contains about 10^{13} cells, while a mouse only has 3×10^9 cells [Baserga, 1985]. Thus, size difference is directly attributable to an increase in cell number. In fact, even among mammals of appreciable different dimensions, cell size does not vary considerably [Teissier, 1939]. Cell proliferation requires the activity of cyclin-dependent kinases (Cdk) [Polyak et al., 1994] and failure to inhibit Cdk complexes leads to increased organ size in mice [Kiyokawa et al., 1996]. Cell number is also controlled through cell cycle exit and apoptosis mediated by the Hippo pathway [Halder and Johnson, 2011]. Disruption of components of this pathway leads to organ overgrowth caused

by sustained proliferation, as was shown in fruit fly [Udan et al., 2003] and mouse [Lee et al., 2010].

Although some molecular players involved in cell growth and cell proliferation have been identified, it is unclear how these two processes are integrated. Several studies suggest that the critical factor that determines body and organ size is total cell mass, rather than cell number or cell size *per se*. Cell number and cell volume in the *Drosophila* wing blade seem to be in an inverse relation to each other [McCabe et al., 1997], i.e. an increase in cell size is accompanied by a decrease in cell number. This suggests that control of wing size is independent of the number of cell divisions. Interesting results were obtained by inducing mitotic recombination in the imaginal discs of *Minute* (*M*) mutants. Flies heterozygous for one of these mutations show severe developmental delay, due to slower cell proliferation, but only mild alterations in final body size. Mitotic recombination in heterozygous M^+/M^- individuals leads to the production of wild type M^+/M^+ clones in an otherwise heterozygous larva. These clones display increased proliferative capability compared to heterozygous cells. Despite the presence of faster proliferating wild type cells, though, final size and shape of the wing appear unchanged [Morata and Ripoll, 1975]. In a similar experiment, inhibition of mitosis entry through inactivation of Cdk1 leads to endoreduplication and cell growth without alterations in wing size and shape [Weigmann et al., 1997]. Likewise, induction of tetraploidy in salamanders leads to a twofold increase in cell volume. Body size of tetraploid individuals, though, is about the same as in diploid salamanders, with tetraploids having fewer but larger cells [Fankhauser, 1952].

In conclusion, increasing cell mass, be it through cell growth

or cell proliferation, is the essence of growth. Dysregulation of this process can have deleterious consequences for the organism and lead to cancerous growth. Therefore, growth needs to be tightly controlled in order to achieve proper size and shape.

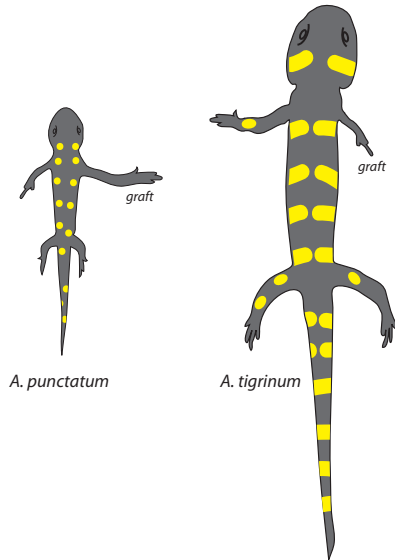


Figure 1.1: Reciprocal transplants of the limb rudiment between *A. punctatum* and *A. tigrinum*. After Twitty and Schwind [1931].

1.1.2 Environmental, systemic and intrinsic factors control growth

The growth of an organ, or in general of a whole organism, can be influenced by extrinsic as well as intrinsic factors, whose contributions can vary depending on the species or even the particular organ within the same animal. For example, when fetal thymus glands are transplanted into a developing mouse, each one of the transplanted organs will grow to the size of an adult thymus, regardless of the number of grafts [Metcalf, 1963]. Here, growth is regulated by intrinsic factors that are autonomous to the organ. In contrast, when the same experiment is repeated using fetal spleens, the total mass of all grafts together will reach the mass of one adult spleen [Metcalf, 1964]. In this case, growth is integrated with external cues that do not originate in the growing organ itself.

Several environmental factors play a role in growth control. It was already mentioned that temperature influences wing size determination in *D. melanogaster* (Sec. 1.1.1). Depletion of food supply in the dung beetle *Onthophagus taurus* induces pupation of the larva and therefore growth cessation [Shafiei et al., 2001], while in the tobacco hornworm *Manduca sexta* metamorphosis is initiated by juvenile hormone degradation, a process that is known to be delayed by starvation [Browder et al., 2001]. The circadian clock also controls growth. Disruption of biological rhythms is associated with breast cancer [Hansen and Stevens, 2012], and impairment of the central circadian clock in mice accelerates tumour growth [Filipski et al., 2002]. In fact, cell cycle progression of cancer cells is known to be controlled by day/night cycles [Wood et al., 2006].

Environmental cues are typically converted into systemic signals such as hormones or growth factors. Body parts can also compete with each other for such factors. Removal of one or both hind wing imaginal discs from the larva of the butterfly *Precis caenia*, results in larger fore wings, suggesting that the different imaginal discs compete for a systemic signal [Nijhout and Emlen, 1998].

In vertebrates, the pituitary synthesised growth hormone (GH) acts on a systemic level to determine body size. Its role is mediated via the production of insulin-like growth factor 1 (IGF-1) [Sarzi-Puttini et al., 2006]. A deficiency in GH causes dwarfism in human and mouse [Rimoin et al., 1966; Eicher and Beamer, 1976] and hypophysectomy in cockerels leads to decreased body size, weight and comb growth [King, 1969]. In humans, overproduction of GH during childhood triggers gigantism, while excessive GH in adulthood results in acromegaly [Lawrence et al., 1970; Eugster and Pescovitz, 1999]. Thyroid hormones (T_3/T_4) also regulate postnatal growth in mammals. Hypothyroidism leads to decreased stature [Rivkees et al., 1988], while increased skeletal growth with premature fusion of the epiphyseal growth plates is observed, if thyroid hormones are produced in excess [Williams, 2009]. Interestingly, both, GH and T_3/T_4 appear to be dispensable during embryonic growth [Bryant and Simpson, 1984].

In fact, often, availability of extrinsic components such as nutrients or hormones does not seem to be the limiting factor determining organ size. Even when cells are provided with saturating amounts of growth factors, they do not grow beyond a certain size [Conlon and Raff, 1999]. For instance, when imaginal discs from first instar *Drosophila* larvae are transplanted

to abdomens of adult flies, they grow to attain their size in prepupal larvae, indicating that the growth is autonomous to the disc [Garcia-Bellido, 1965]. Likewise, pieces of ear cartilage obtained from young rabbits continue growing if grafted to adult hosts, while adult tissue fails to grow in young hosts [Dupertuis, 1941]. Twitty and Schwind [1931] demonstrated that not only growth rate, but also final size can be determined in an organ autonomous manner. Using two species of salamanders that differ in body size, the small *Ambystoma punctatum* and the larger *Ambystoma tigrinum*, they performed reciprocal transplants of either the eye or the limb rudiment between embryos of the two species. The transplanted organs developed within the host to a final size corresponding to that of the donor species (Fig. 1.1). In fact, intrinsic and extrinsic components are often integrated with each other. When Twitty repeated the experiment above with transplanted hearts, he observed that the grafted organs reach the size appropriate for the host, after an initial phase with a donor-specific growth rate [Twitty, 1940]. Therefore, organ growth also involves feedback mechanisms and cross talk between tissues to ensure that proper size is attained. How this is exactly achieved, remains unclear. The identification of genes regulating size and the characterisation of the underlying signalling pathways will be the first steps to understand more about this fascinating phenomenon.

1.2 Body appendages of the zebrafish as a model for organ growth

The problem of growth control in vertebrate development has been tackled mainly in amphibians and avians. However, these organisms lack the molecular and genetic tools to address such questions systematically. The zebrafish (*Danio rerio*) represents an ideal model to understand postembryonic growth in vertebrate development: amenability to mutagenesis screens [Driever et al., 1996; Haffter and Nüsslein-Volhard, 1996; Haffter et al., 1996], an almost completely sequenced genome, well established knockdown and transgenesis techniques [Higashijima et al., 1997; Nasevicius and Ekker, 2000] as well as compact space requirements and a comparably short generation time.

In the present work, I used zebrafish appendages, specifically fins and barbels, to study postembryonic growth. These organs possess diverse, but limited cell types and are amenable to microscopy as well as experimental manipulations. Moreover, they can be removed without compromising survival and they have regenerative capability. Finally, various zebrafish mutants affected in these structures have been isolated over the years [van Eeden et al., 1996; Fisher et al., 2003; Goldsmith et al., 2003; Iovine et al., 2005]. This makes fins and barbels ideal models to address questions of size regulation. In the following sections the basic biology of these appendages will be described.

1.2.1 Fins

With the exception of hagfish, which merely possess a primitive fin fold, fins are present in all fishes. They are generally formed by a framework consisting of rays that support a stratified epidermal layer. In Chondrichthyes (cartilaginous fishes) these rays are keratinous in nature, while in Osteichthyes (bony fishes) they are composed of dermal bone. The major role of fins is to facilitate locomotion and to prevent the body from pitching and rolling. However, in many species, changes in shape and size, conferred them a specialised function e.g. baiting device, copulatory apparatus or sensory organ.

Fins are usually classified into median fins, also known as unpaired fins, and paired fins. Although they share a common repertoire of developmental mechanisms, these two classes are of distinct embryonic origin [Freitas et al., 2006]. The first group arises from somitic mesoderm and is part of the axial skeleton. The median fins comprise one or more dorsal fins as well as the adipose fin on the dorsal side and the anal and caudal fin on the ventral side. The caudal fin is regarded as a ventral fin, since it initially develops ventrally to the caudal notochord (hypochordal development) and only later experiences a reorientation along the antero-posterior axis upon flexion of the notochord. [Kendall Jr. et al., 1984; Marí-Beffa and Murciano, 2010].

Paired fins are part of the appendicular skeleton. They originate from lateral plate mesoderm and comprise pectoral fins as well as the pelvic fins. While median fins are already found in lampreys, paired appendages are a synapomorphy, or

a unique defining characteristic, of jawed vertebrates [Grandel and Schulte-Merker, 1998]. The paired fins of lobed finned fishes (Sarcopterygii) which connect to the axial skeleton through a single bone, are homologous to the limbs within the tetrapod lineage, the forelimbs corresponding to the pectoral fins and the hindlimbs to the pelvic fins. The external fin of ray-finned fishes (Actinopterygii) are characterised by a radial bony scaffold covered by a web of skin that, unlike the sarcopterygian fin, is completely devoid of muscular tissue [Grandel and Schulte-Merker, 1998]. The zebrafish is a ray finned fish and further discussion will focus on the development and anatomy of this class.

Anatomy of the fin

Zebrafish fins consist of a proximal endoskeletal component that ossifies during development from cartilaginous precursors, the endochondral skeleton, and a distal exoskeleton that forms directly via mesenchymal condensation, the dermal skeleton [Grandel and Schulte-Merker, 1998; Bird and Mabee, 2003; Marí-Beffa and Murciano, 2010].

The endochondral skeleton of fins is composed of a variable number of bony supports, the parhypural and the hypurals in the caudal fin and the radials in the other fins. These bones articulate directly with the exoskeletal fin rays or lepidotrichia.

Lepidotrichia extend distally from their endoskeletal support and bifurcate towards the margin of the fin, surrounded by a stratified epidermis. The number of rays, which may fluctuate, occurs to differ even between contralateral fins of the

same individual [Cubbage and Mabee, 1996; Bird and Mabee, 2003]. Each fin ray consists of a pair of dermal ossifications, termed hemirays (Fig. 1.2). These are subdivided into segments by ligaments, or joints [Santamaría and Becerra, 1991; Akimenko et al., 2003; Poss et al., 2003]. Segment length decreases slightly along the proximo-distal axis [Grandel and Schulte-Merker, 1998; Rolland-Lagan et al., 2012]. Importantly, once the boundaries of a segment are established, it does not significantly increase in length [Iovine and Johnson, 2000]. The concave hemirays are synthesised by osteoblasts that secrete bone matrix at the epithelio-mesenchymal interface [Akimenko et al., 2003; Marí-Beffa et al., 1996; Poss et al., 2003; Smith et al., 2008]. The hemirays enclose an intrasegmental region rich in collagen and dermal fibroblasts that embed arterial blood vessels and nerve bundles [Becerra et al., 1983; Huang et al., 2009]. Venous blood vessels leave the intrasegmental region and return to the body running along the lepidotrichia [Tu and Johnson, 2011; Yoshinari and Kawakami, 2011]. Clusters of collagenous spicules, termed actinotrichia, emerge from the tip of each lepidotrichium [Becerra et al., 1983]. The role of these distally located structures is not fully understood, but they seem to be involved in mesenchymal cell migration [Wood and Thorogood, 1984; Zhang et al., 2010].

Morphogenesis of the fin

Although median and paired fins differ in their embryonic origin, they co-opt similar developmental mechanisms [Freitas et al., 2006]. Most studies concentrate on the development of paired fins due to their homology to tetrapod limbs. The fin bud of

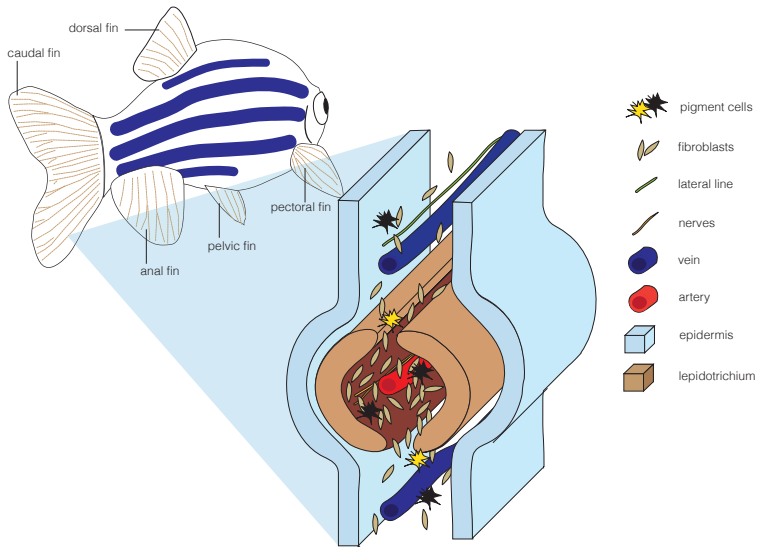


Figure 1.2: Anatomy of the zebrafish fin. The fin is supported by a dermal skeleton (in brown) consisting of segmented lepidotrichia. The blow-up shows a single segment consisting of two hemirays (in brown) surrounded by epidermis (in light blue). Nerve bundles (in orange), fibroblasts (in light brown) and a central artery (in red) extend along the cavity formed by the hemirays, while veins return to the body in the interray area. Pigment cells (in black/yellow) and the lateral line (in green) are also present in the fin tissue. Adapted from Becerra et al. [1983] and Tu and Johnson [2011]

the pectoral fin arises at 23 hpf (staging according to Kimmel et al. 1995) through proliferation of the lateral plate [Grandel and Schulte-Merker, 1998; Freitas et al., 2006; Mari-Beffa and Murciano, 2010]. Two organisers that are homologous to their tetrapod counterparts have been proposed to control pectoral fin development: the apical ectodermal ridge (AER) and the zone of polarising activity (ZPA) [Neumann et al., 1999; Fischer et al., 2003].

The AER in fish controls proximo-distal extension of the pectoral fin bud and appears as an apical thickening of the latter. It soon lifts and develops to an elongated structure, termed apical fold (AF) [Grandel and Schulte-Merker, 1998]. Appearance of the AER has been described also in the developing median fins, where it gives rise to the median fin fold (MFF). This structure has been reported to appear as soon as 18 hpf [Kimmel et al., 1995]. Extension of the fin fold along the proximo-distal axis is a fibroblast growth factor (Fgf) dependent process [Abe et al., 2007]. The ZPA is a second organiser that positions in the posterior mesenchyme of the pectoral fin bud [Neumann et al., 1999]. The corresponding structure in median fins is termed adult caudal fin primordium (ACFP). This signalling centre is thought to regulate antero-posterior patterning via Sonic hedgehog (Shh) signalling [Hadzhiev et al., 2007].

AF and MFF emerge from back-to-back sheets of epidermis. Development of the adult fin begins with the infiltration of the fin fold by mesenchymal cells and formation of actinotrichia [Wood and Thorogood, 1984]. Subsequently, mesenchymal cells migrate distally, along the actinotrichia, to form lepidotrichia [Mari-Beffa and Murciano, 2010; Yano and Tamura, 2012]. During development, bony segments are sequentially added at the

distal tip of the fin [Nabrit, 1929; Goldsmith et al., 2003]. *In situ* hybridisation analysis and bromodeoxyuridine (BrdU) incorporation experiments indicate that this process is saltatory, where proliferative phases are alternating with periods of stasis [Goldsmith et al., 2003]. While growth rate attenuates with age, ontogenetic growth is indeterminate in zebrafish, as both fins and body continue growing throughout a fish's lifetime [Gerhard et al., 2002].

Regeneration of the fin

In addition to the ability to grow indeterminately, zebrafish possess a remarkable regenerative capability. Regeneration has been reported in the most diverse tissues, including the heart, spinal chord, brain, retina, lateral line as well as fins [Dufourcq et al., 2006; Jopling et al., 2010; Fleisch et al., 2011; Yoshinari and Kawakami, 2011].

Fin regeneration in zebrafish is epimorphic, i.e. regeneration of lost tissue involves dedifferentiation and extensive cell proliferation. Upon amputation, epithelial cells are mobilised to cover the wound. In analogy to ontogenic growth, this structure is termed apical epidermal cap (AEC). Intrarary mesenchymal cells of the stump migrate underneath the AEC to give rise to the blastema [Poleo et al., 2001]. 24 hours after amputation the proximal portion of the blastema engages in rapid proliferation cycles [Nechiporuk and Keating, 2002]. These cells migrate distally and eventually reconstitute the amputated tissue.

Fin regeneration is a complex process as cell proliferation needs to be integrated with size regulation in order to reestablish ori-

ginal organ size. Therefore, regeneration entails not only growth initiation and maintenance but also growth arrest. In order to reform a properly patterned organ, positional information has to be provided. In fact, the pace at which an amputated fin regenerates depends on the proximo-distal level of amputation, with proximal amputations regenerating faster than more distal ones [Lee et al., 2005]. Although retinoic acid has been proposed as a fin morphogen [White et al., 1994; Géraudie et al., 1995], to present date it is unclear which signals provide positional information to the regenerating as well as developing fin tissue [Azevedo et al., 2012].

1.2.2 Barbels

The term barbel loosely defines a tendril-like, small, elongated sensory organ located in the mouth region of "lower" vertebrates. Within fishes, barbels are found among hagfish, lampreys, benthic sharks and are widespread in teleosts, especially in catfish [Tanaka, 1973; Georgieva et al., 1979; Fox, 1999; Richardson and Wright, 2003]. Although barbels in fish have been proposed to be homologous to oral cirrhi of *Amphioxus* [Pollard, 1894], several authors disagree with this hypothesis, since barbels are absent from more basal teleosts [Fox, 1999]. Also diversity in location, structure and number rather suggest that these appendages evolved independently, probably several times [Fink and Fink, 1981; Howes, 1991; Zardoya and Doadrio, 1999].

Barbel length differs significantly among teleost fishes, and can reach a considerable percentage of body length. The most striking example is given by the barbeled dragonfish *Ultimostomias*

mirabilis, where barbel length reaches 41.7 cm, which corresponds to ten times the length of the fish [Beebe, 1933]. In such deep-sea fish barbels carry a photophore and are thought to function as lure to attract prey. In other teleosts, such as zebrafish, these structures serve as gustatory and tactile organs.

Anatomy of the barbel

Zebrafish are characterised by two types of barbels: a smaller pair placed on the anterior snout, termed nasal barbels, and a larger pair protruding from the maxilla, termed maxillary barbels [Barman, 1991]. Barbels are hardly described in the literature and most of our current understanding of these appendages has been illustrated in a recent study on the maxillary barbels [LeClair and Topczewski, 2010] .

Like in other cyprinids [Sato, 1937], zebrafish barbels are of the flexible type and lack a bony rod. They possess a refractile core of connective tissue that LeClair and Topczewski [2010] term central rod. This structure appears acellular, non-cartilaginous and non-mineralised as confirmed by negative Alcian Blue or Alizarin Red staining. Two blood vessels extend ventrally along this structure towards the distal tip where they form a capillary loop. Dorsally to the central rod a smaller vessel with tapered end is found, which the authors indicate as a possible lymph vessel. Nerves and pigment cells can also be identified. The inner structure of the barbel is surrounded by a stratified epidermis resting on a thick basement membrane. Mucin secreting glands, the goblet cells, as well as taste buds can be found within the epithelium of the barbel (Fig. 1.3).

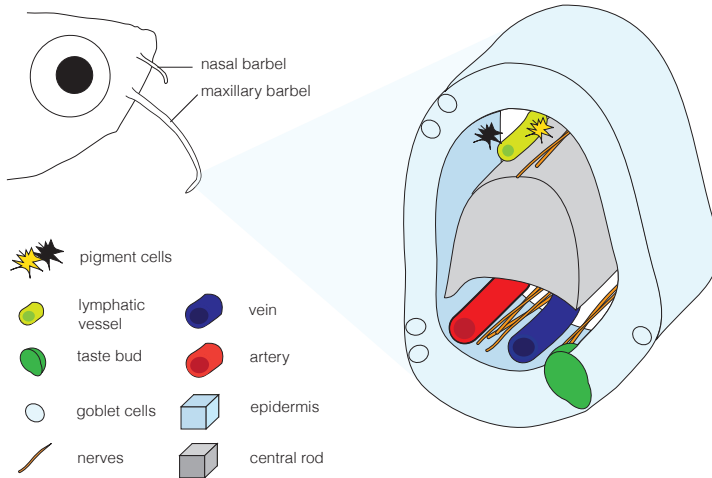


Figure 1.3: Anatomy of the zebrafish barbel. The barbel is supported by an acellular, non-mineralised central rod (in grey) surrounded by epidermis. The barbel contains blood vessels (in red/blue) and a smaller vessel (in light green), possibly a lymphatic vessel. The surface of the barbel is lined with goblet cells (in light blue) that secrete mucin and at the tip of the barbel taste buds are often found (in dark green). After LeClair and Topczewski [2010]

Morphogenesis of the barbel

The barbels originate from epithelial buds that emerge when fish reach a standard length (SL) of about 10 mm (30-40 dpf) [Hansen et al., 2002]. They consist of a mesodermal core covered by an ectodermal jacket [LeClair and Topczewski, 2010]. Within the dorsal portion of the mesodermal component, fine threads of birefringent matrix soon become visible. This structure will give rise to the central rod. During maturation, the barbel bud extends to an elongated structure and angiogenesis, as well as protruding taste buds, can be observed. When the fish exceed a SL of 15 mm, these nascent structures are elongated and enlarged. Identically to fins, barbels show indeterminate growth [LeClair and Topczewski, 2010]. To present date, the molecular mechanisms underlying barbel development remain obscure.

Regeneration of the barbel

Similarly to fins, barbels have the capability to regenerate. Upon amputation, the barbel stump of zebrafish forms an epithelial cap, comparable with the AEC seen in fin regenerates. Subsequently the underlying mesenchyme thickens and forms a blastema [LeClair and Topczewski, 2010]. Seven days post amputation, blood flow is completely reestablished and the stump resembles a smaller version of an uncut barbel. However, in contrast to fins, the regenerative capabilities of barbels are not unlimited. Even six months after amputation, barbels fail to regrow the central rod [LeClair and Topczewski, 2010; Moore et al., 2012] and regrowth of an amputated barbel only restores

45-85% of its original length [LeClair and Topczewski, 2010]. Since the molecular factors regulating barbel regeneration have yet to be investigated, it is not clear what limits the regeneration in the barbels as compared to the fins.

In summary, fins and barbels are relatively simple organs, however, they can vary considerably in size and shape in different fish species where they accomplish diverse functions. Moreover, they possess the remarkable capability of growing indeterminately and to regenerate upon amputation. Together with the ease of manipulation, these features make them a powerful tool to study organ growth and size determination.

1.3 Forward genetics as a means to identify novel factors involved in size determination

As mentioned in the preceding sections, some molecular players involved in fin development and regeneration have been identified; however, to which extent these factors play a role in size determination is not clear. Large-scale mutagenesis led to the identification of several zebrafish mutants that are affected in fins and barbels. Such mutants include *wanda* (*wan*), *stein und bein* (*sub*), *finless* (*fls*), *another longfin* (*alf*) [van Eeden et al., 1996], *chihuahua* (*chi*) [Fisher et al., 2003], *rapunzel* (*rpz*) [Goldsmith et al., 2003] and *shortfin* (*sof*) [Iovine et al., 2005]. In order to find factors involved in organ size control, I decided to study mutants that display an overgrowth phenotype in their appendages. Specifically, I focussed on two classes of mutants: mutants that display generalised fin overgrowth as well as overgrown barbels and mutants that show overgrowth in the dorsal fin only. The first group includes the mutant *alf* that was isolated in the first N-ethyl-N-nitrosourea (ENU) Tübingen mutagenesis screen [Haffter et al., 1996; Haffter and Nüsslein-Volhard, 1996; van Eeden et al., 1996] and the mutant *pfau* which was isolated by Matthew Harris in a subsequent mutagenesis screen focussing on adult specific phenotypes [e.g. Appendix A, Harris et al., 2008], within the Zebrafish Models for Human Development and Disease (zf-Models) project in Tübingen (2004-06). The second class of mutants consists of *segel* (*sgl*) and *segel-like* (*sllk*), which were found in the zf-Models screen, and the mutant *flagge* (*fgg*), which was isolated in a

further screen for dominant mutations affecting adult structures performed during my doctoral studies [e.g. Appendix B, Rohner et al., 2011].

In the present work, I phenotypically characterised these two classes of mutants and mapped them in order to identify the underlying mutations. I also investigated whether the mutations act as intrinsic or systemic factors. Finally, I characterised the mutations at the functional level to gain insight into possible mechanisms of action.

Results

2.1 Analysis of mutants showing generalised enlargement of the fins

Two of the zebrafish mutants analysed in this work display general overgrowth of the fins: *another longfin* (*alf^{dt^y86}*) and *pfau* (*pfau^{dt³⁰mh}*) (Fig. 2.1). Both of these mutants are homozygous viable and also show a dominant phenotype. The *alf* mutant displays enlarged paired and unpaired fins. Moreover, it is characterised by overgrown barbels. In homozygous *alf* fish, the caudal fin tends to break (cf. Appendix C, Fig. 4.3), especially in older animals. This frequently leads to a curvature of the fin, often accompanied by haematomata. The mutants are otherwise healthy, except for slightly slower swimming behaviour than wild type probably due to the bulkiness of the fins. The *pfau* mutant (*pfau^{dt³⁰mh}*) is reminiscent of *alf* fish with overgrown fins and barbels in both heterozygous and homozyg-

ous individuals (Fig. 2.1; Appendix C, Fig. 4.3), although the phenotype is not as severe.

2.1.1 The *alf* and *pfau* mutations map to chromosome 20

In order to determine the genetic lesion underlying the *alf* and *pfau* mutations, a positional cloning approach was taken. The position of a mutated locus is determined in respect to known genetic markers according to the frequency of recombination. For genetic mapping in zebrafish, microsatellites (z-markers) are commonly used as genetic markers [Shimoda et al., 1999]. These repetitive sequences vary in length among zebrafish strains and even individuals and can be detected via polymerase chain reaction (PCR). For the initial mapping, microsatellites that are evenly distributed over the genome are used to assign the mutant locus to a chromosome. In order to genetically map a mutation, mutant carriers are outcrossed to a wild type strain that is highly polymorphic in comparison to the strain where the mutant has been induced [Rauch et al., 1997]. The F₁ progeny will carry one set of chromosomes from each parental strain. In the germ line of these fish meiotic recombination occurs, leading to segregation of loosely or unlinked microsatellites from the mutant locus in the resulting F₂ generation. The closer a genetic marker is to the mutation, the more unlikely a recombination event between the two loci occurs. Hence, the linkage of the mutation to a certain z-marker will be visible in F₂ individuals as co-segregation of the mutant trait with a given marker allele.

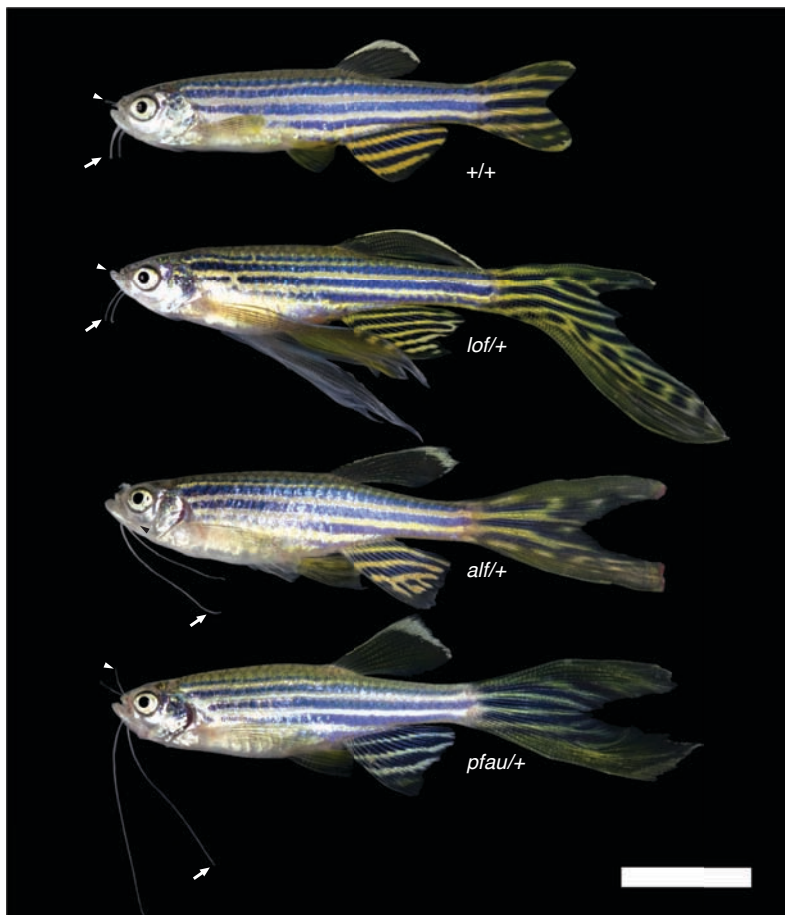
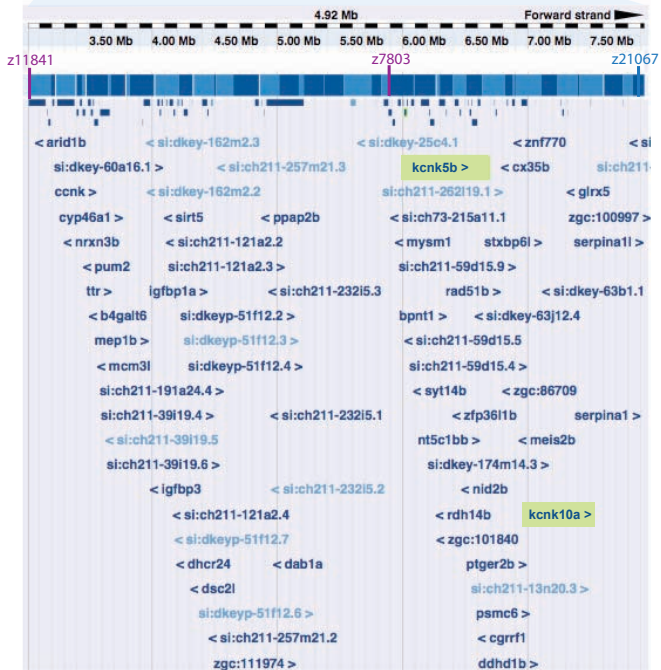
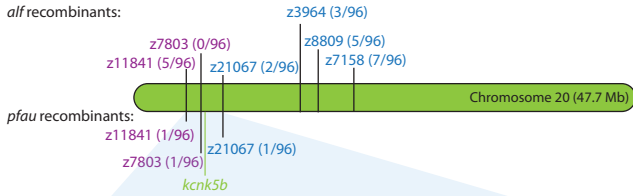


Figure 2.1: Phenotype of *alf* and *pfau* mutants compared to wild type (+/+) and the *longfin* (*lof*) mutant. All mutant fish depicted are heterozygous. Arrows indicate maxillary barbels, arrowheads point to nasal barbels. +/+ : wild type. Scale bar = 10 mm.

alf recombinants:



Assignment of the mutant loci to one of the 25 zebrafish chromosomes (linkage groups) was done by bulk segregant analysis. For this, mutant fish in Tübingen (TÜ) background were outcrossed to the wild type India Kolkata strain (WIK), which is highly polymorphic to TÜ. F₂ progeny was then sorted into mutants and wild type siblings. DNA of 48 individuals was pooled for each group and analysed for linkage with a collection of 192 microsatellites (G4 set) [Geisler et al., 2007]. Since both the *alf* and *pfau* mutations are dominant, assignment to a particular chromosome is performed by observing linkage of z-markers with wild type siblings rather than with the mutant phenotype.

The *alf* mutation showed linkage to z-markers z4329, z9334, z3964 and z9334, the *pfau* mutation was linked to z7158, indicating that both mutations are located on chromosome 20 (cf. Tab. 4.1). The linkage to this chromosome was confirmed on DNA of the individual specimens of the F₂ cross employing additional z-markers. Further analysis led to the assignment of recombinants into one of two groups, depending on whether the recombination occurred upstream (North) or downstream (South) of the mutation (Fig. 2.2 upper panel). The *alf* mutation maps downstream of z11841 (5 recombinants/96 meioses) and upstream of z21067 (2 recombinants /96 meioses), encom-

Figure 2.2 (preceding page): Mapping of *alf* and *pfau* mutations. (Upper panel) Both mutations map to chromosome 20. Purple: North markers; blue: South markers; numbers in brackets: recombinants/meioses. (Lower panel) Genes encoded in the region linked to *alf*. z11841: North marker of *alf*; z7803: North marker of *pfau*; z21067: South marker of *alf* and *pfau*. Two potassium channels are encoded in this interval: *kcnk5b* and *kcnk10a*, highlighted in green.

passing a region of 4.9 Mb (Vertebrate Genome Annotation database zebrafish assembly version 47 - VEGA 47) (Fig. 2.2 lower panel). All recombinants were lost at the position of marker z7803, suggesting that the causative mutation is within 1 cM of this locus. Initial mapping placed the *pfau* mutation to the same region on chromosome 20, between z11841 (1 recombinant/96 meioses) and z21067 (1 recombinant/96 meioses). Subsequent analysis identified z7803 as a North marker of *pfau* (1 recombinant/96 meioses) reducing the genomic interval containing the mutation to 2.0 Mb (VEGA 47) (Fig. 2.2 lower panel) encoding 33 annotated genes (Appendix C, Tab. 4.4).

Thus, analysis indicates that both the *alf* and *pfau* mutations map to an overlapping region on chromosome 20. Together with the similar overgrowth phenotype of barbels and fins, this suggests that the two mutants are allelic.

2.1.2 The *alf* and *pfau* mutants harbour missense mutations in K⁺ channel *kcnk5b*

The mutant *longfin* (*lof^{dt2}*) [Tresnake, 1981] (Fig. 2.1), which also displays patterned fin overgrowth, shows strong linkage to potassium (K⁺) channel *kcnh2a* locus [Johnson and Harris, unpublished data]. In the light of this finding, the intervals linked to the *alf* and *pfau* mutations were scanned for K⁺ channels as possible candidate genes. In fact, these contain, among other candidate genes, two K⁺ channels, namely *kcnk5b* and *kcnk10a*.

Transcripts of candidate genes were amplified from cDNA of *alf* and *pfau* mutants, their respective wild type siblings as well as

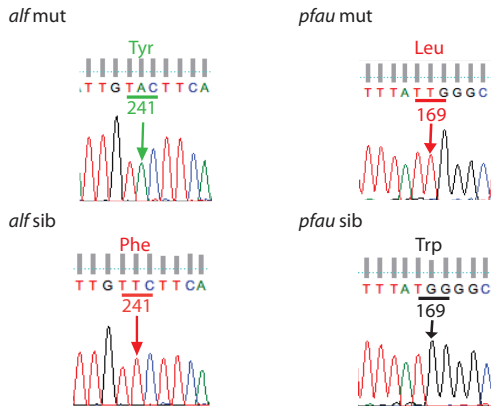


Figure 2.3: Electropherogram of *kcnk5b* at the *pfau* and *alf* locus: A transversion from thymine to adenine turns Phe 241 into Tyr in the *alf* mutant. In *pfau* a guanine transversion into thymine results in a codon encoding Leu instead of Trp 169.

of T \ddot{U} and WIK strains. While none of the mutants contained mutations in *kcnk10a* nor in other selected candidate genes (e.g. nidogen 2b; CASK interacting protein 2, prolyl 4-hydroxylase, alpha polypeptide III), in *alf* and *pfau* fish distinct missense mutations could be identified within the coding sequence of *kcnk5b*. In *pfau* mutants a transversion from guanine to thymine is predicted to change tryptophan (Trp) 169 into a leucine (Leu), while in *alf* phenylalanine (Phe) 241 is exchanged for a tyrosine (Tyr) through a transversion from thymine to adenine (Fig. 2.3). The affected residues are highly conserved in the paralogue of *kcnk5b*, *kcnk5a*, as well as in the orthologues in other vertebrate species (Fig. 2.4). No recombination at the *kcnk5b* locus was observed in F₂ progeny of mapping crosses of both, *alf* and *pfau* mutants. Moreover, the identified mutations in *kcnk5b* were never found in any of the wild type siblings or in any wild type strain. These mutations were consistently used to genotype homozygous and heterozygous fish.

Taken together, *alf* and *pfau* mutants harbour missense mutations in the coding region of the same gene, *kcnk5b*, and, hence, this strongly indicates that they are allelic to this locus.

pfau (W169L)
↓

:.: * : ** : * : : * : . : * : : * : . : * : * * * : * : * : * : * : *

D. re kcnk5b RKVQFICTIVFLLWGFVHLLIIPAFVFMFFENWNTYLEGLYFSFTT
O. la kcnk5b KKVQFTCTALFLLWGLLVHLVIPPFVFMSEGWTYLEGIYFSFIT
G. ac kcnk5b KKVQFTCTALFLLYGLLVHLLIIPPFVFMSEMGWSYVEGLYFSFIT
T. ni kcnk5b KKVQLTCTALFLLWGLLVHLVLPVVFMYMEGWSYLEGFYYSFIT
T. ru kcnk5b KRVQLTCTALFLLWGLLVHLVLPVVFMYMEDWSYLEGLYYSFIT
G. mo kcnk5b KKVQLICTALFLLWGLVMHLVMPPFVFMSELGWSYLEGFYFSFIT
D. re kcnk5a RKTQLTCTAVFLLWGLVIHLVIPPFVFMTOEGWTYIEGLYFSFVT
O. la kcnk5a RKAQFTCTAIFLLWGLVHLVLPVVFFMSEGWTYIEGLYFSFVT
G. ac kcnk5a RKAQFTCTAIFLLWGLVHLVLPVVFMSQEGWTYVEGLYFSFVT
T. ni kcnk5a RKAQFTCTAIFLLWGLVIHLVLPVVFMSQEGWTYIEGFYFSFVT
T. ru kcnk5a RKAQFTCTAIFLLWGLVHLVLPVVFMSQEGWTYLEGFYFSFVT
G. mo kcnk5a RKAQFACTAIFVLWGLVFHLVLPVVFVKSQEGWTYVEGLYFSFIT
G. ga kcnk5 RKAQITCTAIFIVWGLVHLVLPVVFVMVTEGWDIIEGLYYSFIT
X. tr kcnk5 RKAQITCTAIFIIWGLVHLVLPVVFIMKTEGWDIIEGLYFSFIT
M. mu kcnk5 RKAQITCTAIFIVWGLVHLVLPVVFVMVTEWNYIEGLYYSFIT

alf (F241Y)
↓

:.: * : * * * : * * * : * : * : * * : . : * : * * : . : * : : * : * * * * * * * * . : * : *

D. re kcnk5b LTTVGFGDYVAGVDPSVNYPTLYRFFVQLWIYLGLAWSLFFSWN
O. la kcnk5b LTTVGFGDYVAGVNPDIQYPRLYRVCAEIWIYMGLAWSLFFSWN
G. ac kcnk5b LTTVGFGDFVAGVNPNDYPRLYRVFAELWIYMGLAWSLFFSWN
T. ni kcnk5b LTTVGFGDYVAGVNPNIYHRLYKVLAQLWIYMGLAWSLFFSWN
T. ru kcnk5b LTTVGFGDYVAGVNPKNYPRLYRAFAELWIYMGLAWSLFFSWN
G. mo kcnk5b LTTVGFGDYVAGVNPNDYPRLYRVCAEIWVYMGLAWSLFFSWN
D. re kcnk5a LTTIGFGDLVAGVDPNAEYPTLYRYFVEVWIYLGLAWSLFFNWK
O. la kcnk5a LTTIGFGDLVAGVEPNKEYPTLYRYFVEVWIYLGLAWSLFFNWK
G. ac kcnk5a LTTIGFGDLVAGVEPNTEYPTLYRYFVEVWIYLGLAWSLFFNWK
T. ni kcnk5a LTTIGFGDLVAGVEPNKEYPALYRYFVEVWIFLGLAWSLFFNWK
T. ru kcnk5a LTTIGFGDLVAGVEPNKEYPALYRYFVEVWIYLGLAWSLFFNWK
G. mo kcnk5a LTTIGFGDLVAGVDPNDYPTLYRYFVEVWIYLGLAWSLFFNWK
G. ga kcnk5 LTTIGFGDFVAGVNPDANYHALYRYFVELWIYLGLAWSLFFNWK
X. tr kcnk5 LTTIGFGDYVAGVNPKNYNVLYRYFVEIWIYLGLAWSLFFNWK
M. mu kcnk5 LSTIGFGDFVAGVNPSANYHALYRYFVELWIYLGLAWSLFFNWK

Figure 2.4 (preceding page): Conservation of the amino acid sequence of Kcnk5 among vertebrates (residues 156-245 of 448 are shown): Arrows show the amino acids affected in *pfau* (Trp 169 to Leu) and *alf* (Phe 241 to Tyr). D. re *Danio rerio*; O. la *Oryzias latipes*, G. ac *Gasterosteus aculeatus*, T. ru *Takifugu rubripes*, T. ni *Tetraodon nigridoviridis*, G. mo *Gadus morhua*, M. mu *Mus musculus*, G. ga *Gallus gallus*, X. tr *Xenopus tropicalis*. Primary structure of Kcnk5 orthologues was retrieved from the Ensembl database of the respective species.

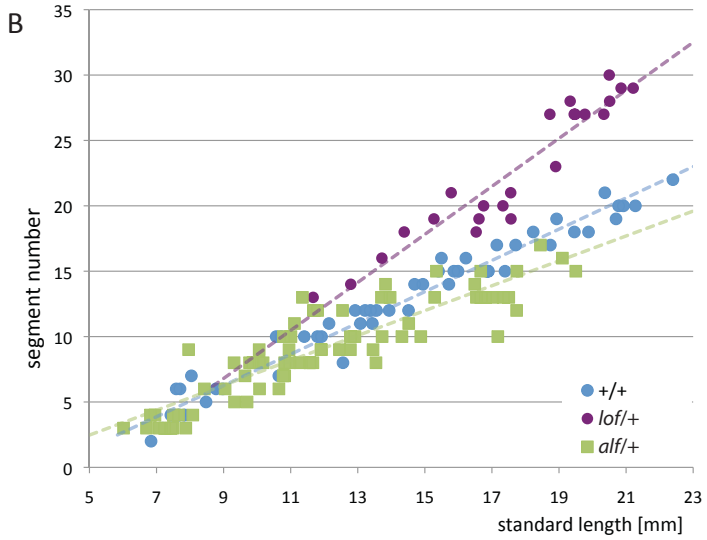
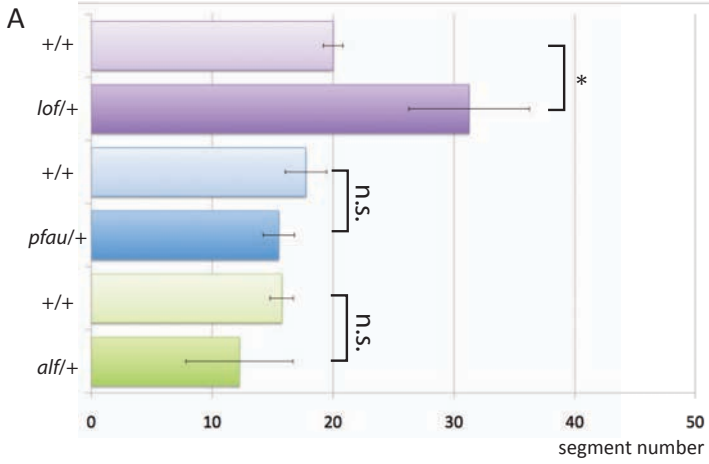
2.1.3 The fins of *kcnk5b* mutants have elongated segments

The bony fin rays (lepidotrichia) are enlarged in both *alf* and *lof* mutants [van Eeden et al., 1996]. Since the lepidotrichia are segmented (cf. Sec. 1.2.1), elongation of fin rays can in principle occur via two different scenarios: multiplication of segment number or expansion of the length of segments.

Previous studies have shown that *lof* mutants have supranumeral segments [Iovine and Johnson, 2000]. Hence, I tested if *alf* and *pfau* mutants also form additional segments in comparison to wild type. Segment number was analysed in the dorsal fin of heterozygous adult mutants (*alf*/+ and *pfau*/+) obtained through a heterozygous outcross and compared to their respective wild type siblings (+/+) as well as to heterozygous *lof* mutants (*lof*/+). Since growth of fish is variable and even siblings raised together can differ considerably in size and developmental stage, fish were compared according to standard length (SL), as described by Parichy et al. [2009]. SL is defined as the distance between the most anterior part of the head excluding the lower jaw, termed snout, and the caudal peduncle, i.e. the most posterior region of the body encompassing the hypural complex, but excluding the caudal fin.

In contrast to *lof*/+, adult *alf*/+ and *pfau*/+ fish do not show an increased number of segments in respect to wild type siblings of comparable SL (Fig. 2.5 panel A). Consistently, during postembryonic development, segment number does not appear to be increased or is even reduced in *alf*/+ mutants compared to fish with wild type fins, whereas in *lof*/+ an

Average segment number



increase in segment number is visible already in juvenile fish (SL 13-16 mm) (Fig. 2.5 panel B).

A detailed analysis of the segments forming the single lepidotrichia reveals that the distance between joints is irregular in *alf/+* (Fig. 2.6). On average, *alf* segments are elongated (*alf/+* mutants: $461 \pm 90 \mu\text{m}$; siblings: $210 \pm 4 \mu\text{m}$; $p < 0.02$) (Fig. 2.7 panel A), although the segmentation pattern is highly variable and segments can also be considerably smaller than in wild type (Fig. 2.6, arrow: $92 \mu\text{m}$). These data are consistent with observations made independently by others [Sims et al., 2009]. Consistently, a similar phenotype is observed in *pfau* mutants (Fig. 2.7 panel A), where segments are on average elongated (*pfau/+* mutants: $361 \pm 18 \mu\text{m}$; siblings: $219 \pm 19 \mu\text{m}$; $p < 0.001$), but also very short segments can be found (Fig. 2.6, arrow: $95 \mu\text{m}$).

In *lof*, segmentation patterning is rather regular, however, segments appear slightly longer than in wild type fish. This dif-

Figure 2.5 (preceding page): Segment number in mutants with generalised fin overgrowth. (A) Segment number in the longest ray of the dorsal fin were counted. Heterozygous mutants were compared to siblings (+/+, sib) of similar standard length (SL). Average SL in mm (N=4): *lof*/sib 25.7/26.4; *alf*/sib 28.4/29.5; *pfau*/sib 31.7/29.7; *: $p < 0.02$, n.s.: not significant ($p > 0.02$) (B) Number of segments during development in *alf/+*, *lof/+* mutants and wild type fish (*alb* fish were used in this case). The number of segments in the longest fin ray of the caudal fin of each individual is plotted against SL. Each data point represents one fish. Dashed lines show linear regression for the respective data points. Blue circles: wild type; green squares: *alf* heterozygous fish; purple circles: *lof* heterozygous fish.

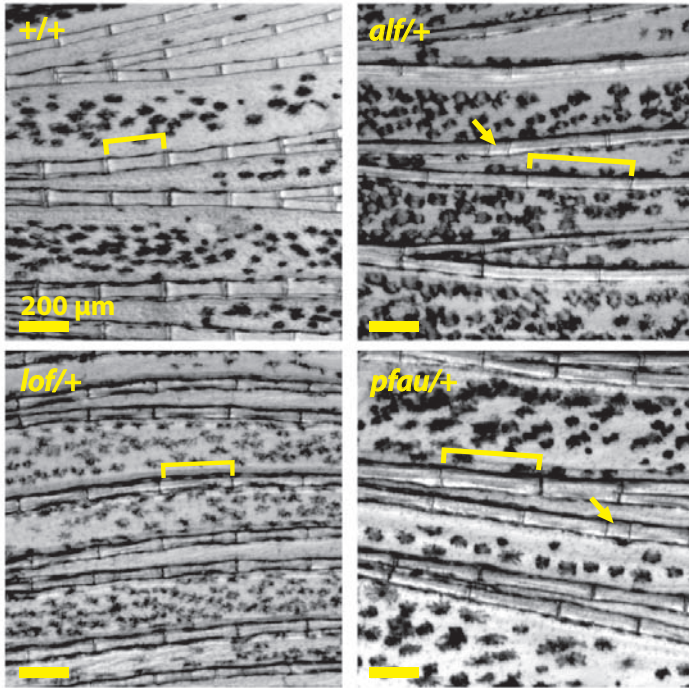
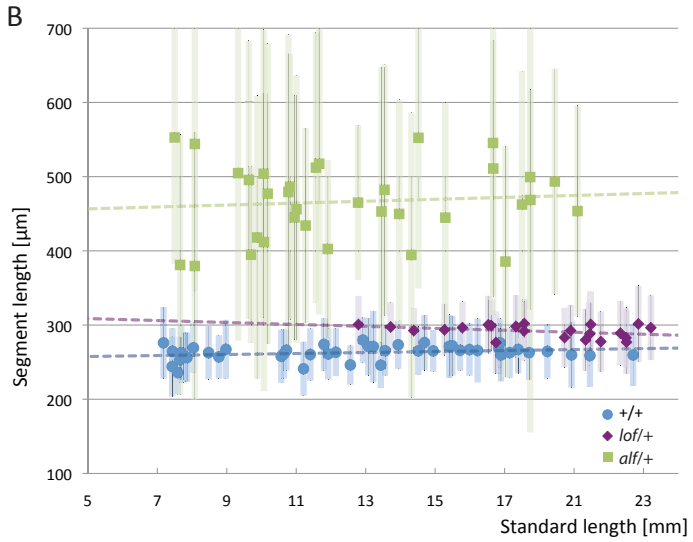
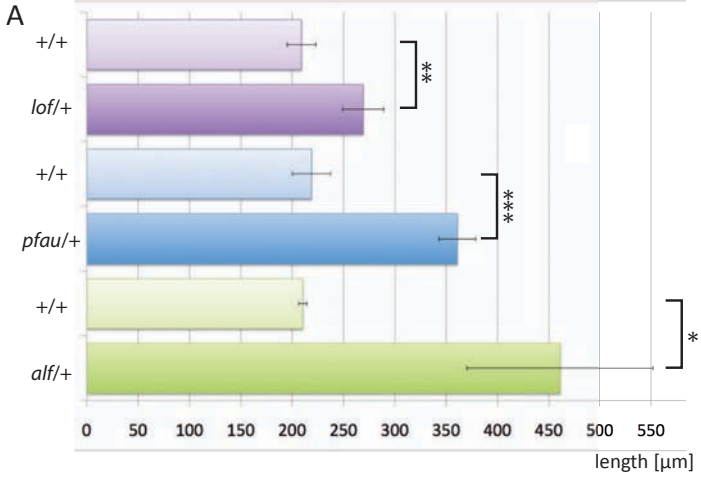


Figure 2.6: Segments in the dorsal fin of wild type and heterozygous mutant fish. Brackets indicate one segment, arrows show short segments in *alf/+* and *pfau/+* mutants. Scale bar: 200 μm

ference is significant (*lof/+* mutants: $269 \pm 20 \mu\text{m}$; siblings: $209 \pm 14 \mu\text{m}$; $p < 0.01$). Enlarged ray segments already appear during development. In *alf* mutants, average segment length is already increased at SL=7 mm (ca. 30 dpf), as soon as the first segments appear in the caudal fin (Fig. 2.7 panel B). Although segment length is extremely variable in this mutant (note error

Average segment length



bars in Fig. 2.7 panel B), the average segment length remains approximately constant during postembryonic development, irrespectively of fish size and is considerably larger than wild type segment length.

In conclusion, *alf* and *pfau* mutants, which are both characterised by elongated fins and barbels, show a very similar phenotype with irregular segmentation patterning and a tendency for elongated segments. Thus, in these mutants, enlarged fins result mainly from an increase in segment length. In contrast, the *lof* mutant, which does not display enlarged barbels, shows only slight segment elongation and achieves enlarged fin size mainly by an increase in segment number. The phenotype arises as soon as first segments are formed suggesting a direct role of *kcnk5b* in segment patterning. Possibly, the elongated and irregular segments observed in *alf* and *pfau* cause a loss of flexibility in the fin and could account for susceptibility to fin breakage.

Figure 2.7 (preceding page): Length of fin ray segments in mutants with generalised fin overgrowth. (A) Segment length in the longest ray of the dorsal fin of adult fin overgrowth mutants was measured. Mutants were compared to wild type siblings (+/+, sib) of similar standard length (SL). Average SL in mm (N=4 fish each): *lof*/sib 25.7/26.4; *alf*/sib 28.4/29.5; *pfau*/sib 31.7/29.7; significance *: $p < 0.02$, **: $p < 0.01$, ***: $p < 0.001$. (B) Length of segments during development. Average length of segments of the caudal fin is plotted against SL. Each data point represents one fish, vertical bars: standard deviation of the average segment length measured in the respective fish, dashed lines: linear regression of the respective data points. Blue circles: wild type; green squares: *alf* heterozygous fish; purple diamonds: *lof* heterozygous fish.

2.1.4 The *pfau* mutation acts locally to increase the size of fins and barbels

A mutation affecting organ size can act at a systemic or local level. Growth can be regulated in an organ-independent manner, through systemic signals, for example when a growth factor is released into the blood stream which stimulates the growth of appendages. Alternatively, a more local mode of action can be envisioned, in which size is determined within the organ through positional information and local interactions. Here, growth could be induced either inside the cells that express the mutated gene or in the surrounding tissue, e.g. through paracrine signalling. Whether a gene acts in an extrinsic or intrinsic fashion can be tested through transplantation experiments. Cells derived from a donor animal are grafted into a host animal with a different phenotype resulting in a chimaeric organism that is composed of a mix of donor and host cells. Donor cells are usually distinguished either by morphology, vital dye tracing or reporter gene expression; therefore, their contribution to the reproduction of the donor phenotype can easily be assessed.

To identify at which level size regulation is altered in *kcnk5b* mutants such transplantation experiments were performed using homozygous *pfau* fish. Despite the weaker phenotype, these mutants were preferred over homozygous *alf* since the fertility is higher in *pfau* fish. These were crossed to homozygous Tg(β -*actin*::GFP) transgenic fish, which express GFP in a wide array of cell types [Higashijima et al., 1997]. Cells from the resulting *pfau*/+; Tg(β -*actin*::GFP)/+ mid-blastula progeny were transplanted into homozygous *albino* (*alb/alb*) hosts of the same developmental stage (Fig. 2.8 panel A and B). The resulting

chimaeras were raised to adulthood and screened for overgrowth phenotypes. In the transplanted fish, cells derived from the *pfau* donor are labelled by the transgene Tg(β -*actin*::GFP), which is ubiquitously expressed. In contrast, host cells are wild type at the *pfau* locus and GFP-negative. In case of a systemic action of the *pfau* mutation, an all-or-nothing response is expected: When the cell population responsible for the *pfau* phenotype is donor derived, chimaeric fish should display overgrowth in all fins and barbels. In contrast, if the mutation induces growth through local effects, chimaeras will show partial overgrowth in barbels or fin parts of donor origin (Fig. 2.8 panel C).

Among the *pfau* chimaeras raised to adulthood, approximately 25% (29/120 adult fish) displayed overgrowth of individual fins (2/120), fin parts (16/120), single overgrown barbels (8/120) or a combination of fins and barbels (3/120) (Fig. 2.9). However, no chimaeras showed an overgrowth phenotype in all of their fins or barbels (0/120). Besides fin overgrowth, no other overt growth anomalies could be observed in chimaeric fish. This type of overgrowth in chimaeras carrying the *pfau* mutant clones shows that the mutation acts locally within fins as well as barbels.

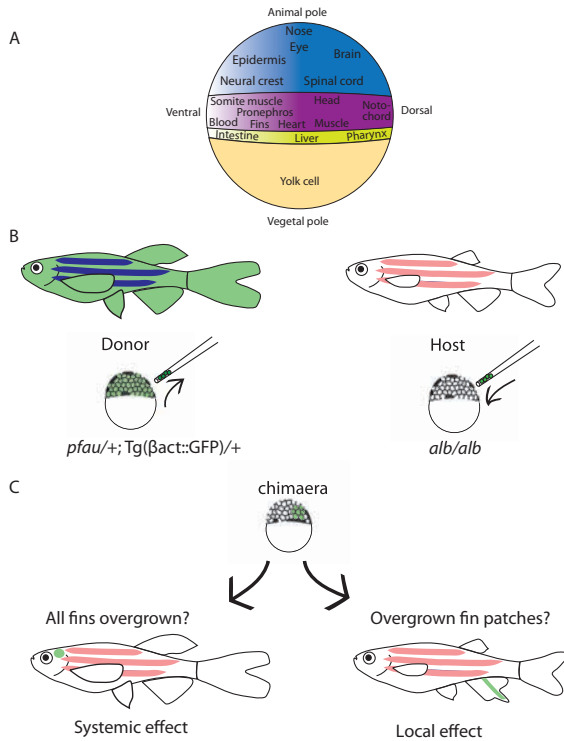


Figure 2.8: Transplantation of *pfau*. (A) Fate map of a fish embryo. Blue: ectoderm, purple: mesoderm, green: endoderm. Adapted from Langeland and Kimmel. [1997]. (B) Cells from a *pfau/+*; *Tg(β-actin::GFP)/+* donor are transplanted into an *alb/alb* host. (C) If the *pfau* mutation acts on a systemic level (e.g. endocrine secretion by the pituitary), the chimaeras show overgrowth in all their fins and barbels. In contrast, if the effect is local, only single fins or parts of fins are expected to overgrow. In this case, the donor cells are expected to be present within or close to the overgrown tissue.

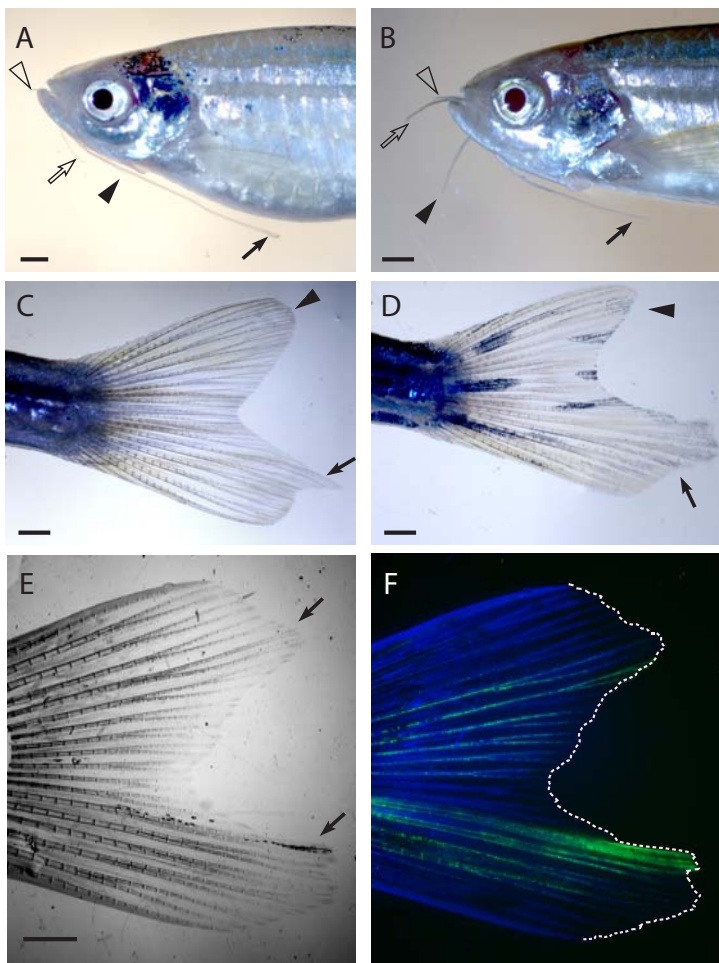


Figure 2.9 (preceding page): Chimaeras resulting from transplantation of *pfau/+; Tg(β -actin::GFP)/+* into *alb:* (A,B) Overgrowth of single barbels. Arrows: overgrown barbels; arrow heads: wild type-sized barbels. Full symbols: maxillary barbels; empty symbols: nasal barbels. (C,D) Caudal fin with partial overgrowth. Arrows: overgrown parts; arrow heads: wild type-sized lobes. (E,F) The presence of GFP expression indicates a correlation between donor cells and overgrowth phenotype. Scale bar: 1 mm

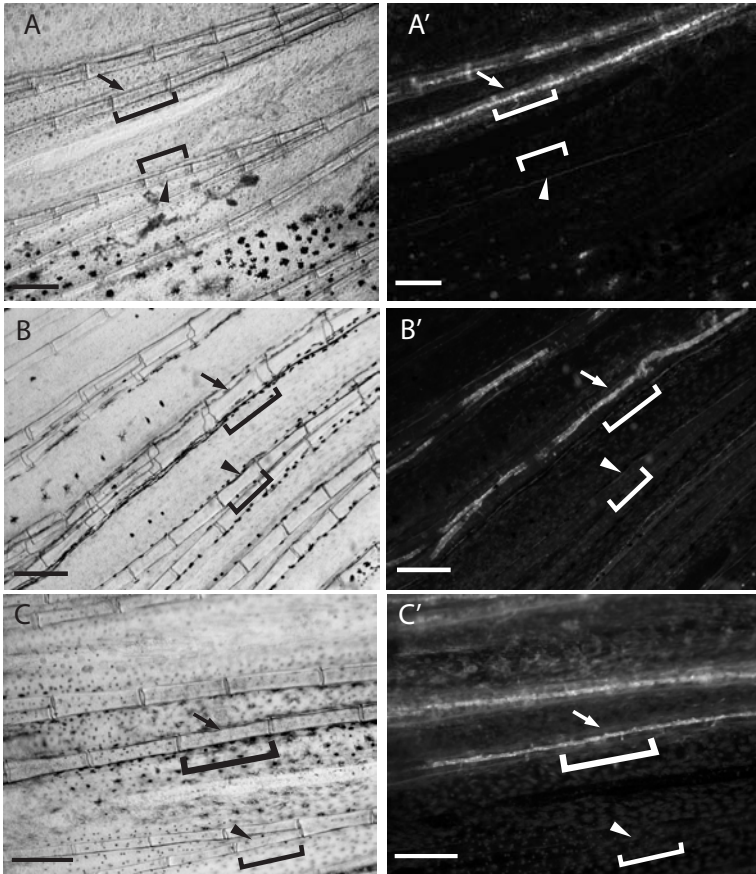


Figure 2.10: Local increased segment length in *pfau/+* clones. Longer segments (A,B,C - arrows) appear close to GFP-positive tissue (A'B'C'). Segments in GFP negative tissue are of normal size (arrow heads). Scale bar: 200 μm .

2.1.5 Vascular clones are often, but not always associated with fin overgrowth in transplantations of *kcnk5b*^{*pfau/+*} cells into *alb* hosts

Next, the question arose as to which tissue type is responsible for the *pfau* overgrowth phenotype. As the donor cells harbouring the *pfau* mutation are also labelled with Tg(β -*actin*::GFP), contribution of donor tissue to the overgrown fin can easily be observed under a fluorescence microscope. In agreement with a local mode of action for the *pfau* mutation, overgrown parts of fins and barbels were consistently labelled by GFP expression (Fig. 2.9 panel E and F). In addition, like in *pfau* fins, segments were increased in length in proximity of GFP-positive clones (Fig. 2.10).

GFP-positive clones were classified according to their cellular morphology as described [Tu and Johnson, 2011]. In most of the chimaeras (23/29), overgrowth was associated with GFP labelled vasculature (Tab. 2.1, Fig. 2.10, Fig. 2.12). Moreover in six of these, no other tissue besides blood vessels was detected as GFP positive. However, in the six remaining chimaeras (6/29) no GFP positive vasculature could be identified. Of these, two showed marked intraray glia in association with overgrowth and four showed no GFP labelling. In one case, GFP-positive clones within the vasculature were found in non-overgrown fin tissue (Fig. 2.12 d'). Although most fin tissues are found to be marked by Tg(β -*actin*::GFP) in *pfau* chimaeras (Fig. 2.11), it is unclear whether the Tg(β -*actin*::GFP) fails to consistently express the reporter gene in the tissue responsible for the phenotype or whether only a subset of vascular *pfau* clones can provoke

proliferation e.g. when present in the distal fin (Fig.2.12 A-D vs D').

To conclude, this analysis showed a potential correlation of overgrowth with vascular tissue. However, this association was not found in all cases. Therefore, it can be assumed that the *pfau* mutation either acts in a subset of blood vessel cell types or in a cell type, that shares a common lineage with vascular tissue, yet is not marked or only inconsistently marked by the transgene.

Table 2.1: GFP positive clones associated with fin overgrowth in *pfau/alb* chimaeras

Labelled tissue in proximity of overgrowth	cases where this is the only detected labelled tissue	cases where this tissue is labelled along with others
vasculature	6	17
intraray glia	2	12
fibroblasts	0	4
pigment cells	0	3
osteoblasts	0	3
lateral line	0	1
epidermis	0	0
no labelling	4	N/A

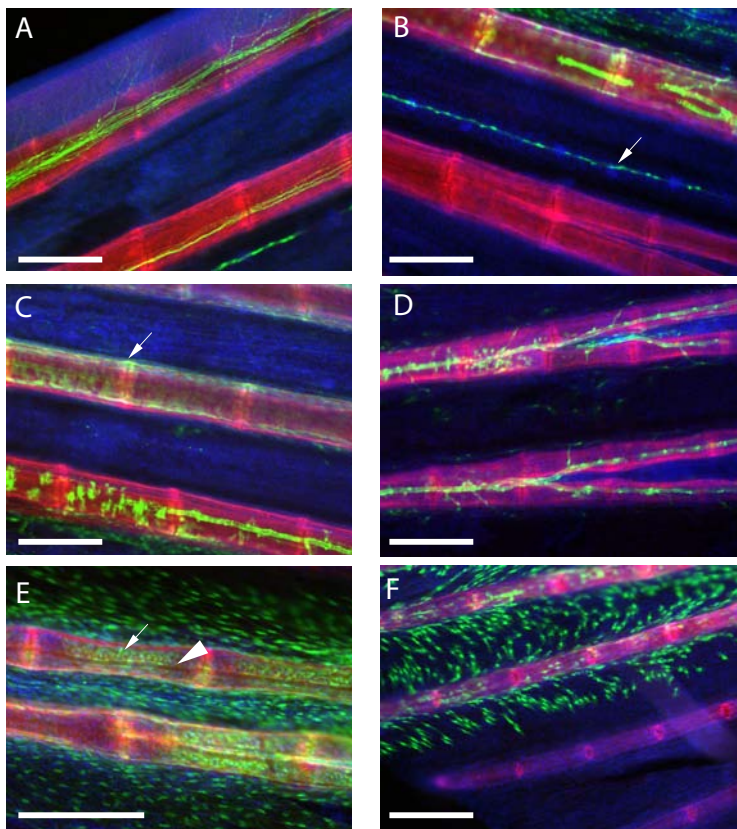


Figure 2.11: GFP positive tissue types found in chimaeric fish. *Tg(β -actin)::GFP* is expressed in a wide range of fin tissue types: intraray glia (A), lateral line (B), osteoblasts (C), vasculature (D), fibroblasts (E), pigment cells (F). Arrow in (B) indicates lateral line; in (E) fibroblasts appear as cells within the fin rays (arrow) surrounding the vasculature (arrow head, GFP negative). Green: α -GFP antibody; red: *zns-5* antibody marking osteoblasts; blue: Hoechst staining of nuclei. Scale bar: 200 μ m.

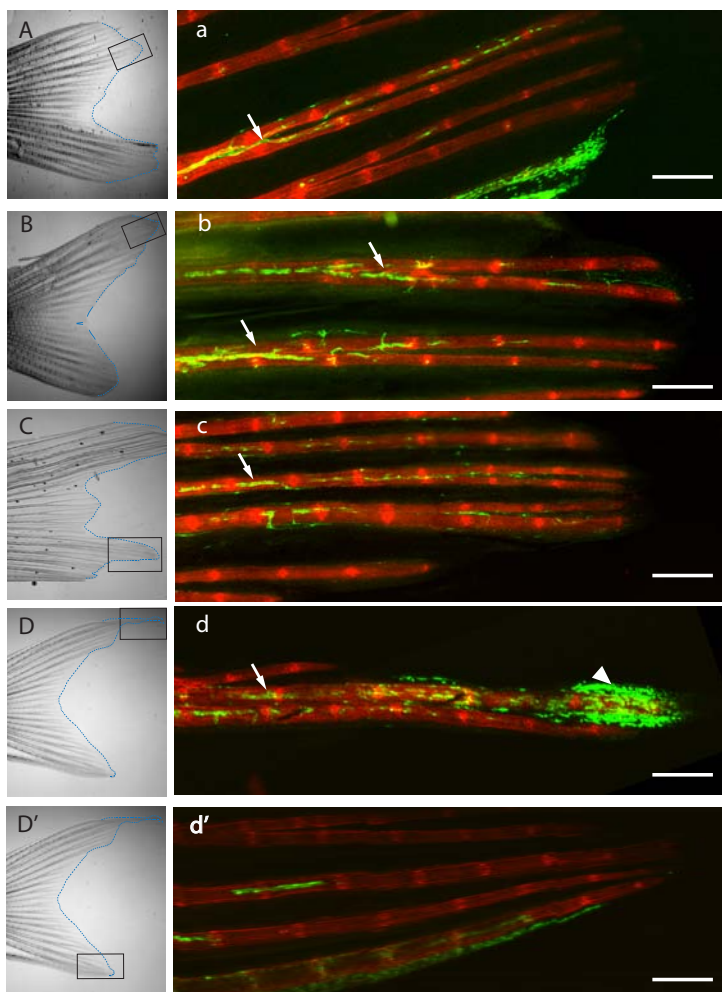


Figure 2.12 (preceding page): Analysis of overgrowth in *pfau* chimaeras. Right panels (lower-case) show the area of fins boxed on the left panel (upper-case). Vasculature was found GFP-positive in the vast majority of chimaeras displaying an overgrowth phenotype. Notice the patchy nature of the GFP positive clones (arrows). Vascular clones were observed also in non overgrown patches (D', d'). Arrowhead: fibroblasts; green : α -GFP antibody; red: *zns-5* antibody marking osteoblasts. Scale bar: 200 μ m

2.1.6 Misexpression of *Kcnk5^{pfau}* leads to local fin overgrowth

To test for the causal relationship between the identified mutations in *kcnk5b* and the overgrowth phenotype of the mutants, *Kcnk5b^{pfau}* was misexpressed in wild type fish. For this purpose, a construct was generated in which *kcnk5b^{pfau}* expression is driven by the ubiquitous promoter of the elongation factor 1 alpha (*ef1a*) from *Xenopus laevis*. To mark the cells that express the mutant channel, expression of a red fluorescent protein from the coral genus *Discosoma* (DsRed) was used. Since even small tag polypeptides have been reported to disrupt K^+ channels function [Hegle et al., 2006], it was decided to express DsRed under a second *ef1a* promoter positioned *in tandem* on the same plasmid (pGEMT *ef1a*:*Kcnk5b^{pfau}*; *ef1a*:DsRed). This plasmid was injected into wild type zebrafish one-cell stage zygotes along with *in vitro* transcribed tol2 transposase mRNA in order to increase the integration efficiency of the construct into the genome. Successful transgene integration into the genome of somatic cells resulted in permanent expression of *Kcnk5b^{pfau}* and DsRed. Injected fish were raised to adulthood and screened for DsRed positive clones in the fins.

When the *ef1a*:DsRed; *ef1a*:*kcnk5b^{pfau}* plasmid was injected at a concentration of 7.5 ng/ μ l, approximately 80% of the surviving fish showed DsRed positive clones in adult fins. Of these, about 40% (22/49) had partial fin overgrowth in paired or unpaired fins (Tab. 2.2, Fig. 2.13). Injection of the *ef1a*:DsRed;*ef1a*:*kcnk5b^{pfau}* plasmid at a higher concentration ($c= 15$ ng/ μ l), had increased lethality and less than 3% of adult fish showed DsRed-positive clones (8/344). Nevertheless, partial fin overgrowth was ob-

served in two cases. No overgrowth was observed in fish injected with a control plasmid, expressing only DsRed under the *ef1a* promoter (n=240, c= 7.5 ng// μ l), despite the fact that these fish developed DsRed-positive clones in various tissues (Fig. 2.14).

Table 2.2: Cases of overgrowth observed in adult wild type fish misexpressing *Kcnk5b^{pfau}* screened for DsRed expression in the fin.

<i>ef1a</i> :DsRed; <i>ef1a:knk5b^{pfau}</i>	7.5 ng/ μ l	15 ng/ μ l
Screened fish	61	344
No. of cases with DsRed expression in fin tissues	49	8
No. of cases with overgrown fin parts	22	2

To identify the tissue(s) responsible for the *pfau* phenotype, samples that displayed overgrowth were analysed for DsRed fluorescence signal. Analysis of these clones showed a strong correlation of DsRed positive dermal fibroblasts with overgrowth (20/22 for 7.5 ng/ μ l and 2/2 for 15 ng/ μ l) (Fig. 2.15 C-F). In two cases no DsRed fluorescence signal could be detected within or next to overgrown fin tissue. This might be due to removal of the reporter via a nonallelic homologous recombination (NAHR) event [Liu et al., 2012] between the two *ef1a* promoters present in the plasmid (cf. Fig. 4.1).

Taken together, these data show that expression of *Kcnk5b^{pfau}* is sufficient to cause fin overgrowth *in vivo*. Overgrown tissue is associated with DsRed positive fibroblasts, although, whether

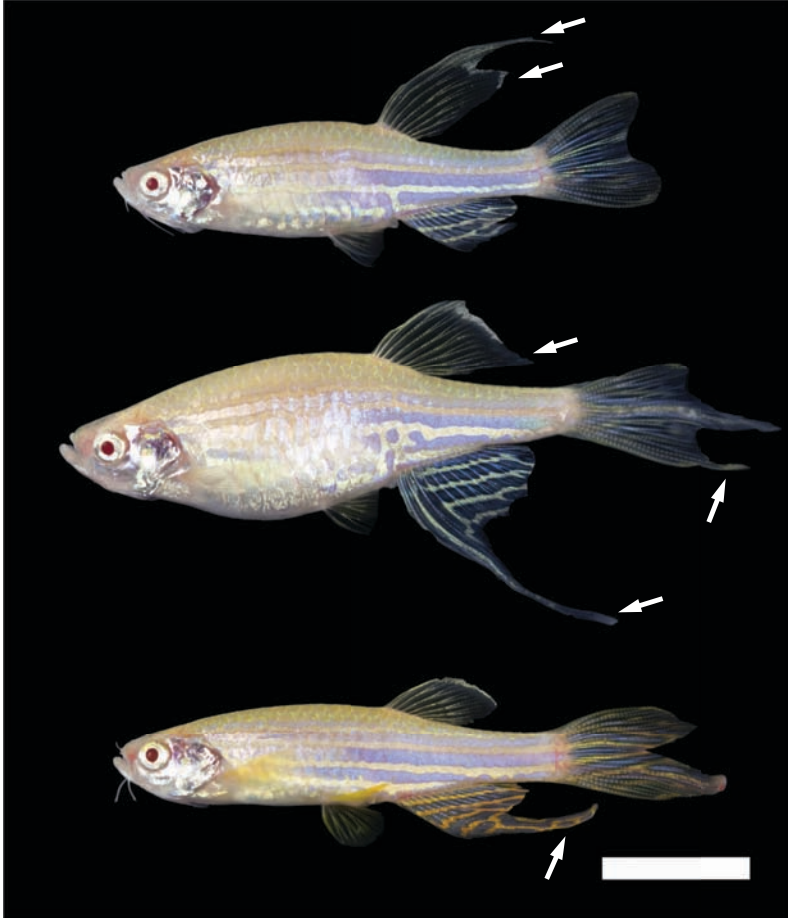


Figure 2.13: Mosaic expression of *ef1*:*DsRed*;*ef1*:*kcnk5b*^{2fa} in wild type fish causes fin overgrowth. Arrows point to overgrown fin parts. Scale bar: 10 mm

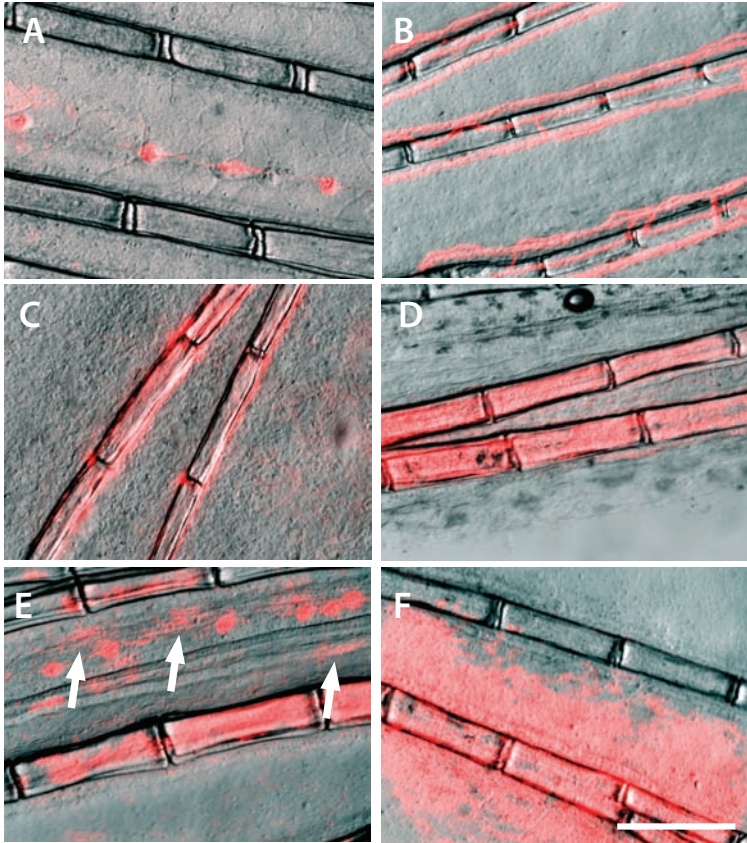
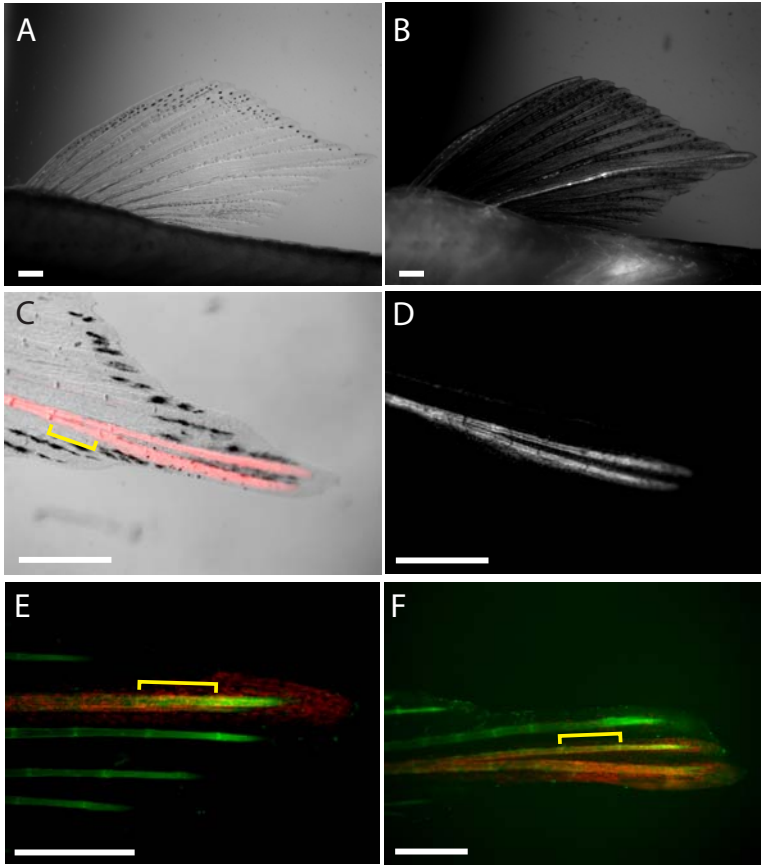


Figure 2.14: The control plasmid *ef1a:DsRed* drives DsRed expression in a wide range of cell types and tissues within the fin: (A) Lateral line, (B) vasculature, (C) osteoblasts, (D) fibroblasts, (E, white arrows) pigment cells and (F) epidermis. Scale bar: 200 μm



this cell type is responsible for the phenotype of *pfau*, needs to be confirmed through expression of $Kcnk5^{pfau}$ via a tissue specific promoter.

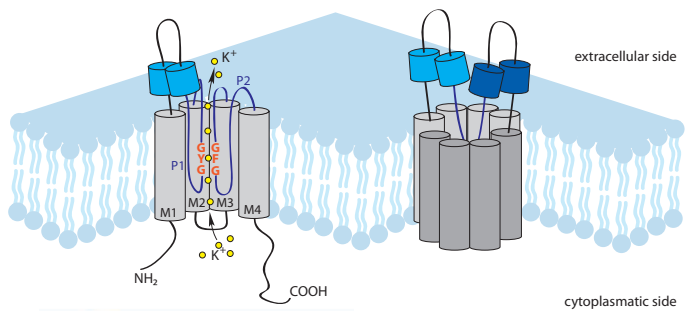
2.1.7 The amino acids altered in *alf* and *pfau* reside within the transmembrane domains of Kcnk5b

To explore the impact of the missense mutations in *alf* and *pfau* on Kcnk5b protein properties, a model of the three-dimensional structure of the protein was generated from the PDB database taking advantage of the MPI toolkit available at <http://toolkit.tuebingen.mpg.de/>. Here, HHpred was used to detect proteins similar to zebrafish Kcnk5b. The program builds a profile hidden Markov model (HMM) from a query sequence and compares it to a database of HMMs corresponding to proteins of known structure [Hildebrand et al., 2009]. Subsequently, the identified sequences with known structures can be used as template for structure prediction.

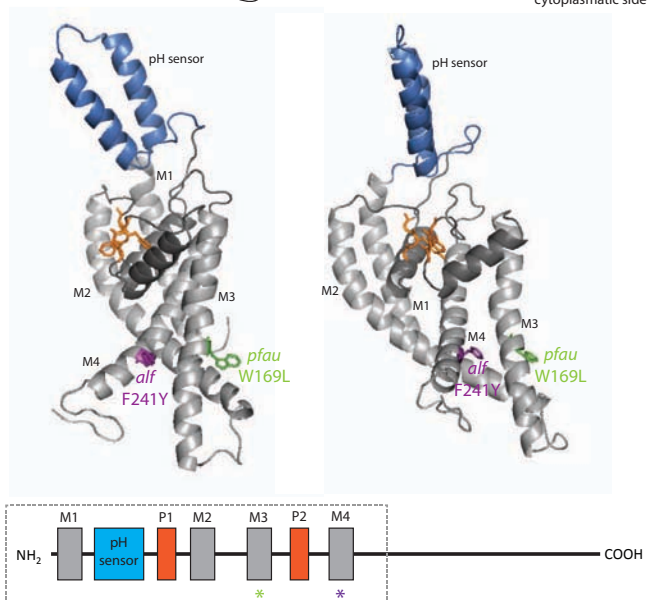
With an identity of 36% and a similarity of 65%, the human K_{2P} channel KCNK4 (K2P4.1) resulted to be the first hit on

Figure 2.15 (preceding page): Clonal misexpression of *ef1a: DsRed*; *ef1a: kcnk5b^{pfau}* in wild type fins. Clonal expression of the mutant protein results in local fin overgrowth (A,B). Overgrown fin parts show DsRed expression within dermal fibroblasts (C-F). Brackets show elongated segments: ca. 320 μm . Red/White: Fluorescence signal of DsRed; green: calcein staining highlighting the bone matrix. Scale bar: 500 μm

A



B



the PDB database (pdb 22nd March 2012). This structure was used as a template for modelling.

Kcnk5b is a tandem pore-domain K⁺ channel (K_{2P}). It is formed by two subunits that homodimerise to form a functional channel. Each subunit consists of four transmembrane (TM) domains, termed M1-M4, and two pore (P) loops, P1 and P2. These P-loops contain a Gly-Tyr-Gly (P1) and a Gly-Tyr-Gly (P2) motif that form the selectivity filter which makes the channel specifically permeable to K⁺ ions (Fig. 2.16 panel A). The extracellular M1-P1 loop contains several charged residues that act as a pH-sensor [Morton et al., 2005].

3D modelling revealed that the *pfau* mutation affects an amino acid in the TM domain M3, while the amino acid substitution in *alf* occurs in TM domain M4 (Fig. 2.16 panel B). The affected amino acids are aromatic and positioned towards the cytoplasmic side of the TM domain. Aromatic amino acids are often found at the interface between cytoplasm and cell

Figure 2.16 (preceding page): Location of the amino acids altered in *alf* and *pfau*. (A) Left: K_{2P} channels possess 4 TM domains (M1-M4). The P1 and P2 loop form the selectivity filter which contains a GYG and GFG motif, respectively. Right: Two subunits assemble two a homodimer to form a functional channel. (B) Modelling of zebrafish Kcnk5b protein on human KCNK4 (K2P4.1). Both amino acid residues altered in *pfau* (green) and *alf* (purple) locate within the vestibulum of the channel. Grey: transmembrane domains (M1-M4), dark grey: pore forming unit, orange: selectivity filter, blue: extracellular pH sensor. The picture shows two different views of the same subunit. Only the amino terminus (dashed box) is depicted in the 3D model.

membrane and seem to stabilise membrane proteins within the membrane [Kelkar and Chattopadhyay, 2006]. In line with this hypothesis, aromaticity in Kcnk5 is fully conserved among vertebrates in the positions affected in *pfau* and the *alf* mutants (cf. Fig. 2.4).

2.1.8 The *alf* and *pfau* mutations lead to an increased conductance of Kcnk5b

In order to assess how the amino acid substitutions found in *alf* and *pfau* mutants might affect Kcnk5b function, the channel properties were tested in a two-electrode voltage clamp experiment [Cole and Moore, 1960] using *X. laevis* oocytes as a heterologous expression system [Gurdon et al., 1971]. In this electrophysiological assay, an oocyte expressing the ion channel of interest is placed in a perfusion chamber and two electrodes are introduced into the cell. One electrode is used to assess the internal potential of the oocyte while the other one is used to inject current. This set-up can be used to clamp the voltage to a certain value. The amount of current that needs to be injected in order to maintain this voltage reflects the amount of current that is flowing through the channel.

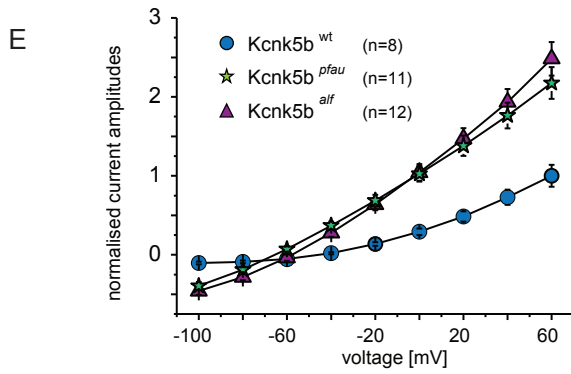
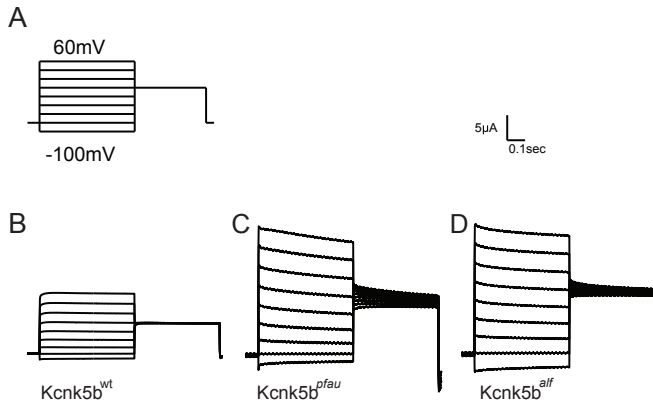
In collaboration with the laboratory of Prof. Guiscard Seeböhm, Ruhr Universität Bochum, I used this system to assess the properties of the channels of wild type and mutant fish. The coding sequences (CDS) of wild type, *alf* and *pfau kcnk5b* were cloned into the pSGEM expression vector. Subsequently, cRNA was synthesised *in vitro* and injected into oocytes for electrophysiological measurements. Voltage clamp experimental

set up pulses from -100 to +60 mV were applied for 0.5 s (Fig. 2.17, A) and the current was simultaneously recorded.

In voltage-dependent potassium (K_V) channels, current typically starts to flow with a delay upon changes in voltage, because these channels have to switch to the open conformation. In contrast, K_{2P} channels, such as *Kcnk5b*, are already open before the voltage changes [Goldstein et al., 2001], therefore the current flow is instant and no delay is observed. Consistently, wild type *Kcnk5b* reacts steadily to a change in voltage and no delay is observed (Fig. 2.17, B). A comparable situation is also seen in both mutant channels. However, both *pfau* and *alf* variants show an almost double increment in K^+ conductance over that of wild type zebrafish *Kcnk5b* (Fig. 2.17 C,D).

The current-voltage relationship of wild type *Kcnk5b* (Fig. 2.17 panel E, blue circles) shows the typical outward rectification of K_{2P} channels, i.e. current flows preferentially out of the cell, from the side of high K^+ concentration to the side of low K^+ concentration [Enyedi and Czirjak, 2010] (see Box 1 for details). In contrast, outward rectification is reduced in both *pfau* and *alf* (Fig. 2.17 panel E, green stars and purple triangles), since inward currents are still observed at -100 mV. This might be a direct consequence of the increased K^+ conductance. Increased ion flow will reduce the difference between intracellular and extracellular K^+ ion concentration and therefore reduce the preferential flow towards the extracellular side.

K_{2P} channels are often referred to as leakage channels, since they account for the constant, "leaking" current that sets the resting membrane potential observed in neurons. In fact, K_{2P} channels are known to control cell excitability as well as membrane



potential (V_m) [Lesage and Lazdunski, 2000]. When a channel type that is selective for a specific ion dominates within the membrane, e.g. because other ion channels are closed, V_m will move towards the equilibrium potential of this ion species. The equilibrium potential for K^+ (E_K) is roughly -100 mV in *Xenopus* oocytes [Kusano et al., 1982; Miledi and Parker, 1984]. Therefore, if *Kcnk5b* plays a major role in determining V_m , V_m should be shifted towards E_K in oocytes expressing the channel.

Indeed, V_m values of oocytes injected with wild type and mutant *kcnk5b* mRNA correlate to the amplitude of the ion current measured at a voltage of 50 mV (Fig. 2.18): The higher the conductance for K^+ measured at 50 mV, the lower the V_m of the oocyte. Consistently, oocytes injected with mutant *kcnk5b* mRNA showed more negative V_m than oocytes injected with wild type mRNA. These findings indicate that V_m in the oo-

Figure 2.17 (preceding page): Voltage clamp on *Xenopus* oocytes injected with cRNA of wild type and mutant *kcnk5b*. A series of voltage steps were delivered to the injected oocytes for 0.5 s (A). The two-pore domain potassium channel *Kcnk5b* displays the typical behaviour of a leakage channel: current changes instantly to a new steady level as soon as a voltage step is delivered (B). In comparison to the wild type channel (B), *pfau* (C) and *alf* (D) show a significant increment in K^+ current. As in wild type, the mutant channels show no delay before current starts to flow upon a change in voltage. Graphs show representative examples of recorded oocytes. (E) Current-voltage characteristic of *Kcnk5b*. Outward rectification is apparent in wild type *Kcnk5b*. *alf* and *pfau* channels fail to rectify and show increased conductance. Circles: wild type, triangles: *alf*, stars: *pfau*. Current was normalised to the measurement of wild type current at 60 mV.

cyte is determined primarily by *Kcnk5b* and that the alterations found in *Kcnk5b^{alf}* and *Kcnk5b^{pfau}* channel lead to a hyperpolarisation of V_m *in ovo*.

In conclusion, the *alf* and *pfau* mutations increase the conductance of *Kcnk5b* and cause hyperpolarisation of *Xenopus* oocytes. Therefore, the mutations might promote hyperpolarisation of the cell *in vivo*.

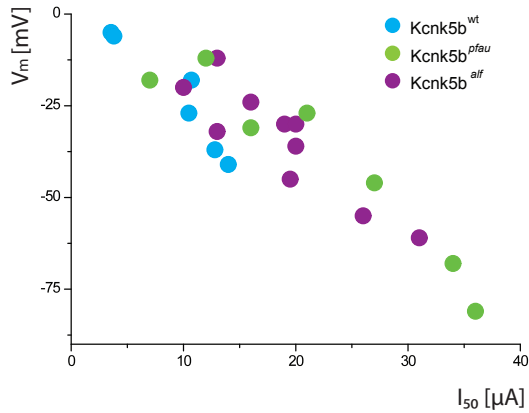


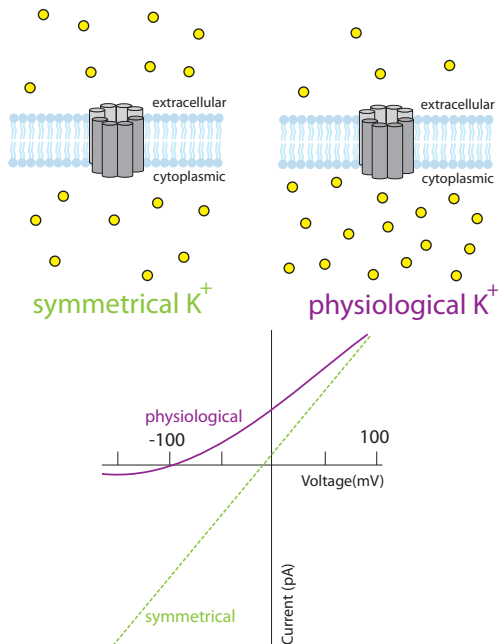
Figure 2.18: *Kcnk5b* influences membrane potential (V_m). Current (I_{50}) recorded at a potential of 50 mV correlates with V_m measured at rest. Each point represents one oocyte. Blue: wild type mRNA; green: *pfau*; purple: *alf*.

Box 1. Outward rectification in K_{2P} channels.

When K⁺ ion concentrations are equal across the membrane (symmetrical K⁺) K_{2P} channels behave like an Ohmic resistance and the current-voltage relationship is nearly linear (broken green line). When K⁺ concentration is high inside the cell and low outside the cell (physiological conditions), the passage of outward currents is favoured (solid purple line). This phenomenon is predicted by the Goldman-Hodgkin-Katz current equation:

$$I_{K^+} = Pz^2 \frac{V_m F^2}{RT} \frac{[K^+]_{int} - [K^+]_{ext} \cdot e^{-z \frac{V_m F}{RT}}}{1 - e^{-z \frac{V_m F}{RT}}}$$

and is therefore termed Goldman-Hodgkin-Katz rectification or outward rectification. I_{K^+} : total K⁺ current; P : ion permeability; z : ion valence; F : Faraday constant; R : gas constant; T : temperature in Kelvin; $[K^+]_{int}$ and $[K^+]_{ext}$: internal and external ion concentration. Figure adapted from Goldstein et al. [2001].



2.2 Analysis of mutants showing dorsal fin overgrowth

The second part of this study concentrates on three mutants that display overgrowth exclusively in the dorsal fin: *segel* (sgl^{dt31mh}), *segel-like* ($sllk^{dt32mh}$) and *flagge* (fgg^{dt3nr}) (Fig. 2.19). These three mutants are characterised by an enlarged dorsal fin, which typically reaches the length of the anal fin or beyond (2.19). As in the case of the *kcnk5b* mutants, *sgl*, *sllk* and *fgg* act dominantly. Homozygotes are virtually indistinguishable from heterozygous individuals. Homozygous *sgl* fish show reduced fitness as is apparent from mapping crosses (cf. Sec. 2.2.1) where only one fish out of 48 *segel* carriers was homozygous (versus 16/48 expected). It is unclear, whether lethality is due to a second mutation linked to the *sgl* locus, or whether homozygosity of the *sgl* mutation itself results in reduced viability.

2.2.1 The mutants *sgl*, *sllk* and *fgg* harbour missense mutations in the potassium channel *kcnh1a*

A mapping approach as described in section 2.1.1 was used to identify the mutation causing the *sgl* phenotype. Bulk segregant analysis revealed that the *sgl* mutant is linked to z-markers z4268 and z22674, placing the mutation on chromosome 17. PCR analysis on individual DNA samples reduced the mapping interval to a region of 4.49 Mb (Vega 47) between z15718 and z21435 (Fig. 2.20).

Based on the results obtained with the *alf* and *pfau* mutants (cf. Sec. 2.1.1), the mapping interval was scanned for K^+ channels. K_V channel *kcnh1a* was identified in the middle of the genomic

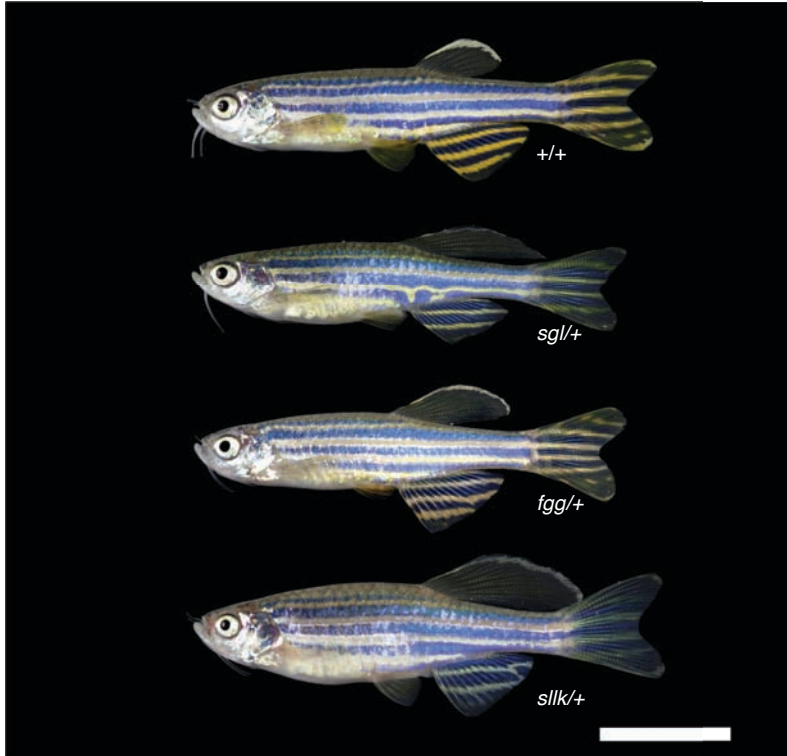
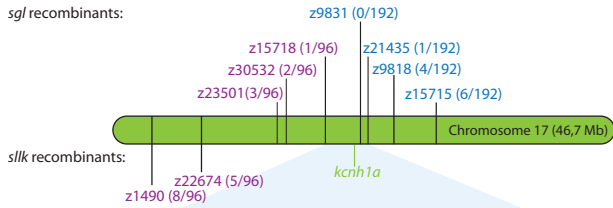


Figure 2.19: Phenotype of *sgl*, *fgg* and *slk* mutants. In wild type (+/+) the dorsal fin reaches to two thirds of the length of the anal fin, while in mutants, the dorsal fin is at least as long as the anal fin. All mutant fish represented are heterozygous. Homozygous mutant fish show a virtually identical phenotype. Scale bar = 10 mm



interval as a potential candidate (Fig. 2.20). No recombinants could be found in proximity to this locus (z9831 in Fig. 2.20). Sequencing of the CDS of *kcnh1a* from *sgl* revealed a change of adenine to guanine resulting in an amino acid substitution of glutamine (Gln) 474 to arginine (Arg) (Fig. 2.21). Mapping for *sllk* showed strong linkage to z-markers z31650, z23501, z55190

Figure 2.20 (preceding page): Mapping of *sgl* and *sllk* mutations. (Upper panel) The *sgl* and *sllk* mutations map to chromosome 17. Purple: North markers; blue: South markers; numbers in brackets: recombinants/meioses. (Lower panel) Genes encoded in the region linked to *sgl*. z15718: North marker of *sgl*; z21435: South marker of *sgl*; z9831: loss of recombination. K⁺ channel *kcnh1a* is encoded in this interval (highlighted in green).

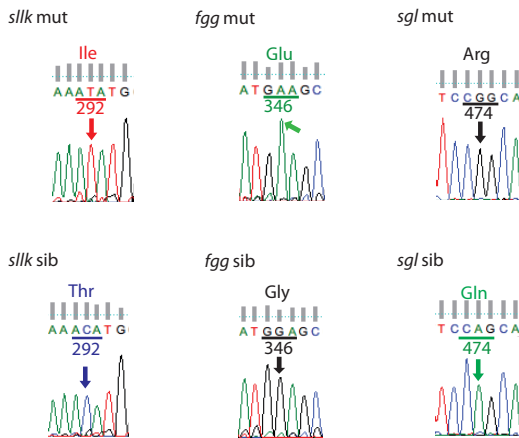


Figure 2.21: Electropherogram of *kcnh1a* at the *sllk*, *fgg* and *sgl* locus

and z22279, placing the mutation on the same chromosome. Analysis of DNA from single F₂ individuals indicated z1490 and z22574 as being linked to the mutation (Fig. 2.20).

Given the close resemblance of *sllk*, *fgg* and *sgl* mutants and due to the linkage of *sllk* to chromosome 17, *kcnh1a* seemed to be the ideal candidate gene for the *sllk* and *fgg* mutations. Indeed, the *sllk* and *fgg* mutants also harbour missense mutations within this gene. In *sllk* a transversion from cytosine to adenine changes threonine (Thr) 292 into isoleucine (Ile). In *fgg* glycine (Gly) 346 is converted to glutamic acid (Glu) through a transition from guanine to adenine (Fig. 2.21). The residues in *kcnh1a* affected in the three dorsal fin mutants are highly conserved within metazoans (Fig. 2.22).

Since the mutations found in the dorsal fin overgrowth mutants are all dominant, with similar phenotypic expressivity in hetero- and homozygous animals, a complementation test cannot be used to genetically support their allelic nature. Instead a segregation test by transheterozygous outcrossing was performed. Here, *sgl/sllk* transheterozygous fish, i.e. fish that are heterozygous for both mutations, were obtained by crossing *sgl* heterozygous fish to *sllk* homozygous mutants. The progeny was raised, genotyped for the presence of both mutations and subsequently outcrossed to *alb* fish. If the *sgl* and *sllk* mutants are allelic, recombination events between the two mutations are highly unlikely. However, in the case of non-allelism, the larger the distance between the affected loci, the more likely are recombination events. Therefore, if number of progeny is sufficiently high, the presence of some wild type fish would be detected in the F₁ fish. In contrast, in case of allelism, each

↓ *slk* (T292)

```

*****:***:.*:.* **.*:*.*****:.*.
Tru-kcnh1a LNFHTTFVGPAGEVISDPKLIRMNYLKTWFVIDLLSCLPYDVINAFENV
Gac-kcnh1a LNFHTTFVGPAGEVISDPKLIRMNYLKTWFVIDLLSCLPYDVINAFENV
Dre-kcnh1a LNFHTTFVGPAGEVISDPKLIRMNYLKTWFVIDLLSCLPYDVINAFENV
Mmu-kcnh1 LNFHTTFVGPAGEVISDPKLIRMNYLKTWFVIDLLSCLPYDVINAFENV
Hsa-kcnh1 LNFHTTFVGPAGEVISDPKLIRMNYLKTWFVIDLLSCLPYDVINAFENV
Gga-kcnh1 LNFHTTFVGPAGEVISDPKLIRMNYLKTWFVIDLLSCLPYDVINAFENV
Xtr-kcnh1 LNFHTTFVGPAGEVISDPKLIRMNYLKTWFVIDLLSCLPYDVINAFENV
Dre-kcnh1b LNFHTTFVGPAGEVISDPKLIRMNYVKTWFVIDLLSCLPYDVINAFENV
Ola-kcnh1a LNFHTTFVGPAGEVISDPKLIRMNYVKTWFVIDLLSCLPYDVINAFENV
Aae-eag LNFHTTFVGGGGEVSDPKVIRMNYLKSWFIIIDLLSCLPYDVFNADFHD
Dme-eag LNFHTTFVGGGGEVSDPKVIRMNYLKSWFIIIDLLSCLPYDVFNADFDR
Cel-egl2 LNFHTTFVGGGGEVIEPSVIRQNYFKSWFLIDLLSCLPYDIFYMEKRD

```

↓ *fgg* (G346E)

```

.***:*****.***.*.***** *.*.* :.*.***:
Tru-kcnh1a SSLSFSSLKVVRLRLGRVARKLDHYIEYGAAVLVLLVCVFGLAHHLAC
Gac-kcnh1a SSLSFSSLKVVRLRLGRVARKLDHYIEYGAAVLVLLVCVFGLAHHLAC
Dre-kcnh1a SSLSFSSLKVVRLRLGRVARKLDHYIEYGAAVLVLLVCVFGLAHHLAC
Mmu-kcnh1 SSLSFSSLKVVRLRLGRVARKLDHYIEYGAAVLVLLVCVFGLAHWMAC
Hsa-kcnh1 SSLSFSSLKVVRLRLGRVARKLDHYIEYGAAVLVLLVCVFGLAHWMAC
Gga-kcnh1 SSLSFSSLKVVRLRLGRVARKLDHYIEYGAAVLVLLVCVFGLAHHLAC
Xtr-kcnh1 SSLSFSSLKVVRLRLGRVARKLDHYIEYGAAVLVLLVCVFGLAHHLAC
Dre-kcnh1b SSLSFSSLKVVRLRLGRVARKLDHYIEYGAAVLVLLVCVFGLAHHLAC
Ola-kcnh1a SSLSFSSLKVVRLRLGRVARKLDHYIEYGAAVLVLLVCVFGLAHHLAC
Aae-eag GSLFSALKVVRLRLGRVVRKLDRYLEYGAAMLILLCFYMLVAHWLAC
Dme-eag GSLFSALKVVRLRLGRVVRKLDRYLEYGAAMLILLCFYMLVAHWLAC
Cel-egl2 GSLFSALKVVRLRLGRVARKLDNYLEYGAATLLLLCAVYVAHWLAC

```

↓ *sgl* (Q474R)

```

*.:.*.*:*****.***:.*:.* **.*:*.***:*.***:*.***:
Tru-kcnh1a FAVAMMMIGSLLYATIFGNVTTIFQOMYANTNRYHEMLNSVRDFLKLYQ
Gac-kcnh1a FAVAMMMIGSLLYATIFGNVTTIFQOMYANTNRYHEMLNSVRDFLKLYQ
Dre-kcnh1a FAVAMMMIGSLLYATIFGNVTTIFQOMYANTNRYHEMLNSVRDFLKLYQ
Mmu-kcnh1 FAVAIMMIGSLLYATIFGNVTTIFQOMYANTNRYHEMLNSVRDFLKLYQ
Hsa-kcnh1 FAVAIMMIGSLLYATIFGNVTTIFQOMYANTNRYHEMLNSVRDFLKLYQ
Gga-kcnh1 FAVAMMMIGSLLYATIFGNVTTIFQOMYANTNRYHEMLNSVRDFLKLYQ
Xtr-kcnh1 FAVAMMMIGSLLYATIFGNVTTIFQOMYANTNRYHEMLNSVRDFLKLYQ
Dre-kcnh1b FAVAMMMIGSLLYATIFGNVTNIFQOMYANTNRYHEMLNSVRDFLKLYQ
Ola-kcnh1a FAVAMMMIGSLLYATIFGNVTTIFQOMYANTNRYHEMLNSVRDFLKLYQ
Aae-eag FTICMMIIAALLYATIFGHVTTIIQQMTSATAKYHDMLNNVREFMKLHE
Dme-eag FTICMMIIAALLYATIFGHVTTIIQQMTSATAKYHDMLNNVREFMKLHE
Cel-egl2 FGVCMIIISALLYAAIFGHMTTIIQQMTSSTVRYHEMINSNVREFIKLQE

```

mutation resides on one parental chromosome and all progeny is expected to carry either the *sgl* or the *sllk* mutation.

All the progeny scored from the *sgl/sllk* transheterozygous outcrosses (n= 240 adult individuals) showed an overgrown dorsal fin. This indicates that the two loci are not more than 0.4 cM apart, which corresponds to roughly 0.4 Mb. These findings confirm therefore the mapping data. An attempt to perform this non-segregation test with *fgg* was not successful, since no transheterozygous fish for *sgl* and *fgg* could be identified due to lethality. However, for all three mutants, *sgl*, *sllk* and *fgg*, phenotype and genetic lesion in *kcnh1a* correlated fully and was consistently used for genotyping purposes.

In summary, mapping of *sgl* and *sllk* as well as test crossings show that these two mutations are linked and located on the same region on chromosome 17. Together with the mutant *fgg*, these three dorsal fin mutants carry missense mutations in conserved amino acids within the K⁺ channel *kcnh1a* encoded in the identified genomic interval. Therefore, hereafter the mutants *sgl*, *sllk* and *fgg* will be considered allelic.

Figure 2.22 (preceding page): Conservation of the amino acid sequence of Kcnh1/Eag/Egl2 among metazoans (residues shown: top 265-312; middle 318-366; bottom 450-498.). The primary structure of the Kcnh1a homologue was retrieved from the Ensembl database of the respective species. Arrows point to the amino acid altered in the different mutants. Tru *Takifugu rubripes*, Gac *Gasterosteus aculeatus*, Dre *Danio rerio*, Mmu *Mus musculus*, Hsa *Homo sapiens*, Gga *Gallus gallus*, Xtr *Xenopus tropicalis*, Ola *Oryzias latipes*, Aae *Aedes aegypti*, Dme *Drosophila melanogaster*, Cel *Caenorhabditis elegans*.

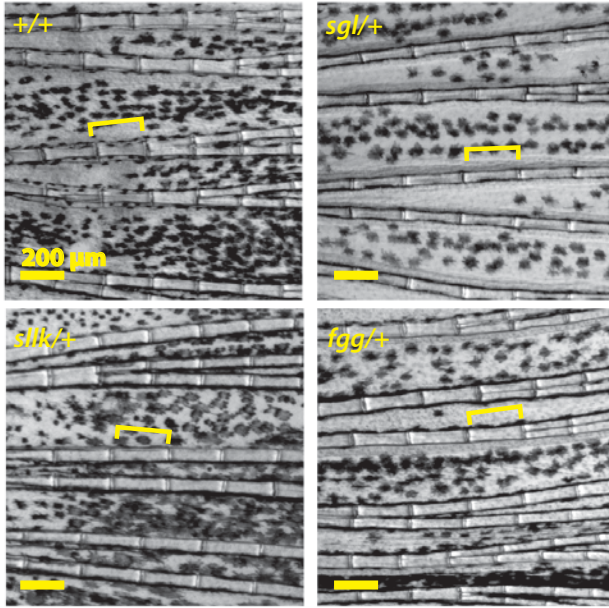
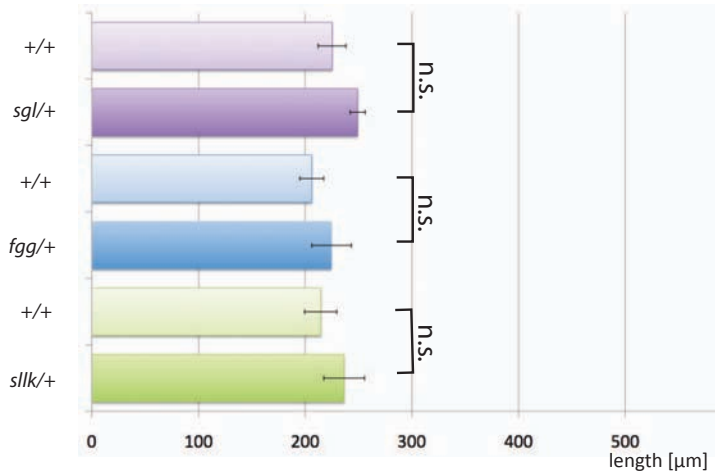


Figure 2.23: Dorsal fin ray segments in wild type and dorsal fin mutants. Brackets indicate individual segments. All mutants shown are heterozygous. Scale bar: 200 μ m

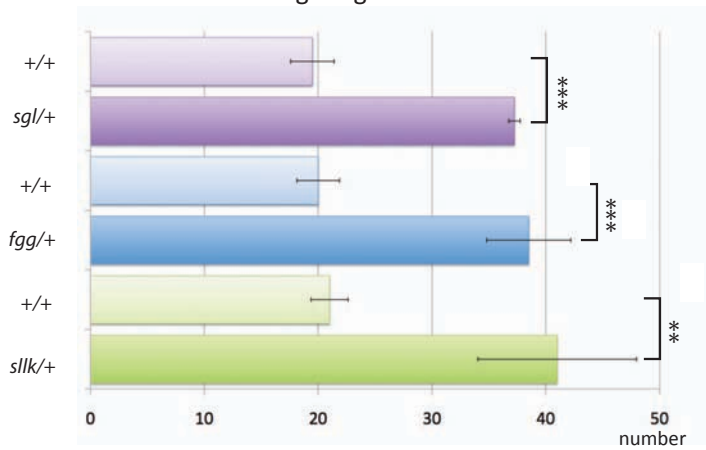
2.2.2 The fins of the *kcnh1a* mutants show an increase in segment number

As discussed previously (Sec. 2.1.3), an increase in fin size can be ascribed to an increase in fin ray segment length or to the addition of segments. The *kcnk5b* mutants showed an irregular segmentation pattern and an increase in segment size, while in *lof* fin enlargement is mainly due to an increase in segment number. Therefore, segments were analysed in *sgl/+*, *slk/+*

Average segment length



Average segment number



and *fgg*/+ mutants. In all three dorsal fin mutants, segmentation appears regular (Fig. 2.23), similarly to what is observed for wild type. Likewise, segment length is not significantly increased in these dorsal fin mutants compared to their siblings (*sgl*/+ mutants: $249 \pm 7 \mu\text{m}$; siblings: $225 \pm 16 \mu\text{m}$; $p > 0.02$; *fgg*/+ mutants: $225 \pm 19 \mu\text{m}$; siblings: $206 \pm 11 \mu\text{m}$; $p > 0.1$; *sllk*/+ mutants: $225 \pm 14 \mu\text{m}$; siblings: $214 \pm 11 \mu\text{m}$; $p > 0.2$). In contrast, when segment number was counted, a significant increase was observed in mutants compared to siblings, similarly to what can be observed in *lof* mutants (Fig. 2.24) (*sgl*/+ mutants: 37 ± 1 segment; siblings: 20 ± 2 segments; $p < 0.001$; *fgg*/+ mutants: 39 ± 4 segments; siblings: 20 ± 2 segments; $p < 0.001$; *sllk*/+ mutants: 41 ± 7 segments; siblings: 21 ± 2 segments; $p < 0.01$. The average segment number is expressed as integer).

In summary, the three dorsal fin mutants *sgl*, *sllk* and *fgg* show a regular segmentation pattern in the dorsal fin with segment length being comparable to wild type. However, similarly to the *lof* mutant, segment number is considerably increased.

Figure 2.24 (preceding page): Segment length and segment number in heterozygous dorsal fin mutants compared to their siblings (+/+, sib). (A) Segment length in the longest ray of the adult dorsal fin (B) Segment number in the longest ray of the dorsal fin of adult. Mutants were compared to siblings of similar standard length (SL). Average SL in mm (N=4): *sgl*/sib 28.6/31; *fgg*/sib 23.9/25; *sllk*/sib 30.8/30.0; **: $p < 0.01$, ***: $p < 0.001$, n.s. not significant ($p > 0.02$).

2.2.3 Transplantation experiments suggest a local role for the *sllk* mutation

Although in the mutants *sgl*, *fgg* and *sllk* organ overgrowth is confined to the dorsal fin, it is still possible that the mutations causing these phenotypes act on a systemic level.

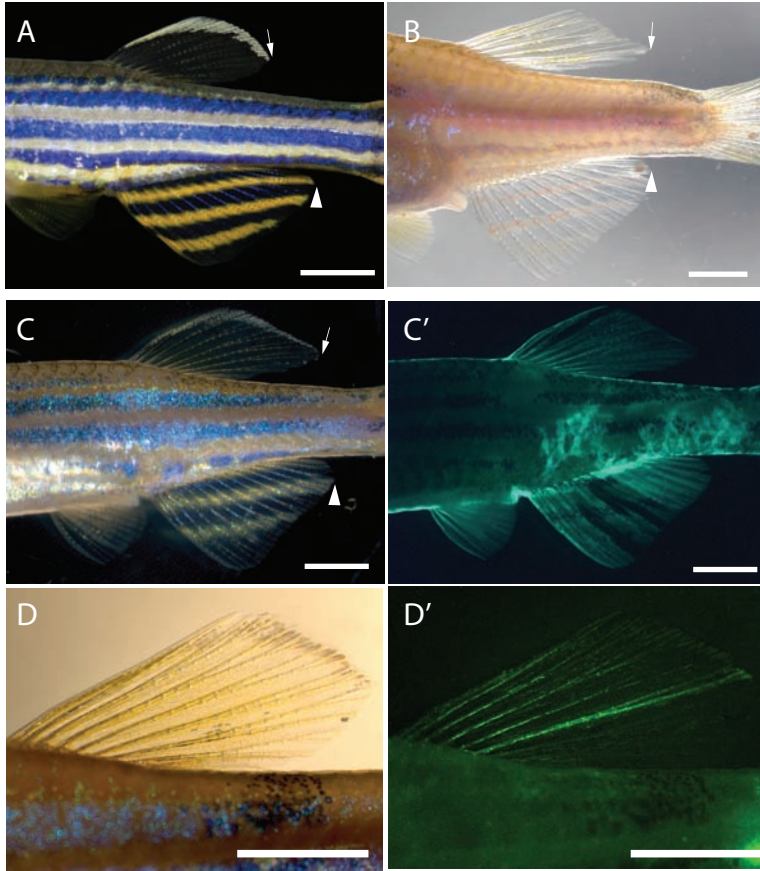
In order to find out whether these mutations act systemically or locally, blastula transplantation experiments with *sllk* mutants were performed, similarly to what was done for *pfau* (cf. Sec. 2.1.4). This particular mutant was chosen because homozygous individuals do not appear to have reduced fitness. Homozygous *sllk* fish were crossed to homozygous Tg(β -actin::GFP) fish and cells from the resulting embryos (*sllk*/+ ; Tg(β -actin::GFP)/+) were transplanted into *alb* hosts. Subsequently, these fish were raised to adulthood.

More than 200 chimaeric adult fish were screened for overgrowth in the dorsal fin. In total, five fish showed a complete or partial overgrowth phenotype (Fig. 2.25). In fact, in two animals, overgrowth was restricted to parts of the dorsal fin, supporting the hypothesis of a local role of the *sllk* mutation. In four cases out of five, donor derived GFP signal could be detected in various tissue types within the overgrown fin (Fig. 2.25, Tab. 2.3). The failure to detect GFP in one case could be explained with variegation of the Tg(β -actin::GFP), i.e inactivation of the transgene in some cells [Burket et al., 2008].

Although further analysis of more transplants will be needed to dissect the tissue type containing the overgrowth, these data favour the idea of a local role of the *sllk* mutation.

Table 2.3: GFP positive tissue types found in *sllk/alb* chimaeras

Donor derived tissue	No. of clones	Associated cases of dorsal fin overgrowth
pigment cells	36	4
muscle	21	3
caudal fin	7	-
dorsal fin	7	4
anal fin	2	1
pectoral fin	1	-
barbels	3	-
axial skeleton	5	-
skin	3	-
scales	2	1
neurons	3	-
brain/eyes	4	-
gills	2	-



2.2.4 A revertant of *sllk* shows a second mutation within *kcnh1a*

To confirm that the identified mutation in *kcnh1a* causes the phenotype of the dorsal fin mutants, a reversion screen was performed to identify compensatory mutations which revert the mutant phenotype to a wild type phenotypic outcome. A gain of function mutation, such as a hypermorphic (increased gene function), a neomorphic (novel gene function) or an antimorphic (dominant negative) mutation, can be reversed through a null mutation or a missense mutation that counteracts the effect of the original mutation.

Such an experiment was performed in *sllk* mutants, due to its increased fitness in respect to the other putative alleles. Homozygous *sllk* mutant males were mutagenised with ENU as described [Appendix B, Rohner et al., 2011] and subsequently outcrossed to *alb* females. As the *sllk* phenotype is dominant and the *alb* phenotype being recessive, the resulting progeny will show dorsal fin overgrowth and normal pigmentation. However, random mutations in spermatogonial cells during mutagenesis may disrupt the *sllk* or *alb* locus. If such event occurs, individual

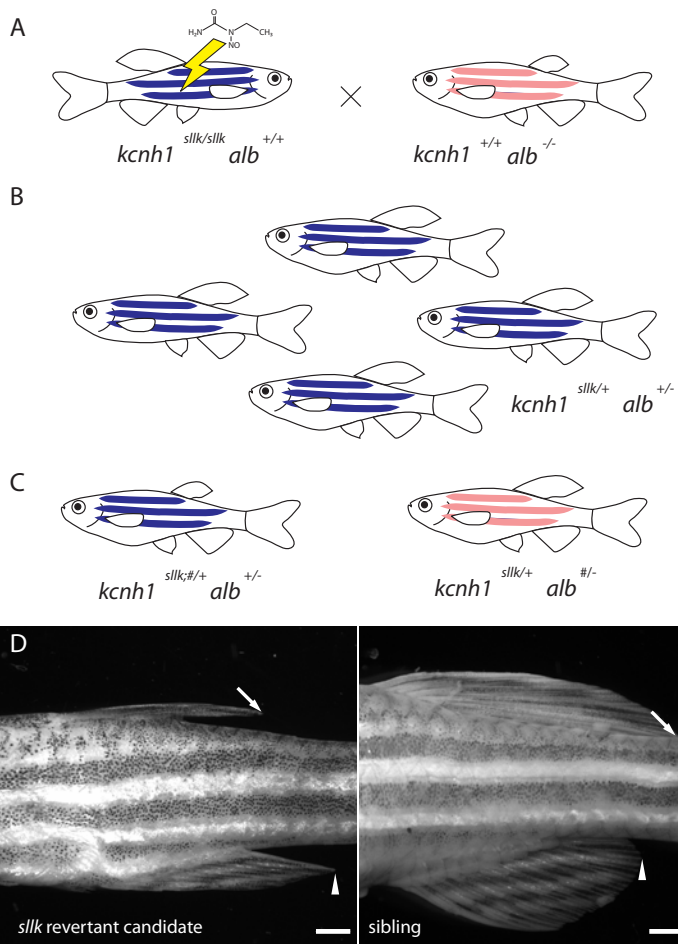
Figure 2.25 (preceding page): Chimaeras resulting from transplantation of *sllk*/+ cells into *alb* blastulas: (A) wild type dorsal fin. (B) Partial overgrowth and full overgrowth (C) in the dorsal fin of two chimaeras. Arrows indicate the tip of the dorsal fin, arrowheads point to the posterior part of the anal fin. In four cases out of five, overgrowth was associated with donor-derived GFP positive cells in the dorsal fin (C,C',D,D'). Scale bar = 2 mm.

F₁ fish are expected to show a normally sized dorsal fin and unpigmented melanophores, respectively (Fig. 2.26).

Interestingly, homozygous *sllk* mutants appeared to be particularly sensitive to the mutagenesis treatment, since mortality was much higher than in wild type T \ddot{U} fish (Tab. 2.4). Out of the six mutagenised *sllk* males that survived the ENU treatment, only one gave progeny. 70 fish were reared to adulthood. Among these, one showed a wild type dorsal fin (2.26, panel D), while another one had an *alb* phenotype, with overgrown dorsal fin (not shown). To exclude that the candidate revertant was a wild type fish that accidentally was introduced into the clutch, the fish was genotyped for the *sllk* mutation. As expected, the fish was heterozygous for the *kcnh1a*^{*sllk*} mutation. A second missense mutation was identified within the coding region of *kcnh1a*. It results in the substitution of a highly conserved valine (Val 335), located within the voltage sensor of the potassium channel, by a methionine (Met) (Fig. 2.27). Unfortunately, the

Table 2.4: Mutagenesis of *sllk* fish

	wild type (T \ddot{U})	homozygous <i>sllk</i>
initial amount of fish	28	28
survivors 1 st treatment	28 (100%)	20 (71%)
survivors 2 nd treatment	22 (78%)	12 (42%)
survivors 3 rd treatment	22 (78%)	10 (36%)
survivors 4 th treatment	20 (71%)	6 (21%)
survivors 5 th treatment	19 (68%)	N/A



potential revertant candidate died during the first mating attempt. An endeavour to perform *in vitro* fertilisation with the sperm of the animal failed. Therefore it was not possible to maintain the mutant and assess linkage analysis to confirm that the identified mutation is causative for the phenotype reversion. However, these findings support the idea that the mutation in the *kcnh1a* gene is responsible for the dorsal fin phenotype of the *sllk* mutant.

2.2.5 The mutations in *sgl*, *sllk* and *fgg* affect the TM domains of Kcnh1a

In order to assess which domains in Kcnh1a are affected by amino acid substitutions found in the dorsal fin mutants, HH-pred was used to construct a 3D model (cf. 2.1.7). The cyclic nucleotide-gated potassium channel MII3241 from the alphapro-

Figure 2.26 (preceding page): Reversion screen for *sllk*: Homozygous *sllk* mutant males were mutagenised with ENU and outcrossed to *alb* females (A). The offspring is expected to show a dorsal fin phenotype and display a wild type pigmentation (B). If the mutagenesis leads to a compensatory mutation in the *sllk* locus, individual fish of the clutch are expected to show a wild type dorsal fin. Likewise, if a deleterious mutation arises in the *alb* locus, single fish with elongated dorsal fin are expected to show unpigmented melanophores (C). A candidate revertant (D, left) was found among the progeny of a mutagenised male. The dorsal fin (arrow) reached only half of the length of the anal fin (arrowhead). In contrast, in siblings the dorsal fin showed the typical *sllk* overgrowth phenotype (D, right). Scale bar: 1 mm

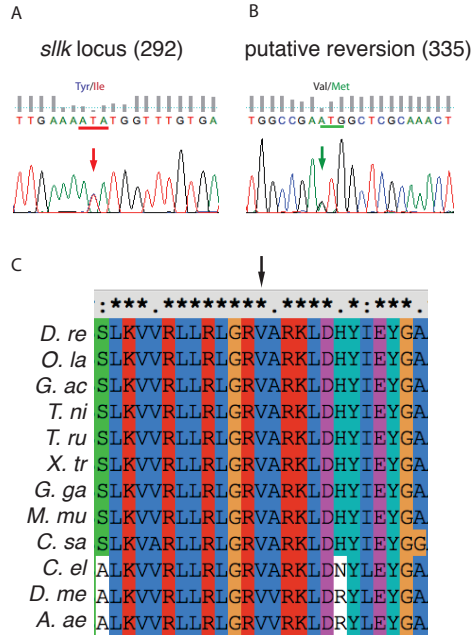
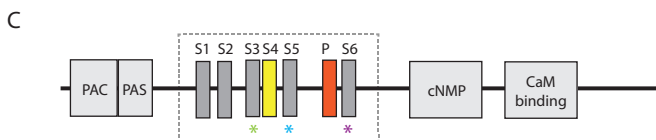
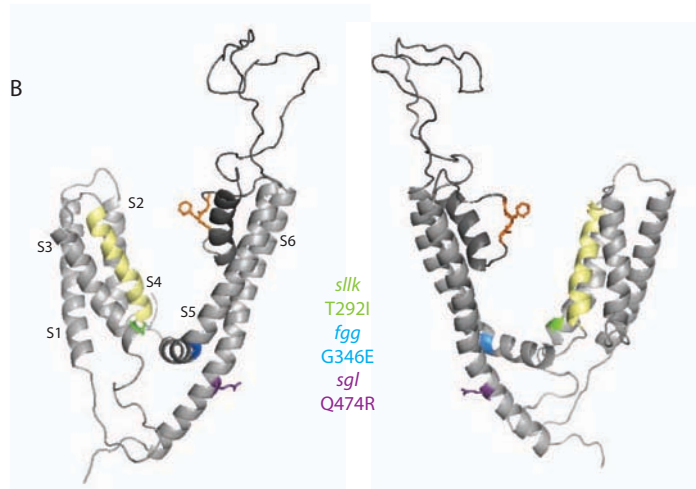
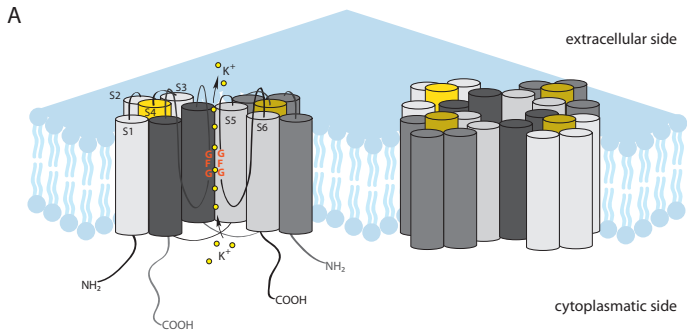


Figure 2.27: Potential revertant of *sllk* shows an amino acid substitution in *kcnh1a*. (A) Electropherogram of the *sllk* locus in the candidate revertant. The fact that the fish is heterozygous for the *sllk* mutation suggests that the isolated specimen was a revertant or a strong suppressor of *sllk*. (B) Mutation in *kcnh1a* that potentially reverts the effect of the *sllk* mutation. (C) The affected amino acid is highly conserved across metazoans.

teobacterium *Mesorhizobium loti* showed an identity of 19% and a similarity of 23.8% with zebrafish Kcnh1a (pdb 20th May 2012). This structure served as a template to predict the position of the altered residues in the Kcnh1a protein.

Kcnh1a is a voltage-dependent K⁺ (K_V) channel formed by four subunits. A channel subunit is composed of six TM domains (S1-S6) and one P-loop containing the selectivity filter with a Gly-Phe-Gly motif (Fig. 2.28 panel A). The core of the channel is formed by the fifth and sixth TM regions (S5 and S6), that are connected by the P-loop, while helix S4 acts as a voltage sensor. K_V channels are closed at resting V_m. However, upon depolarisation, they change conformation and open. The S4 helix contains several positively charged residues, that sense changes in V_m and cause activation of the channel [Jiang et al., 2003].

The amino acid changes identified in the dorsal fin mutants locate to the second third of the protein, where the transmembrane region of the channel is encoded (Fig. 2.28 panel C). This is reminiscent of the situation in *alf* and *pfau* and could potentially lead to changes in the electrophysiological properties of Kcnh1a. The substituted residues found in *fgg* and *sgl* are directly located in the TM domains that form the core of the channel, S5 and S6, respectively, while the change found in *slk* is in helix S3, which interacts with the voltage sensor (Fig. 2.28 panel B).

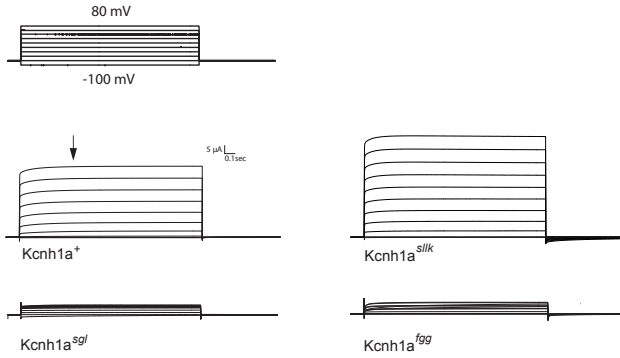


2.2.6 The electrophysiological properties of the mutant Kcnh1a variants are altered

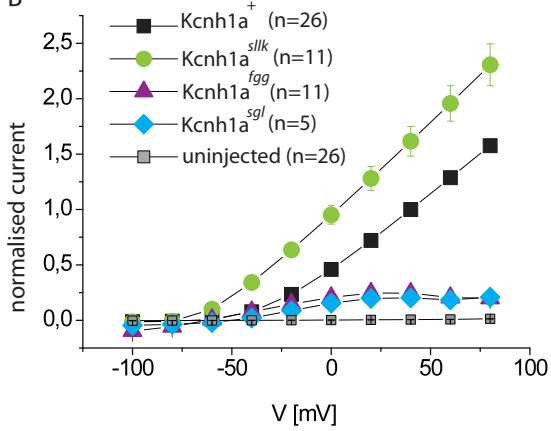
To assess if these amino acid substitutions affect the electrophysiological function of Kcnh1a, conductance was measured using the two-electrode voltage clamp approach (cf. Sec.2.1.8). *Xenopus* oocytes were measured three days after injection of 2 ng of *kcnh1a* mRNA using a holding potential of -60 mV. Higher amounts of *kcnh1a* seemed to have a lethal effect on the oocyte. Pulses from -100 to +80 mV were applied and the current was simultaneously recorded. It should be noted that the voltage step is applied for 2.15 s. This is in contrast to the measurements of *kcnk5b*, where the voltage step was applied for only 0.5 s (cf. Sec. 2.1.8). In Kcnh1a, the ion current reaches a plateau only after this time point. This delay in current flow reflects the necessity of the channel to switch from the closed

Figure 2.28 (preceding page): Modelling of Kcnh1a protein on the cyclic nucleotide-gated potassium channel Mll3241 from the alphaproteobacterium *Mesorhizobium loti*. (A) Left: K_V channels have 6 TM domains (S1-S6). The P-loop forms the selectivity filter of the channel containing a GFG motif. A second subunit is shown in dark grey. Right: Four subunits tetramerise to form a functional channel. (B) The identified amino acid substitutions of the dorsal fin overgrowth mutants all map to transmembrane domains of Kcnh1a: purple: *sgl*; blue: *fgg*; green: *sllk*; light grey: transmembrane domains; dark grey: pore forming unit, orange: selectivity pore within the pore forming unit, yellow: voltage sensor (S4). Picture shows two different views of the same monomer. (C) Only the content of the dashed box is illustrated in the 3D model (B), amino and carboxyl terminus are omitted.

A



B



conformation to an open conformation, as it is expected for a K_V channel.

The current to voltage (I-V) characteristic of Kcnh1a (Fig. 2.29) shows a linear dependency of the current on the voltage for the wild type channel at depolarised states. At hyperpolarised states the channel is in the closed conformation and hence is no longer permeable for K^+ ions. The *sllk* variant experiences a left shift and switches to the open conformation at relatively low voltage values. In contrast, the *sgl* variant displays a conspicuous reduction in K^+ conductance. Interestingly, a very similar situation is observed in the *fgg* variant.

Thus, while all three amino acid substitutions alter the properties of Kcnh1a, the *sgl* and *fgg* variants show a reduced channel conductance and the *sllk* variant increases K^+ flow. This apparent inconsistency will be discussed below (cf. Sec. 3.5.2).

Figure 2.29 (preceding page): Voltage clamp on *Xenopus* oocytes injected with cRNA encoding wild type and mutant Kcnh1a variants. (A) A series of voltage steps were delivered to the injected oocytes for 2.15 s. In Kcnh1a⁺ current flow is slightly delayed when the voltage is changed and reaches a plateau only after 0.5 s (arrow) because Kcnh1a has to switch to the open conformation before current can flow. Such delay is reduced in Kcnh1a^{sllk}. (B) Kcnh1a^{sllk} shows increased conductance and opens at lower V_m values compared to Kcnh1a⁺, whereas Kcnh1a^{sgl} and Kcnh1a^{fgg} have strongly reduced conductances. Black squares: wild type; green circles: *sllk*; blue diamonds: *sgl*, purple triangles: *fgg*; grey squares: uninjected oocytes. Current was normalised to the measurement of wild type current at 40 mV.

2.2.7 The gene *kcnh1a* might play a role in fin length variation of poecilid fish

The present work provides evidence that several fin overgrowth mutants appear to harbour mutations in genes involved in K^+ flux. This leads to the question whether K^+ channels also play a role in organ size modulation in natural populations. Within the *Poecilia* genus, the sailfin mollies are characterised by sexually dimorphic overgrowth of the dorsal fin (cf. Fig. 2.30), a phenotype that is reminiscent of the zebrafish dorsal fin overgrowth mutants. Each dorsal fin mutant identified so far bears a mutation in *kcnh1a*. The bias towards this gene suggests that *kcnh1a* in particular could be a preferred target for sexual selection to increase dorsal fin size. For this reason, the sequence of *kcnh1a* was examined in the sailfin molly *P. latipinna* and in its close relative, the short finned molly *P. sphenops*.

In the absence of a published poecilid genome sequence, degenerated primers designed on the *kcnh1a* sequence from *D. rerio* and *O. latipes* were used to amplify a stretch of 1.4 kb, covering most of the channel forming unit, from both *P. sphenops* and *P. latipinna* cDNA (4 individuals each). Comparison of the resulting partial Kcnh1a protein sequences revealed a variation in residue 396 between the two species. No other species specific amino acid changes could be identified in the sequenced region. The Thr 396 in the shortfin molly *P. sphenops* is substituted by an Ala in the longfinned *P. latipinna*. Interestingly, this position appears to be well conserved in other non-mammalian vertebrates, where either a Thr or a Ser is found, while in mouse this position is taken by a phosphomimetic amino acid (Fig. 2.31).

I hypothesised that if the amino acid substitution is important for the sailfin phenotype, a change in the same position should be found in the sailfinned molly *P. velifera*, the sister species of *P. latipinna*, but not in the shortfin *P. latipunctata*, which represents the outgroup of the two sailfin mollies. Indeed sequencing of these two species (4 individuals each) revealed a Tyr at this locus for the shortfinned *P. latipunctata* and an Ala for the sailfinned *P. velifera* (Fig. 2.31). To exclude the possibility that the *P. velifera* sample was contaminated with cDNA from *P. latipinna*, the cDNAs were compared for SNPs. A synonymous substitution specific for the *P. velifera* samples could be identified within the third base of the triplet encoding for Tyr 401 (cf. Tab. 4.6), confirming that the *P. velifera* and the *P. latipinna* sequences derived from independent cDNA samples.

To test whether the variation in the amino acid at position 396 has any effect on zebrafish *Kcnh1a*, a plasmid was generated via PCR mutagenesis, in which the codon for Ser 396 was mutated to produce an Ala. The cRNA transcribed from this plasmid as well as *kcnh1a*⁺ were injected into *Xenopus* oocytes and currents were recorded using two-electrode voltage clamp. No difference between *Kcnh1*⁺ and *Kcnh1*^{S396A} could be observed with this method (cf. Appendix C Fig. 4.6). However, *in vivo*, *Kcnh1* could require post-translational modifications, such as phosphorylation, that might not occur in the *Xenopus* oocyte, and therefore differences in the electrophysiological properties of the two channels might not be visible in this system. In fact, the mouse homologue carries an Asp in this position, which could mimic a phosphorylated Thr or Ser.

In conclusion, an amino acid substitution in a conserved residue

within *Kcnh1a* could be identified in the two sailfin species *P. velifera* and *P. latipinna* in respect to two closely related short-finned species. These findings open the possibility for a role of *Kcnh1a* in dorsal fin overgrowth observed in sailfin mollies. While these results are preliminary, it will be interesting to determine whether the sailfin *kcnh1a* induces dorsal fin overgrowth in zebrafish.

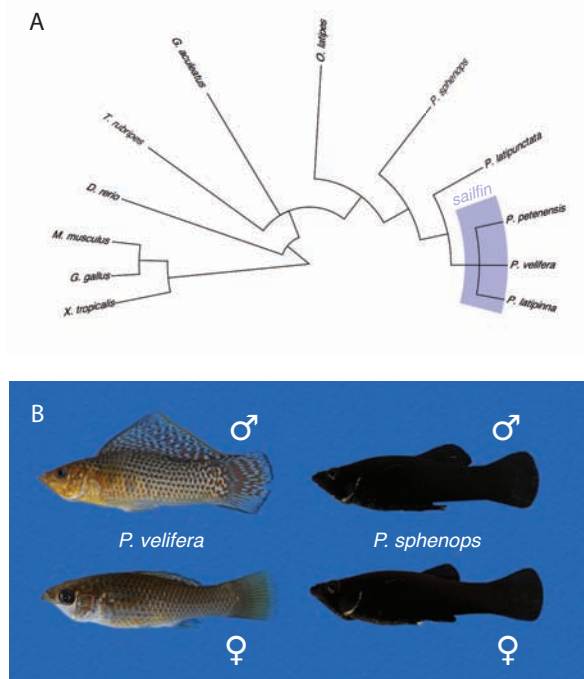


Figure 2.30: Sexually dimorphic growth of the dorsal fin in sailfin mollies. (A) Phylogenetic relationships among mollies. Adapted from Ptacek [1998]. (B) In *Poecilia velifera* males display overgrowth of the dorsal fin, however, the closely related *P. sphenops* does not show enlarged dorsal fin.

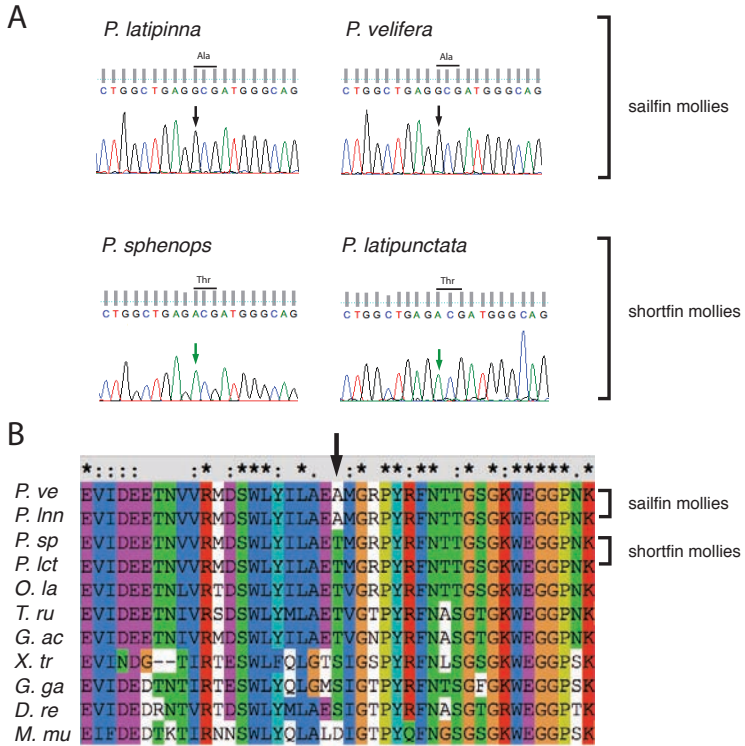


Figure 2.31: *kcnh1a* sequence from poeciliids. (A) Electropherograms show base pair variations found in the sailfinned (top) and shortfinned (bottom) poeciliid species resulting in a different amino acid. (B) With the exception of the sailfin mollies, a Ser or Thr is found at this position in all non-mammalian vertebrates, while mouse shows an Asp at this position.

CHAPTER 3

Discussion

Classical embryological manipulations in insect and amphibian models have taught us a lot about how organ size is determined [Twitty and Schwind, 1931; Fankhauser, 1952; Garcia-Bellido, 1965; Nijhout and Emlen, 1998]. However, the molecular mechanisms underlying growth control remain largely obscure. In an attempt to identify new genes involved in growth control, I took advantage of the zebrafish model system to study mutants showing aberrant growth of the fins. Multiple zebrafish mutants displaying adult-specific fin phenotypes have been isolated in the past three decades [Tresnake, 1981; van Eeden et al., 1996; Fisher et al., 2003; Goldsmith et al., 2003; Iovine et al., 2005]. Most of these show absent or reduced fins. The former might have defective instructive signals, like *fls* [Appendix A, Harris et al., 2008], while the latter are likely to be the result of secondary effects, like defects in bone growth as it is the case for *chi* mutants [Fisher et al., 2003]. In my doctoral studies I decided to focus on mutants that show an increase in fin size, with the aim to identify genes that directly contribute to growth control.

3.1 Changes in K⁺ channel activity underlie the phenotype of several fin overgrowth mutants

In the present study, I characterised several fin overgrowth mutants that display either generalised overgrowth of fins and barbels or overgrowth restricted to the dorsal fin.

The first group comprises the mutants *alf* and *pfau*, which display very similar phenotypes. Mutant fish have elongated maxillary and nasal barbels and show overgrowth in all, paired and unpaired fins (Fig. 2.1). Both mutations act dominantly and homozygous individuals are particularly susceptible to fin breakage. Within fin rays, segment length (Fig. 2.7) [Sims et al., 2009], but not segment number (Fig. 2.5), is increased in these mutants. Such an increase in segment size is observed as soon as the first segments are formed (Fig. 2.7 and not shown). Occasionally, in both *alf* and *pfau* mutants very short segments are found (Fig. 2.6), which might be due to mismatching joint formation in the two hemisegments of the fin ray [Murciano et al., 2007].

I show that the mutants *alf* and *pfau* are defective in the K⁺ channel *kcnk5b*. Several lines of evidence support this conclusion: (i) Positional cloning indicates strong linkage of the *alf* and *pfau* mutations to *kcnk5b* (Fig. 2.2) and (ii) both mutants harbour a missense mutation in this gene (Fig. 2.3). (iii) The affected residues are highly conserved within vertebrates (Fig. 2.4) and (iv) occupy a similar position within the transmembrane (TM) region of the channel (Fig. 2.16). Moreover, (v) the two

mutant variants of the channel show a very similar behaviour in electrophysiological assays (Fig. 2.17). Finally, (vi) misexpression of *Kcnk5b^{pfau}* in wild type fish mimics the mutant phenotype (Fig. 2.13). In accordance to these findings, γ -ray induced disruption of *kcnk5b^{alf}* reverts the phenotype of *alf* fish to wild type sized fins and barbels [Johnson, unpublished data].

The second group of mutants analysed includes *sgl*, *sllk* and *fgg*. These mutants are affected in the dorsal fin only (Fig. 2.19). The mutations act dominantly and homozygous individuals are virtually indistinguishable from heterozygous fish. Similarly to the *lof* mutant, they show an increase in fin ray segment number (Fig. 2.24), while segment length is not significantly increased. Results of my work indicate that these mutants are defective in the K^+ channel *kcnh1a*: (i) Mapping of *sgl* and *sllk* shows that these mutations are linked to *kcnh1a* (Fig. 2.20). (ii) All three mutants show amino acid substitutions in this gene (Fig. 2.21). (iii) The affected amino acids locate to TM regions in the channel and are highly conserved across metazoans (Fig. 2.28, Fig. 2.22). Furthermore, (iv) the electrophysiological properties are altered in the mutant variants of the channel (Fig. 2.29). Lastly, (v) a potential revertant of *sllk*, shows an additional missense mutation affecting a conserved amino acid within *kcnh1a* (Fig. 2.27). Altogether, these data provide strong indications that improper function of *Kcnh1a* leads to the phenotype of *sgl*, *sllk* and *fgg*. Consistent with this idea, the mutant *mohawk* (*mhk*), which also shows elongated dorsal fins, maps to *kcnh1a* and carries a missense mutation in this gene [Johnson, unpublished data].

Interestingly, the *lof* mutant maps to another K^+ channel on chromosome 2, *kcnh2a* [Johnson and Harris, personal commu-

nication] and two independent *lof* revertants show a nonsense mutation in *kcnh2a* [Harris, unpublished data], strongly indicating that this gene is responsible for the *lof* phenotype. Moreover, the mutant *schleierschwanz* (*szz*), which displays a similar phenotype to *kcnk5b* mutants, appears to be mutated in a K^+/Cl^- co-transporter [Harris, unpublished data]. Moreover, the mutant *sof*, which is characterised by fins decreased in size, is defective in *connexin43* (*cx43*) [Iovine et al., 2005], a gene that mediates electrical coupling between cells through formation of gap junctions.

In summary, numerous mutants altered in fin size, which were isolated independently, appear to be defective in molecules regulating ion flow (Tab. 3.1), indicating that ion homeostasis might play an important role in size determination of the zebrafish fin.

3.2 K^+ channels can intrinsically determine fin size

Transplantation and misexpression experiments show that cells expressing $Kcnk5b^{pfau}$ induce local fin overgrowth (Fig. 2.9, Fig. 2.13). Lepidotrichial segments are elongated in proximity of *pfau* mutant cells, supporting a paracrine or cell autonomous mode of action within the fin. Consistently, *kcnk5b* mRNA can be detected in uncut fins as well as regenerative fin blastema via RT-PCR (not shown). It is unclear, if such local mode of action also applies to *kcnh1a* mutants. Scoring for overgrowth in *sllk/alb* transplantations resulted being challenging, since, if *kcnh1a* act

Table 3.1: Fin mutants affecting ion homeostasis

Gene	Protein	Function (GO term)	Phenotype	Effect on segments	Mutant(s)	Reference
<i>kenk5b</i>	K _{2p} channel, subfamily K, member 5b	channel	enlarged fins, barbels	longer	<i>alf</i> , <i>pfau</i>	this work;
<i>kenh1a</i>	K _V channel, subfamily H, member 1a	channel	enlarged dorsal fin	more	<i>sgl</i> , <i>slk</i> , <i>f9g</i> , <i>mhk</i>	this work; Johnson [unpublished];
<i>kenh2a</i>	K _V channel, subfamily H, member 2a	channel	enlarged fins	more	<i>lof</i>	Harris, Johnson [unpublished];
<i>kcc4</i>	K ⁺ /Cl ⁻ cotransp. 4	transporter	enlarged fins, barbels	longer	<i>ssz</i>	Harris [unpublished];
<i>cx43</i>	Connexin 43	gap junction	reduced fins	shorter	<i>sof</i>	Iovine et al. [2005];

in an organ autonomous fashion, only *sllk* clones present in the dorsal fin, but not clones present in other fins, would presumably lead to local overgrowth. Also, the *sllk* phenotype is more subtle, as it does not lead to an increase in segment size and overgrown fin patches in the dorsal fin cannot be compared to contralateral fins or to dorsal and ventral fin lobes. Although a higher number of chimaeras is still required, preliminary results presented here suggest that *kcnh1a* can act locally in the dorsal fin (Fig. 2.25). These findings indicate that K^+ channels have an intrinsic role in fin overgrowth of these mutants.

3.3 Tissues involved in the overgrowth phenotype of *kcnk5b* mutants

While transplantations and misexpression experiments show that *kcnk5b* acts locally in the fin, it is not clear in which tissue this gene is expressed. In transplants of *pfau* cells labelled with Tg(β -*actin1*:GFP), overgrowth was mostly associated with GFP-positive vascular clones and to a lower extent with labelled intraray glia (Fig. 2.12 and Tab. 2.1). However, in four cases local overgrowth was observed in the absence of GFP fluorescence. The most likely cause of this discrepancy is variegation of the β -*actin1* promoter in fin tissues [Burket et al., 2008]. Consequently, the cells responsible for the overgrowth phenotype might not express the transgene. This prevented the conclusion that the expression of $Kcnk5b^{pfau}$ in the vasculature is responsible for the overgrowth phenotype.

Surprisingly, in *Kcnk5b^{pfau}* expressing clones marked in parallel by red fluorescence, overgrown fin parts were never associated with fluorescent signal in the vasculature, despite the fact that the *ef1a* promoter used in these experiments activated expression of the *kcnk5b^{pfau}* transgene in vascular tissues (cf. Fig. 4.4 D, Appendix C). This indicates that *Kcnk5b^{pfau}* action in vasculature may not be responsible for the overgrowth phenotype. In fact, the misexpression experiments rather point towards fibroblasts as the causative cell type. Among the 24 fish with fin overgrowth, 22 showed a correlation with fluorescent labelling of fibroblasts. In the two remaining cases, no fluorescence was observed in concomitance with overgrown fin parts. It is conceivable that in these two cases integration into the genome occurred concomitantly with a disruption of the fluorescent protein CDS or that reporter expression was prevented due to recombination between the two *ef1a* promoters residing in the transgene. These findings suggest that *Kcnk5b^{pfau}* expression within fibroblasts is sufficient to cause fin outgrowth. However, whether *kcnk5b* is expressed endogenously in fibroblasts, remains to be determined.

An alternative approach to analyse *kcnk5b* gene activity consists in the detection of its transcripts by RNA *in situ* hybridisation. Numerous attempts were made to detect the *kcnk5b* transcripts in embryos as well as adult fins. Several different probes and protocols were employed, however specific signals were never detected, although the transcript could be amplified via RT-PCR from adult tissue. An effort in detecting *kcnk5b* expression through a Gal4/UAS:GFP reporter line, using the 6.7 kb upstream sequence of *kcnk5b* as promoter, showed expression of GFP protein in the caudal fin primordium at 48

hpf (cf. Fig. 4.7) and in the notochord at 5 dpf (not shown). However, in adult fins, no expression was detected. It remains unclear whether the upstream sequence used in this plasmid might not be sufficient to faithfully report endogenous *kcnk5b* expression, since downstream sequences, such as introns, often carry important enhancer elements [Müller et al., 1999; Prasad et al., 2011; Sundström et al., 2012]. Therefore, following the protocol of Bussmann and Schulte-Merker [2011], a bacterial artificial chromosome (BAC) containing the *kcnk5b* locus in a larger genomic context (200 kb) was engineered by substituting the first exon of *kcnk5b* with a cassette containing the yeast transcriptional activator Gal4. This driver construct might turn out to be useful not only to detect the expression pattern of *kcnk5b* in the fin, but could also be employed to dissect the role of membrane potential (V_m) in fin growth by expressing various channels or ion pumps under the control of a UAS sequence. At the time of writing the results of this experiment were still pending.

In summary, it is not clear, which tissue is responsible for the overgrowth phenotype in *alf* and *pfau*, although misexpression experiments indicate that fibroblasts might be important in this process. Further studies on endogenous gene expression are necessary to confirm the nature of the tissue inducing overgrowth in *kcnk5b* mutants.

3.4 Fin growth and ray segment formation

Lepidotrichia are of segmented nature [Becerra et al., 1983] and formation of such segments has been proposed to be linked to

fin growth [Sims et al., 2009]. In fact, the *kcnk5b* mutants (*alf* and *pfau*) show an increase in fin size that is accompanied by elongated segments (Fig. 2.7) [Sims et al., 2009]. Likewise, the *sof* mutant, is characterised by fins of reduced size and shorter ray segments [Iovine and Johnson, 2000; Iovine et al., 2005].

In *sof*, reduction in segment length is due to loss of function in *cx43* [Sims et al., 2009]. This gap junction protein has been proposed to promote the diffusion of a joint-inhibiting signal [Rolland-Lagan et al., 2012]. Interestingly, connexins are known to be voltage-dependent [Hervé and Derangeon, 2012] and the rat, chicken as well as *Xenopus* homologues of *cx43* are reported to decrease their conductance upon depolarisation [González et al., 2007]. Therefore, the hyperpolarising effect of mutant *kcnk5b* on V_m might activate Cx43 channels and thereby promote diffusion of the joint-inhibiting morphogen postulated by Rolland-Lagan et al. [2012]. Intriguingly, *cx43* transcripts were found to be increased in *alf* mutants and decreased in *sof* mutants [Sims et al., 2009], indicating a positive feedback regulation of *cx43* gene expression.

Connexins are relatively unselective and a joint-inhibiting morphogen could include numerous little solutes, like second messengers, amino acids, sugars or ions themselves. In fact, it is known from regenerative studies in planaria, that ionic currents mediated by gap junctions can provide positional information and determine patterning [Oviedo et al., 2010; Beane et al., 2011].

However, segment length does not seem to be crucial in determining fin size. In fact, *kcnh1a* (*sgl*, *sllk*, *fgg*) and *kcnh2a* (*lof*) mutants show elongated fins without considerably increasing segment size (Fig. 2.24, Fig. 2.7) [Iovine and Johnson, 2000].

Also, a mutation in *evx*, which completely abolishes the formation of segments, does not affect fin ray length of wild type or *lof* fish [Schulte et al., 2011]. These findings suggest that fin outgrowth is independent of segment formation.

3.5 Ion channels and growth control

How K^+ channels might regulate fin size itself remains unclear. Intrinsic effects on fin growth could, for example, include paracrine secretion of growth factors, reduction of apoptosis or promotion of cell proliferation. Although none of these hypotheses can be excluded *a priori* and need to be tested particularly for fin overgrowth in zebrafish, existing evidence supports the idea that numerous K^+ channels might play a role in cell proliferation.

3.5.1 Kcnk5b and the role of K^+ currents in cell proliferation

Electrophysiological assays (cf. Fig. 2.17) showed that mutant forms of Kcnk5b have increased conductance compared to the wild type channel and lead to hyperpolarisation of *Xenopus* oocytes (cf. Fig. 2.18). Interestingly, hyperpolarisation has been reported to be associated with cell proliferation. Vascular endothelial growth factor (VEGF) is known to promote proliferation of endothelial cells *in vitro* and angiogenesis *in vivo* via intracellular Ca^{2+} increase and nitric oxide (NO) synthesis. This process has been proposed to be mediated by hyperpolar-

isation of the cell as mitosis can be inhibited by the K^+ channel blocker margatoxin [Erdogan et al., 2005].

In *ex vivo* cultures of Schwann cells from leporine sciatic nerve, proliferation is accompanied by an increased K^+ current and a progressive hyperpolarisation of V_m [Chiu and Wilson, 1989]. In these experiments, proliferation was inhibited by culturing cells in depolarising culture media or administration of K^+ channel blockers such as quinine, tetraethylammonium (TEA) and 4-aminopyridine (4-AP). Interestingly, treatment with TEA, but not with quinine or 4-AP, had a weaker effect on proliferation than on current inhibition. Remarkably, K_{2P} channels, such as *Kcnk5b*, are relatively insensitive to TEA [Richter et al., 2004; Clark et al., 2011]. The strong reduction in conductance observed with TEA, might therefore be due to preferential blocking of other types of K^+ channels, while the anti-proliferative effect is only visible when TEA reaches concentrations sufficient to target K_{2P} channels. This raises the question whether K_{2P} channels are particularly prone to promote cell proliferation and whether this property is connected to their K^+ conducting function.

Depletion of *KCNK5* was shown to decrease oestrogen-induced proliferation of two breast cancer cell lines [Alvarez-Baron et al., 2011]. Growth of human breast tumour requires oestrogen stimulation via oestrogen receptor α ($ER\alpha$). The enhancer region of *KCNK5* shows oestrogen-responsive elements; stimulation of $ER\alpha$ signalling increases *KCNK5* at the transcript and protein level and is accompanied by enlarged K^+ currents. In another study, several K_{2P} channels (*KCNK5*, *KCNK16* and *KCNK17*) were found to be associated with human cancer with *KCNK5* being upregulated in more than half of the 23 cancer cell lines

analysed [Santarius et al., 2010]. KCNK9 (TASK3) has also been reported to play a role in cancer as it is frequently upregulated in breast, lung, colon, and metastatic prostate cancers [Mu et al., 2003]. Importantly, cells expressing the wild type but not a dominant negative version (G95E) of this channel induces tumour formation in nude mice [Pei et al., 2003]. Overexpression of KCNK2 (TREK1), a K_{2P} channel whose expression is correlated with prostate cancer, increases proliferation of normal prostate epithelial cells (NPE) and Chinese hamster ovary (CHO) cells. A dominant negative form of KCNK2 bearing two mutations in the selectivity filter (G161E; G268E) inhibits proliferation of PC3 cells, a prostate cancer cell line that endogenously expresses the channel [Voloshyna et al., 2008].

Taken together these data indicate that K_{2P} channel overexpression and/or dysregulation play a role in uncontrolled growth of tumourigenic tissue. The present work provides first evidence that changes in the activity of K^+ channels are sufficient to modify organ size during development, since expression of $Kcnk5^{pfau}$ in wild type fins phenocopies the fin overgrowth of *pfau* mutants. This overgrowth may be due to cell autonomous stimulation of proliferation, since the mutation acts locally in the fin, fin overgrowth is accompanied by the presence of $Kcnk5^{pfau}$ expressing cells and numerous K^+ channels have been implicated in proliferation. The effect of mutant $Kcnk5b$ is probably mediated by hyperpolarisation of the cell as a result of increased conductance. The necessity of K^+ permeation for promoting the overgrowth phenotype will be tested by expression of a non-conducting version of the channel (cf. Appendix C, Fig. 4.5), carrying a mutagenised P2 selectivity filter. If ion conductance is required to promote overgrowth, no overgrowth

should be observed with such non-conducting channel.

3.5.2 *Kcnh1* and its current-independent role in cell proliferation

Similarly to what was observed for *Kcnk5b*, protein structure models of *Kcnh1a* revealed that the amino acids affected in the *sgl*, *sllk* and *fgg* variants locate within the TM domains of the channel. While all three variants altered the properties of the channel, the effect of *Kcnh1a^{sllk}* on ion current was opposite to what was observed for *Kcnh1a^{sgl}* and *Kcnh1a^{fgg}* (cf. Fig. 2.29). These results suggest that K^+ permeation *per se* is not responsible for the overgrowth phenotype of the dorsal fin mutants.

Interestingly, a similar current-voltage characteristic to *Kcnh1a^{fgg}* and *Kcnh1a^{sgl}* is observed in rat KCNH1 after progesterone treatment [Brüggemann et al., 1997] (Fig. 3.1). This hormone promotes maturation of *Xenopus* oocytes, as it causes release of the cell from arrest in G_2 phase and thereby enables completion of meiosis. Its action is mediated by mitosis-promoting factor (MPF), a complex of CDK1 and Cyclin B. Brüggemann et al. [1997] showed that progesterone application or MPF injection into oocytes changes the conducting properties of murine KCNH1. Before MPF activation, the current-voltage relationship is almost linear at depolarised potentials, similar to what was observed for wild type *Kcnh1a* (cf. Fig. 2.29, panel B black squares). With activation of MPF, K^+ current experiences inward rectification, i.e. outward current is strongly reduced. This resembles the current-voltage characteristic of *Kcnh1a^{fgg}*

and *Kcnh1a^{sgl}*. The MPF-induced rectification of K^+ current was specific to this channel and was not observed for other K^+ channels like KCNA4 or the *Shaker* H4 channel from *D. melanogaster*. This suggests that cell cycle progression can lead to post-transcriptional modifications of KCNH1.

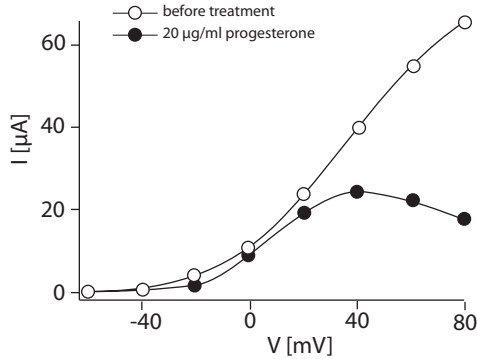
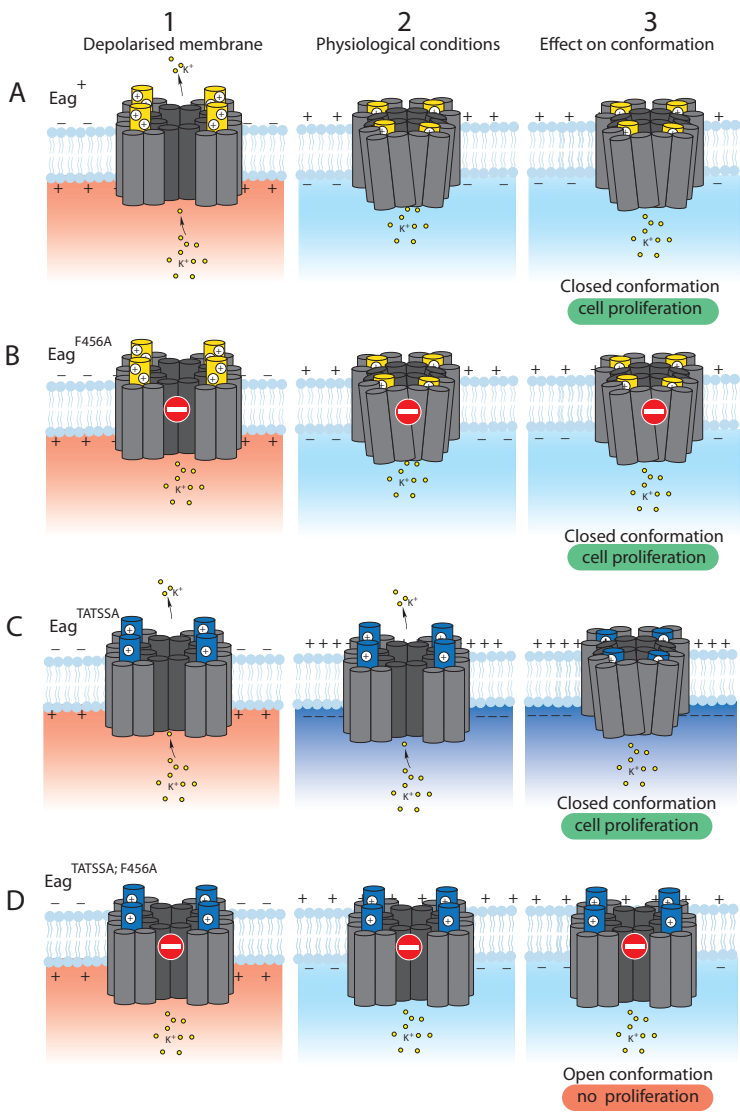


Figure 3.1: Current–voltage relationships of rat KCNH1 obtained from the same oocyte before (open circles) and after (filled circles) treatment with 20 $\mu\text{g}/\text{ml}$ progesterone. Adapted from Brüggemann et al. [1997]

As a K_V channel, *Kcnh1a* channels assume an open conformation at depolarised states and a closed conformation at hyperpolarised states [Stengel et al., 2012]. Intriguingly, the *Drosophila* homologue of *Kcnh1a*, *Eag* has been reported to induce proliferation in cell culture, depending on the conformational status [Hegle et al., 2006]. Surprisingly, this effect is independent of K^+ permeation, as both wild type Eag^+ and the non-conducting

Eag^{F456A} stimulate proliferation of NIH 3T3 fibroblasts cultured in serum free media. By employing a mutant channel that switches to the open conformation even with hyperpolarised V_m but is unable to conduct K^+ ions, the authors showed that proliferation is regulated by the position of the voltage sensor (see Fig. 3.2 for details).

Human KCNH1 has also been shown to stimulate proliferation independently from its ion-conducting function. Allografts of NIH 3T3 cells transfected with a non-conducting mutant of KCNH1 still induce tumours in severe combined immunodeficient (SCID) mice [Downie et al., 2008]. This finding seemingly contrasts with the observation that blockade of KCNH1 via the K^+ channel inhibitor astemizole also reduces tumour size. However, astemizole locks KCNH1 in the open, non-proliferative conformation [Downie et al., 2008], thus inhibiting a conformation-induced proliferative response. The findings presented above support the view that *Kcnh1a* channel can promote overgrowth independently of its K^+ conducting function. The current-voltage relationship of *Kcnh1a*^{*sgl*} and *Kcnh1a*^{*fgg*} closely resembles the curve of rat KCNH1 upon MPF treatment. Therefore, the *sgl* and *fgg* mutations could mimic the effect of a mitogen on wild type *Kcnh1a* and would therefore transduce a proliferative signal. On the other hand, *Kcnh1a*^{*sllk*} shows increased conductance in respect to wild type (cf. Fig. 2.29). This effect contrasts with what is observed in the *sgl* and *fgg* channels and resembles more the hyperpolarising behaviour of *Kcnk5b*^{*alf*} and *Kcnk5b*^{*pfau*}. Therefore *sllk* might act in a similar way as *pfau* and *alf*. Moreover, since *Kcnh1a* is voltage-dependent, such hyperpolarisation might in turn promote the closed conformation of the channel and hence induce



proliferation.

Further *in vitro* and *in vivo* studies are required to resolve the difference between these allelic variants of *Kcnh1a*. However, the commonality of their effect on dorsal fin growth versus their different electrophysiological behaviour would favour a model in which channel conformation and not ion conductance induces a proliferative response.

Figure 3.2 (preceding page): The *Drosophila* homologue of *Kcnh1a*, *Eag*, was shown to induce cell proliferation of fibroblasts depending on the channel conformation, but not on K^+ permeation [Hegle et al., 2006]. (A) Eag^+ is open at depolarised states of the membrane (1A) and causes K^+ outflow. Under physiological conditions, with a negative V_m (2A) the voltage sensor (in yellow) causes the channel to close (3A). (B) The same behaviour is observed in the non conducting mutant, Eag^{F456A} . (C) The mutant Eag^{TATSSA} is affected in the voltage sensor (in blue), which makes this channel less sensitive to negative V_m . This channel conducts K^+ currents at depolarised states (1C) as well as at polarised states (2C). Since the channel conducts also under physiological conditions, K^+ outflow will cause hyperpolarisation (V_m will become even more negative) and Eag^{TATSSA} will eventually switch to the closed conformation (3C). When these two mutations are combined (D), the channel will not be permeable to K^+ ions (1D), but will still show low sensitivity to negative V_m (2D). Therefore under physiological conditions, this channel stays in the open conformation (3D). Only when *Eag* is in the closed conformation (3A-C) (note the position of the voltage sensor) it is able to stimulate cell proliferation. Change in conformation might be crucial to allow interactions with other macromolecules that transduce a proliferative signal. Indeed, *Eag* was shown to bind and activate CaMK II [Sun et al., 2004] via its carboxyl terminus.

3.5.3 K⁺ channels and growth: possible mechanisms

Several growth factors and mitogens, such as IGF-1, oestrogen and prolactin are known to promote K⁺ currents [Van Coppenolle et al., 2004; Borowiec et al., 2007; Alvarez-Baron et al., 2011]. This process is dependent on protein kinase activity [Van Coppenolle et al., 2004; Borowiec et al., 2007]. Conductance of human KCNK5, for example, was shown to be modulated by tyrosine phosphorylation of the channel [Kirkegaard et al., 2010]. Growth factors are also reported to promote *de novo* transcription of human *KCNK5* and *KCNH1* [Borowiec et al., 2007; Alvarez-Baron et al., 2011]. Additionally, *KCNH1* has recently been reported to promote expression of the G₁/S phase cyclins cycD1 and cycE in MCF-7 cells [Borowiec et al., 2011]. As discussed, numerous studies suggest that K⁺ channels are actively involved in cell proliferation. Therefore, gain of function mutations in genes encoding for K⁺ channels, such as those described in this work, could mimic the modulation of channels by growth factors and mitogens and, hence, induce cell cycle progression. By which means K⁺ channels stimulate mitosis is yet unclear, however several scenarios can be envisioned.

Hyperpolarisation

The primary role of K⁺ channels is regulation of transmembrane potential (V_m). V_m and K⁺ conductivity are known to be modulated during cell cycle progression [Cone, 1969; Bregestovski et al., 1992], with cells arrested in G₀/G₁ showing a relatively depolarised state, and cells entering into S phase experiencing

hyperpolarisation [Orr et al., 1972; Canady et al., 1990; Wonderlin et al., 1995]. In contrast, the G₂/M phase transition is accompanied by depolarisation of the cell and reduced K⁺ conductance [Blackiston et al., 2009]. Such oscillation in V_m and K⁺ conductance was observed also during cleavage stage in early embryogenesis of the weather loach *Misgurnus fossilis* [Bregestovski et al., 1992].

Activation of K⁺ channels during cell cycle progression and the consequent hyperpolarisation of the cell could modulate the activity of voltage-dependent channels, such as voltage-dependent calcium (Ca²⁺) channels or connexins, and therefore directly or indirectly increase cytosolic Ca²⁺ concentrations [Nilius and Droogmans, 1994]. Ca²⁺ regulates a plethora of biological processes and many authors have proposed it as a regulator of cell cycle progression [Kahl and Means, 2003; Capiod, 2011]. In fact, blockers of Ca²⁺ channels have antiproliferative effect in several tissues [Taylor and Simpson, 1992; Haverstick et al., 2000] and Ca²⁺ is required in the extracellular environment and in intracellular compartments for growth and proliferation of many cell types. Increases in cytosolic Ca²⁺ can directly affect protein behaviour, as in the case of Ca²⁺-dependent K⁺ channels (K_{Ca}), or can be transduced by intracellular Ca²⁺ receptors such as calmodulin (CaM). CaM in turn controls many intracellular targets like CaM-dependent protein kinase (CaMK), the phosphatase calcineurin and endothelial NO synthase (eNOS) and is required for cell cycle progression through the restriction point via hyperphosphorylation of Retinoblastoma-associated (Rb) protein [Kahl and Means, 2003; Whitaker, 2006].

Interestingly, blockade of K⁺ channels inhibits the rise of cytosolic

lic Ca^{2+} and proliferation of T lymphocytes [Lin et al., 1993]. In contrast, proliferation of tumour cells is independent of Ca^{2+} [Owen and Villereal, 1985], but still can be inhibited by K^+ channel blockers [Balk, 1971; Dubois and Rouzair-Dubois, 1993; Rouzair-Dubois and Dubois, 2004]. Therefore, while Ca^{2+} mediated effects on cell proliferation are one plausible mechanism, it is certainly not the only way by which K^+ channels can stimulate growth. Hyperpolarisation also increases the electrochemical gradient for Na^+ , which has been proposed as a mitogen by some authors [Kaplan and Owens, 1980; Dubois and Rouzair-Dubois, 1993; Klausen et al., 2010]. Moreover, a more negative V_m enhances the activity of various metabolite transporters such as the voltage-dependent Na^+ -amino acid co-transporter [Dubois and Rouzair-Dubois, 1993] and the voltage-dependent serotonin transporter [Blackiston et al., 2009].

Volume regulation

K^+ channels are notoriously involved in cell volume regulation [Hoffmann, 2011]. This is an active process that is essential for homeostasis, since cells undergo intense changes in cell volume as they grow, divide and migrate [Lang et al., 1998]. When a cell is exposed to a hypotonic solution, i.e. a solution low in osmolytes, it initially experiences swelling due to osmosis. Subsequently, it responds by releasing osmolytes into the extracellular environment through membrane transporters and channels [Deutsch et al., 1982]. This causes the efflux of H_2O and, hence, a reduction of cell volume. Such process is referred to as regulatory volume decrease (RVD), and is mainly due to

the action of K^+ and Cl^- channels. KCNK5 is known to account for RVD in Ehrlich ascites tumour cells [Niemeyer et al., 2001]. Moreover, KCNK5 overexpression in HEK293 cells accelerates RVD [Kirkegaard et al., 2010]. This process is accompanied by phosphorylation and activation of KCNK5, and can be inhibited by blocking the JAK/STAT pathway. In fact, changes in cell volume have also been reported to lead to activation of protein kinases of the MAPK pathway [Schliess et al., 1995; Szász et al., 1997].

Several studies suggest that cell volume regulation is linked to cell proliferation [Xu et al., 1996; Rouzaine-Dubois and Dubois, 1998; Rouzaine-Dubois et al., 2000; Di Giusto et al., 2012; Zhu et al., 2012]. Quiescent mouse L2 clone T-lymphocytes express low levels of K^+ channels and do not exhibit RVD. Interestingly, however, when L2 cells are induced to proliferate by administration of the cytokine interleukin 2 (IL-2), K^+ conductance increases and the ability to engage in RVD in response to hypotonicity is restored [Lee et al., 1988]. In a series of experiments on mammalian neuroblastoma cells it was observed that blockage of K^+ channels with TEA, 4-AP or caesium (Cs^+) ions increases cell volume and decreases cell proliferation in a dose-dependent manner [Rouzaine-Dubois and Dubois, 1998]. In the same study, this inverse relationship between cell proliferation and volume was shown also by inducing volume changes through osmotic challenges, blockage of Cl^- channels or use of antibiotic-free medium. Similarly, 4-AP blocking of K_V channels in human myeloblastic ML-1 cells induces a volume increase of 37% and arrests the cells in G_1 phase. Here, inhibition of the ion channels was accompanied by dephosphorylation of Rb protein, a crucial factor for entry into S phase. This effect

was specific for $G_{0/1}$ phase, since cell cycle progression of myeloblasts that were already past the restriction point was not affected by the K^+ channel blocker [Xu et al., 1996]. These findings suggest that volume decrease might play a role in cell cycle progression. Reduction of volume has been proposed to directly increase the concentration of cell cycle relevant factors, such as cyclins, CdKs and pRb [Dubois and Rouzair-Dubois, 1993; Nilius, 2001].

Protein-protein interactions

In the last years, evidence has been accumulating that K^+ channels can trigger cell proliferation independently of their function as ion-conducting molecules [Hegle et al., 2006; Downie et al., 2008; Millership et al., 2011; Ciudad et al., 2012]. In fact, in several cases, K^+ channels have mitogenic effects even if they are rendered non-conductive by mutating the selectivity pore. A conformational switch in the channel has been proposed to underlie activation of the MAPK pathway and proliferation of fibroblasts expressing Eag [Hegle et al., 2006] (cf. Sec. 3.5.2). Structural change has been proposed as activator of MAPK signalling also for the Ca^{2+} -dependent K^+ channel (K_{Ca}) KCNN4 (IK1) [Millership et al., 2011]. KCNN4 was shown to increase cell proliferation in HEK293 cells. This occurred independently of its ion conducting function, as was shown for the non-conducting mutant KCNN4^{GYGAAA} (G252A; Y253A; G254A), and even independently of its presence at the cell membrane, as observed in the trafficking mutant KCNN4^{LLAA} (L18A; L25A) [Miller-ship et al., 2011]. This suggests that ion channels might have additional functional properties besides ion conductance. The

transient receptor potential (TRP) cation channel TRPM7, for example, also displays kinase activity [Runnels et al., 2001] and is known to interact with phospholipase C (PLC). Moreover, the *Drosophila* Slowpoke binding protein (Slob), which interacts with the K_{Ca} channel Slowpoke (Slo, KCNMA family), acts as a kinase [Zeng et al., 2004]. It is possible that K^+ channels act as sensors for changes in V_m [Cidad et al., 2012] or cytosolic Ca^{2+} [Millership et al., 2011]. Conformational change could therefore be transduced to intracellular components via binding sites on the large amino and carboxyl terminal regions of these transmembrane proteins. In fact, Eag has been shown to bind and activate CaMKII upon local Ca^{2+} CaM exposure [Sun et al., 2004].

Whether the phenotype of the *kcnk5b* and *kcnh1a* mutants can be ascribed to a cell autonomous role of these channels in cell proliferation still needs to be confirmed experimentally. This hypothesis will be tested in cell culture, since this system allows not only to assess proliferative capability, but also cytosolic Ca^{2+} concentration and changes in cell volume. Another question that still remains open is how fin growth in the mutants is integrated to achieve an enlarged but correctly patterned organ with all its tissues rather than a lump of uncontrolled proliferating cells. K^+ channels such as *Kcnk5b* and *Kcnh1a* could indirectly affect patterning and positional information by acting on instructive signals in the developing fin, possibly through regulation of Cx43 (cf. Sec. 3.4). Intriguingly, Cx43 has been reported to control Fgf mediated limb outgrowth in the AER of chick [Makarenkova and Patel, 1999]. In this context, it will be interesting to see

whether K^+ channels regulate connexin activity to establish and maintain signalling centres such as the AER and ZPA.

3.6 Extrapolating the role of K^+ channels in fin growth to natural populations

In fishes, the development of enlarged fins has been proposed as a low cost strategy to increase apparent body size in aggressive interactions between males as well as to target female choice. Such a phenomenon is particularly apparent in several poeciliid species and is subject to sexual selection [Rosenthal and Evans, 1998; Gumm et al., 2009]. To date, the genes involved in these exaggerated phenotypes are not known.

In the present study, I analysed five zebrafish mutants with overgrown fins and provide evidence that they carry mutations in two K^+ channel encoding genes. Moreover, fin overgrowth mutants studied by others also appear to be affected in genes involved in K^+ homeostasis. The phenotype of the *lof* mutant can be reverted by a nonsense mutation in K^+ channel *kcnh2a* [Johnson and Harris, unpublished data] and *szz* bears a mutation in a gene coding for a K^+/Cl^- co-transporter [Harris, unpublished data]. Additionally, the dorsal fin overgrowth mutant *mhk* is altered in *kcnh1a*, the same gene defective in the dorsal fin mutants presented in this work. Therefore, K^+ channels in general, and *Kcnh1a* in particular, may play a role in dorsal fin size determination.

To test this hypothesis, *kcnh1a* was analysed in the sailfinned *P. latipinna* and *P. velifera* as well as in the shortfinned spe-

cies, *P. latipunctata* and *P. sphenops*. The longfinned species *P. latipinna* and *P. velifera* both show an Ala at position 396 of *kcnh1a*, in a residue that is conserved in other teleosts. Electrophysiological measurements employing the zebrafish *kcnh1a* harbouring the mutation S396A did not show any difference in conducting properties in comparison to the zebrafish wild type channel (cf. Fig. 4.6). However, *in vivo* this channel might be subject to posttranslational modifications. In fact, all the other vertebrate species analysed, showed either a phosphorylatable (Ser/Thr) or phosphomimetic residue (Asp) in this position. As was shown for KCNK5 [Kirkegaard et al., 2010] and proposed for KCNH1 [Borowiec et al., 2007], phosphorylation of *kcnh1a* might regulate channel activity. Further studies will be needed to assess if this is the case, and whether the sailfin variants of *kcnh1a* are able to induce dorsal fin overgrowth in zebrafish.

In the future it will be interesting to see if the numerous cases of enlarged fins found in natural populations of fishes, such as flying fish (*Exocoetidae*) and swordtails (*Xiphophorus* sp), also involve modulation of K^+ channels or other ion flow controlling proteins.

Materials & Methods

4.1 Fish maintenance

Zebrafish were bred and maintained as previously described [Nüsslein-Volhard and Dahm, 2002] at 28°C. Eggs were collected in E3 medium (5 mM NaCl, 0.17 mM KCl, 0.33 mM CaCl₂, 0.33 mM MgSO₄ in ddH₂O) containing 200 µg/l methylene blue (Merck, 1283) to avoid growth of mold.

4.2 Bleaching of fish eggs

In order to decrease the risk of spreading diseases, embryos to be raised to adulthood were treated with 360 µl/l of bleaching agent (12% NaClO, Carl Roth 9062.3) in tub water for 5 min, followed by a 5 min wash in tub water. This treatment was repeated for a second time. Bleaching was performed after completion of epiboly and before the chorion starts to dissolve

at 28 hpf. After bleaching, pronase from *Streptomyces griseus* (Roche, 70306722) was added to E3 medium at an approximate final concentration of 3.5 µg/ml in order to facilitate hatching.

4.3 Anaesthesia

Fish were anaesthetised in 1× tricaine solution diluted in fish water (30× stock tricaine solution: 0.5 % (w/v) Ethyl 3-aminobenzoate methanesulfonate salt (Sigma-Aldrich, A5040) 1% (w/v) Na₂HPO₄ in ddH₂O). A 4× solution was used to euthanise fish.

4.4 Measurements

Fish were euthanised in tricaine solution, fixed overnight in 4% PFA in PBS and gradually (25%, 50%, 75%, 100%) dehydrated in EtOH/PBS and stored in 100% EtOH until further processing. Fish were imaged under a stereo microscope (Zeiss, SteREO Discovery) and measurements were performed using AxioVision software (Zeiss).

4.5 Generation of *fgg* mutant fish and *sllk* revertant

For the *fgg* mutant, six month old TÜ wild type males were mutagenised six times at one week interval as described [Rohner

et al., 2011] (Appendix B). The fish were outcrossed to *alb* females. Progeny was reared to adulthood and screened for fin overgrowth phenotypes. For the *slk* revertant, homozygous *slk* males were identified by genotyping and treated as above. Progeny was screened for loss of *slk* phenotype.

4.6 DNA preparation

Fish were anaesthetised in tricaine solution (Sec. 4.3) and transferred to a piece of parafilm with a spoon. Caudal fin was removed with a sterile scalpel leaving a proximal stump of ca. 5 mm, so to allow the fin to regenerate. The amputated fin was immediately transferred to lysis buffer (100 mM Tris-HCl pH 8, 200 mM NaCl, 0.2% SDS, 5 mM EDTA pH 8) supplemented with 0.1 mg/ml proteinase K (Merck, 1245680500) and fish were promptly put back to regular fish water for recovery. Samples were incubated overnight at 55°C with vigorous shaking. The next day, proteinase K was inactivated through a 20 min incubation at 90°C. Then samples were put on ice and vortexed vigorously after addition of 800 µl of isopropanol (propan-2-ol). Samples were centrifuged at 4°C with 12000 g for 30 min, supernatant was discarded and tubes were briefly dried on bench paper. After adding 200 µl of 70% EtOH, samples were briefly vortexed and centrifuged for another 5 min. Supernatant was carefully removed and tubes were put at 55°C for 10 min to allow evaporation of the remaining ethanol. DNA was resuspended in H₂O and incubated for 30 minutes at 55°C shaking. DNA was diluted to a final concentration of 100 ng/µl.

4.7 Mapping

Mapping was performed as described in [Nüsslein-Volhard and Dahm, 2002]. Mutant fish in T \ddot{U} background were crossed to wild type WIK fish. Siblings of the F₁ progeny were incrossed, and F₂ progeny was sorted into mutant and sibling fish. For rough mapping bulk segregant analysis was used. Pooled DNA of 48 mutant individuals was diluted to 35 ng/ μ l and compared to the DNA of 48 non-mutant siblings using the standard G4 set primers [Geisler et al., 2007]. For single PCRs DNA was diluted to 10 ng/ μ l. The DNA was amplified with following conditions using eppgradient Mastercycler (Eppendorf):

Genomic DNA	10-35 ng/ μ l	5.0 μ l
PCR buffer (Genaxxon)	10 \times	2.0 μ l
MgCl ₂ (Genaxxon)	25 mM	2.0 μ l
Forward primer	10 μ M	0.5 μ l
Reverse primer	10 μ M	0.5 μ l
dNTPs (Fermentas)	10 mM each	0.4 μ l
<i>Taq</i> polymerase S (Genaxxon)	5U/ μ l	0.5 μ l
ddH ₂ O μ l		11.9 μ l
Total volumel		<u>20 μl</u>

10 \times PCR buffer (Genaxxon) contains: 100mM Tris-HCl (pH 9.0 at 25°C), 500mM KCl, 1.0 % Triton X-100. Amplification program:

94°C	30 s	initial denaturation
94°C	30 s	} 40 cycles
60°C	45 s	
73°C	60 s	

73°C 30 s final elongation

PCR amplicons were analysed via agarose gel electrophoresis (2% w/v) for co-segregation with the non-mutant phenotype in bulk segregant analysis as well as recombination in single DNA PCRs. For further mapping additional z-markers were retrieved from Ensembl Zv9 and VEGA47 zebrafish genome assembly databases.

4.8 Total RNA isolation

Fish were euthanised and tissue was removed with a clean scalpel. Tissue was placed in a clean tube with 500 µl Trizol[®] and subsequently homogenised with a nuclease-free pestle. Following 15 min incubation, 100µl chloroform were added. The probe was incubated for 15 min at RT and centrifuge with a table centrifuge for 15 min at 13000 rpm. The aqueous phase was collected to a fresh tube and precipitated with 250 µl isopropanol and incubation at -20°C for 10 min. The sample was then centrifuged for 30 min at 4°C at 13000 rpm, supernatant was discarded and pellet was washed with 500 µl EtOH 75% and centrifuged for another 5 min. Supernatant was carefully removed and sample was allowed to dry for 10-15 min at 65°C. 20 µl DEPC-H₂O (0.1% diethylpyrocarbonate, autoclaved) were added and pellet was solubilised at 65°C and subsequently verified through gel electrophoresis for smear-free rRNA bands and concentration was measured through spectrophotometry (NanoDrop).

4.9 cDNA synthesis

Following components were mixed:

Oligo(dT) [0.5 µg/ µl]	1 µl
Total RNA	1-5 µg
dNTP(Fermentas) [10 mM]	0.2 µl
DEPC-H ₂ O	q.s.
Total volume	<hr/> 12 µl

The mixture was heated to 65°C and quick chilled on ice. Subsequently following components were added:

5× First-Strand Buffer (Invitrogen)	4 µl
0.1 M DTT	2 µl
RiboLock RI (Fermentas)	1 µl
Total volume	<hr/> 19 µl

After mixing, the sample was incubated at 42°C for 2 min and 1 µl of SuperScript™ III (Invitrogen) was added and mixed by pipetting. After an incubation time of 2 h, the reaction was inactivated by heating for 15 min at 70°C and put on ice. Finally, 2.5 µl of *E. coli* RNase H [5U/µl] (Fermentas) were added to remove RNA from cDNA and diluted 5× prior to PCR reaction.

4.10 Cloning of *kcnk5b* and *kcnh1a* cDNA

LA *Taq* polymerase (TaKaRa) was used for amplifying full length cDNA of caudal fin blastema. CDS of *kcnk5b* and *kcnh1a* were amplified with following conditions:

gene	forward primer	reverse primer	annealing temp.	cycles
<i>kcnk5b</i>	OSP-379	OSP-382	60°C	45×
<i>kcnh1a</i>	OSP-128	OSP-129	63°C	35×
cDNA				1-5 μ l
Buffer (TaKaRa)			10×	5.0 μ l
MgCl ₂ (TaKaRa)			25 mM	5.0 μ l
Forward primer			10 μ M	1.5 μ l
Reverse primer			10 μ M	1.5 μ l
dNTPs (TaKaRa)		2.5 mM each		8 μ l
LA <i>Taq</i> polymerase (TaKaRa)			5U/ μ l	0.5 μ l
ddH ₂ O				q.s.
Total volume				<hr/> 50 μ l

Amplification program:

94°C 4 min initial denaturation

94°C	30 s	} 35-45 cycles
xx°C	30 s	
72°C	60 s/1 kb	

72°C 4 min final elongation

An aliquot of PCR product was run on 1% agarose gel to verify successful amplification. If gel electrophoresis showed a unique clean band, the remaining PCR product was directly processed for ligation (*vide infra*). In the case of multiple amplicons, DNA bands were excised and cleaned up with Wizard[®] SV Gel and PCR Clean-Up System according to the manufacturer's instructions. Briefly, excised band was dissolved with Membrane Binding Solution (1 µl/mg gel) at 65°C and transferred to a binding column. After 1 min incubation, the sample was centrifuged at maximum speed (16,000 g) in a table centrifuge for 1 min and flowthrough was discarded. Subsequently sample was washed through centrifugation with 700 µl Membrane Wash Solution for 1 min, followed by 500 µl for 5 min. The column was then dried through centrifugation for 2 min and placed to a clean tube. 30 µl ddH₂O were applied to the top of the column and incubated for 1 min. Finally, sample was centrifuged for 2 min to eluted DNA and then stored on ice. The PCR product was then ligated overnight at 4°C to the pGEM[®]-T Easy (Promega) vector:

PCR product	3.0 μ l
Buffer 2 \times	5.0 μ l
pGEM [®] -T Easy Vector [50 ng/ μ l]	1.0 μ l
T4 DNA Ligase (3 Weiss units/ μ l)	1.0 μ l
Total volume	<u>10.0 μl</u>

The sample was then processed for transformation (cf. Sec. 4.13). Clones positive to blue/white screen were verified by sequencing. *Kcnk5b* was subcloned to pSGEM through SacII and SpeI restriction sites. *Kcnh1a* was subcloned to pSGEM KS⁻ through EcoRI digestion. The destination vector was dephosphorylated with rAPid Alkaline Phosphatase (Roche) for at least 1h:

Vector DNA	<1 μ g
10 \times rAPid Alkaline Phosphatase buffer	2 μ l
rAPid Alkaline Phosphatase (1U/ μ l)	1 μ l
ddH ₂ O	<u>q.s.</u>
Total volume	10 μ l

Ligation reaction was performed for 10 min using Quick Ligation[™] Kit (NEB):

Vector DNA	50 ng
Insert (molar ratio vector:insert = 1:3)	x μ l
2 \times Quick Ligase buffer	10 μ l
Quick Ligase	1 μ l
ddH ₂ O	<u>q.s.</u>
Total volume	10 μ l

4.11 Cloning of *kcnh1a* cDNA from poecilids

Partial sequence of *P. latipinna kcnh1a* cDNA was amplified with LA *Taq* polymerase (TaKaRa) using degenerated primers OSP-137 and OSP-138 designed on zebrafish and medaka *kcnh1a*. The resulting sequence was used to design the poecilid specific primers OSP-151 and OSP-163.

4.12 Competent cells

One shot[®] TOP10 *E. coli* cells (F⁻ *mcrA* Δ (*mrr-hsdRMS-mcrBC*) Φ 80*lacZ* Δ M15 Δ *lac* X74 *recA1* *araD*139 Δ (*ara-leu*)7697 *galU galK rpsL* (Str^R) *endA1 nupG*) were purchased at Invitrogen, diluted 1:1,000 and 1:10,000, plated on LB plates w/o antibiotics and incubated overnight at 37°C. A single colony was inoculated in 6 ml LB overnight. The culture was diluted 1:100 with pre-warmed LB medium and grown to OD₆₀₀ = 0.5. Bacteria were aliquoted in 50 ml Falcon tubes, centrifuged at 3000 rpm for 15 min at 4°C and pellet was resuspended in ice-cold 16.5 ml RF1 buffer (100 mM RbCl, 30 mM KOAc, 10 mM CaCl₂ · 2 H₂O, 50 mM MnCl₂ · 4 H₂O, 15% glycerol (w/v), pH set to 5.8 with HCl, sterilised with 0,22 µm filter). After 1 h incubation, samples were centrifuged at 2500 rpm for 12 min at 4°C and resuspended in 4 ml RF2 (10 mM MOPS, 10 mM RbCl, 75 mM CaCl₂ · 2 H₂O 15% glycerol pH set to 6.8 with NaOH, sterilised with 0.22 µm filter). Bacteria were incubated

15 min on ice, quickly aliquoted in 50 μ l in pre-cooled tubes, shock frozen in liquid N₂ and stored at -80°C until used.

4.13 Transformation

Competent cells were thawed 5 min on ice. 1 μ l plasmid DNA was added, sample was gently resuspended and placed on ice for another 30 min. Cells were heat shocked for 45 s at 42°C and immediately placed on ice for 5 min. 250 μ l LB were added, bacteria were incubated on a thermoshaker (300 rpm) for 45 min at 37°, before plating on LB plates containing the appropriate antibiotic. For blue/white screening, 40 μ l x-gal (20 mg/ml in N-N dimethyl formamide) were plated to each dish.

4.14 Plasmid purification

Plasmids were purified using QIAprep Spin Miniprep Kit (Qia-
gen) or Quantum Prep™ Plasmid Midiprep Kit (Bio Rad) ac-
cording to manufacturer's instructions.

4.15 Digestions with restriction enzymes

Generally, for analytical restriction enzyme digestions following conditions were used:

DNA	0.5 µg
Appropriate buffer (NEB/Fermentas)	2 µl
BSA 100×(NEB)	0.2 µl
Restriction enzyme (NEB/Fermentas)	5U/µg DNA
ddH ₂ O	q.s.
Total volume	<hr/> 20 µl

For preparative digestions following conditions were used:

DNA	5-10 µg
Appropriate buffer (NEB/Fermentas)	10 µl
BSA 100×(NEB)	1 µl
Restriction enzyme (NEB/Fermentas)	5U/µg DNA
ddH ₂ O	q.s.
Total volume	<hr/> 100 µl

4.16 Sequencing

DNA sequence was determined by taking advantage of the sequencing facility of the Max Planck Institute for Developmental Biology. Following conditions were used to set up the sequencing reaction:

BigDye Terminator (Applied Biosystems)	0.75 µl
Sequencing buffer	1.90 µl
Sequencing primer [10µM]	1.90 µl
DNA [100 ng/µl]	1.90 µl
ddH ₂ O q.s. to 10 µl	5.85 µl

The sequencing buffer contains: 350 mM Tris HCl pH 9, 2.5 mM MgCl₂.

4.17 Genotyping

DNA was isolated from caudal fins (cf. Sec. 4.6) and amplified with following primer pairs:

locus	forward primer	reverse primer
<i>alf</i>	OSP-377	OSP-378
<i>pfau</i>	OSP-57	OSP-58
<i>sgl</i>	OSP-21	OSP-22
<i>sllk</i>	OSP-105	OSP-106
<i>fgg</i>	OSP-175	OSP-176

Genomic DNA		100 ng
PCR buffer (Genaxxon)	10×	2.0 μ l
MgCl ₂ (Genaxxon)	25 mM	2.0 μ l
Forward primer	10 μ M	1 μ l
Reverse primer	10 μ M	1 μ l
dNTPs (Fermentas)	10 mM each	1 μ l
<i>Taq</i> polymerase S (Genaxxon)	5U/ μ l	0.5 μ l
ddH ₂ O μ l		q.s. μ l
Total volumel		<hr/> 20 μ l

Amplification program:

94°C	4 min	initial denaturation
94°C	30 s	} 35 cycles
60°C	30 s	
72°C	60 s	
72°C	4 min	final elongation

Successful amplification was verified by running an aliquote on 1% agarose gel. PCR product was diluted 1:10 and processed for sequencing.

4.18 Transplantations

Transplantation were performed as previously described [Nüsslein-Volhard and Dahm, 2002]. Donors were obtained by crossing β -*actin1*:GFP transgenic fish to *pfau* homozygous fish and regular *alb* fish were used as hosts. At mid blastula stage (1000 cell stage), about 20-40 cells were transplanted from the donor into the recipient at a position where, according to the fate map [Langeland and Kimmel., 1997], the prospective fins are located. Transplantation recipients were raised to adulthood.

4.19 Injections

Plasmids (5-20 ng/ μ l), Tol2 mRNA (25 ng/ μ l) and 20% (v/v) phenol red solution (Sigma-Aldrich, P0290-100ML) were injected into the zygote of 1-cell stage embryos under a dissecting microscope (Zeiss, Stemi 2000) using 275 Pa (40 psi) injecting pressure for 100 ms (World Precision Instruments, Pneumatic PicoPump PV820).

4.20 Calcein staining

Calcein (Sigma-Aldrich, C0875) was dissolved to 0.2% (w/v) in ddH₂O and pH was set to neutral values with NaOH. Live fish were bathed in the calcein solution for 10 min, washed in normal fish water for 10 min and processed for imaging.

4.21 cRNA Preparation

10 µg of template plasmid were linearised by digestion with 50 U of the appropriate restriction enzyme in a total volume of 100 µl.

construct	gene	enzyme	polymerase
PSi01	<i>kcnh1a</i> ⁺	NheI	T7
PSi02	<i>kcnh1a</i> ^{sgl}	NheI	T7
PSi03	<i>kcnh1a</i> ^{sgl}	NheI	T7
PSi51	<i>kcnh1a</i> ^{f9g}	NheI	T7
PSi05	<i>kcnk5b</i> ⁺	NheI	T7
PSi06	<i>kcnk5b</i> ^{pfau}	NheI	T7
PSi07	<i>kcnk5b</i> ^{alf}	NheI	T7
PSi08	<i>kcnk5b</i> ^{GFGAAA}	NheI	T7
PSi82	Tol2 transposase	NotI	Sp6

Proper linearisation was confirmed on 1 µl by agarose gel electrophoresis and ethidium bromide staining. Subsequently, template DNA was extracted through phenol/chloroform precipitation using Phase Lock Gel Heavy 2 ml tubes (5 Prime): An isovolume of phenol:chloroform:isoamyl alcohol 25:24:1 (Carl Roth) was added to the sample. Solution was mixed through shaking.

Samples were centrifuged for 5 min at 13,000 rpm. The aqueous, upper phase was carefully pipetted in a new Phase Lock Gel Heavy 2 ml tube, an isovolume of chloroform was added and, after vigorous mixing, samples were centrifuged for another 5 min. The aqueous phase was again transferred to a fresh tube and supplemented with $1/10$ volume of 3 M sodium acetate and 2.5 volumes of absolute ethanol. Mixing was followed by an incubation of 1 hour at -80°C and a centrifugation at 4°C with 12000 rpm for 10 min. Pellet was washed twice with 70% ethanol and 14000 rpm for 5 minutes. Subsequently pellet was dissolved in 10 μl ddH₂O (ca. 1 $\mu\text{g}/\mu\text{l}$). The transcription reaction was performed using Ambion mMessage mMachine (Invitrogen) according to manufacturer's instructions (total volume 20 μl). The DNA template was then digested through incubation with 2 μl TURBO DNase for 15 min at 37°C and successful transcription was verified through agarose gel electrophoresis and ethidium bromide staining on 1 μl of the reaction. For Tol2 mediated transgenesis mRNA was purified as follows: After transcription, mRNA was precipitated through addition of 30 μl of nuclease free H₂O and 30 μl of lithium chloride precipitation solution. Samples were mixed thoroughly, incubated for 1 hour at -20°C and centrifuged at 4°C with 12000g for 15 minutes. The pellet was washed via centrifugation with 1 ml 70% ethanol for 5 min, resuspended in 50 μl nuclease free H₂O and diluted to a final concentration of 250 ng/ μl . mRNA was aliquoted in batches of 2 μl and stored at -80°C . mRNA for expression in *Xenopus* oocytes was clean up using mRNeasy Mini Kit (Qiagen) according to the manufacturer's protocol and stored at -80°C .

4.22 Electrophysiology

Xenopus laevis oocytes were harvested according to German law as described previously [Strutz-Seebohm et al., 2007]. Briefly, animals were tricaine anaesthetised and ovary lobes were removed from frogs and digested with collagenase (Type II, Worthington, 1 mg/ml in Ca^{2+} -free Barth's solution) for 120 min. Stage V oocytes were collected and injected with cRNA (*kcnk5b* single alleles: 4 ng of wild type or mutant *kcnk5b* cRNA; coinjections of two *kcnk5b* alleles: 2 ng cRNA each, for a total of 4 ng; measurements of *kcnh1a*: 2 ng of wild type or mutant *kcnh1a* cRNA per oocyte). Injected oocytes were stored for 3-4 days at 17°C in Barth's solution containing (in mM): 88 NaCl, 1.1 KCl, 2.4 NaHCO_3 , 0.3 $\text{Ca}(\text{NO}_3)_2$, 0.3 CaCl_2 , 0.8 MgSO_4 , 15 HEPES-NaOH, penicillin-G (31 mg/l), streptomycin sulphate (20 mg/l), gentamycin (50 mg/l), pH 7.6.

Standard TEVC recordings were performed at 22-23°C using a Turbo Tec-10CX (NPI, Germany) amplifier equipped with an ITC-16 interface and pCLAMP 8.0 software (Axon Instruments Inc./Molecular Devices, USA) and analyzed with Clampfit 8.0 and Origin 6.0 (Additive, Germany). From a holding potential of -80 mV 0.5 s (*kcnk5b*) or 2.15 s (*kcnh1a*) long pulses from -100 to +60 mV with increments of 20 mV were applied. Recording pipettes were filled with 3M KCl and had resistances of 0.4-1 M Ω . Channel currents were recorded in ND96 recording solution containing (in mM): 96 NaCl, 4 KCl, 1.8 MgCl_2 , 1.0 CaCl_2 , 5 HEPES; pH 7.6.

Recorded currents (n=5-26) were averaged and normalised to the mean value recorded for oocytes injected with the wild type

channel at +60 mV (*kcnk5b*) or +40 mV (*kcnh1a*).

4.23 Immunohistochemistry

Fins were cut and fixed in 4% PFA rotating overnight at 4°C. The next day fins were briefly rinsed in PBS and gradually dehydrated through 5 min washes of 25%, 50%, 75%, 90% and 100% MetOH in PBST (PBS + 0.1% Tween20). Samples were kept overnight in MetOH at -20°C and subsequently rehydrated through 5 min washes in 90%, 75%, 50%, 25% MetOH in PBST. Fins were then permeabilised through three washes in PBT (PBS + 0.3% Triton-X) of 5 min and digested with proteinase K (10 µg/ml in PBST) digestion for 70 min at room temperature. The reaction was stopped with two quick washes in PBST. Fins were then postfixed with 4% PFA at RT for 20 min and washed for another 4-5 times. The samples were then blocked for at least 1 h at RT with 10% NGS (normal goat serum), and incubated overnight with the primary antibody (mouse α -zns-5: 1:200, rabbit α -GFP: 1:500) in 1% NGS and PBST. The next day fins were washed for at least 5 times with PBST at RT and incubated overnight with the secondary antibody (1:400 α -mouse Cy3, α -rabbit Alexa488) in 1% NGS and PBST. Subsequently samples were washed several times in PBST and mounted on a microscope slide in Aquamount. A small amount of silicon was applied on the borders as spacer, samples were covered with a cover slip and sealed with nail polish.

4.24 Imaging

Following microscopes were used for imaging:

Microscope	illumination	Software
Zeiss SteREO	KL2500	AxioVision 4.8
Discovery V20	LCD/HXP120	
Zeiss Apotome	HAL100/HXP120	AxioVision 4.8
Zeiss LSM 5LIVE	DPSS 405/ Di-odes 488 561 635	Zen 2009

Images were processed using:

- ImageJ 1.45s
- Adobe Photoshop CS4
- Adobe Illustrator CS4

4.25 Cloning of misexpression constructs

The backbone (PSi75) of the misexpression construct was generated by excising the *cmc*:EGFP cassette from vector PSi30 (587jk, kind gift of Dr. Jana Krauß) through BglII restriction. At this site a *ef1a*DsRed cassette generated from PSi73 (Ale237, kind gift of Alessandro Mongera) was inserted through In-Fusion[®] Advantage (Clontech) cloning using following conditions:

PSi73 DNA 10 ng/ μ l	1.00 μ l
10 \times Buffer for KOD Hot Start DNA Polymerase (Toyobo)	5.00 μ l
25 mM MgSO ₄ (Toyobo)	3.00 μ l
dNTPs (2 mM each) (Toyobo)	5.00 μ l
OSP-295 primer 10 μ M	1.25 μ l
OSP-304 primer 10 μ M	1.25 μ l
KOD Hot Start DNA polymerase (Toyobo) (1U/ μ l)	1.00 μ l
ddH ₂ O μ l	32.50 μ l
Total volume	<u>50 μl</u>

Amplification program:

95°C	2 min	initial denaturation
95°C	20 s	} 30 cycles
59°C	10 s	
72°C	30 s	

An aliquot of 1 μ l was verified on a 1% agarose gel and the remaining sample was digested with 1 μ l DpnI enzyme (10 U/ μ l, Fermentas) for 8 h, cleaned up with Wizard[®] SV Gel and PCR Clean-Up System as above, using an isovolume of Membrane binding solution. Insert was processed for In-Fusion[®] Advantage reaction to obtain PSi76:

PSi75	50 ng
Insert (vector:insert ratio = 1:2)	60 ng
Buffer	2 μ l
Enzyme	1 μ l
ddH ₂ O	q.s.
Total volume	<u>10 μl</u>

The *ef1 α :kcnk5b^{pfau}* cassette (PSi74) was obtained by inserting the *ef1 α* promoter from PSi73 into PSi06. The promoter was amplified from PSi73 using KOD Hot Start DNA Polymerase (Toyobo) with OSP-297 and OSP-298 primers and inserted into PSi06 via In-Fusion[®] Advantage through a KpnI cutting site using the same conditions as above.

This cassette was finally amplified from PSi74 by PCR with OSP-313 and OSP-314 primers which contain AvrII cutting sites, using KOD Hot Start DNA Polymerase (Toyobo) as above, digested with AvrII after Wizard[®] SV Gel and PCR Clean-Up clean up and ligated into PSi76, which was previously digested with SpeI and dephosphorylated with rAPid Alkaline Phosphatase (Roche), using Quick Ligase[™] (NEB) as above to obtain PSi81. The *ef1 α :kcnk5b⁺* version (PSi96) was obtained by substituting the CDS of PSi81 through SalI and XbaI cutting sites with the *kcnk5b* wild type sequence obtained from PSi05 with the same restriction enzymes.

4.26 PCR mutagenesis

In order to generate the pore mutant *kcnk5b*^{GF₃GAAA} and the pSGEM Kcnh1^{S396A}, PCR mutagenesis was performed as described [Zheng et al., 2004] using primer pairs OSP-15/16 on PSi05 and OSP-155/156 on PSi01, respectively and following conditions:

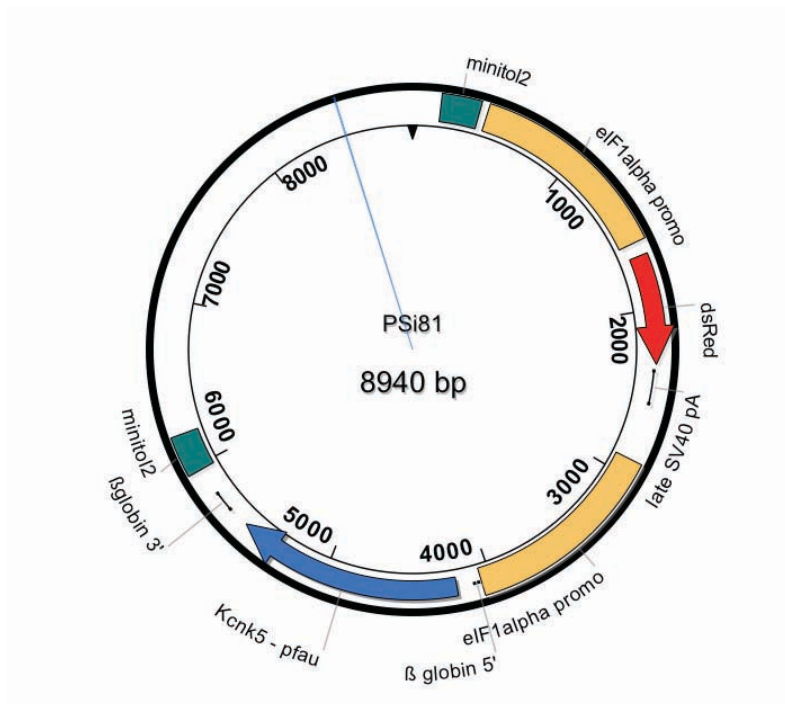


Figure 4.1: Map of *ef1 :DsRed; ef1 :kcnk5b^{pfau}* plasmid

Template DNA (PSi05/PSi01)	200 ng/ μ l	1 ng
Pfu polymerase buffer (Fermentas)	10 \times	2.5 μ l
Forward primer	10 μ M	1 μ l
Reverse primer	10 μ M	1 μ l
dNTPs (each)	12.5 mM	1 μ l
<i>Pfu</i> polymerase (Fermentas)	2.5U/ μ l	1 μ l
ddH ₂ O μ l		37 μ l
Total volume		<hr/> 50 μ l

Amplification program:

95°C 2 min initial denaturation

95°C 15 s	}	30 cycles
70°C 1 min		
72°C 10 min		

An aliquot of 10 μ l was verified on a 1% agarose gel and the remaining sample was digested with 1 μ l DpnI enzyme (10 U/ μ l, Fermentas) for 8 h and processed for transformation.

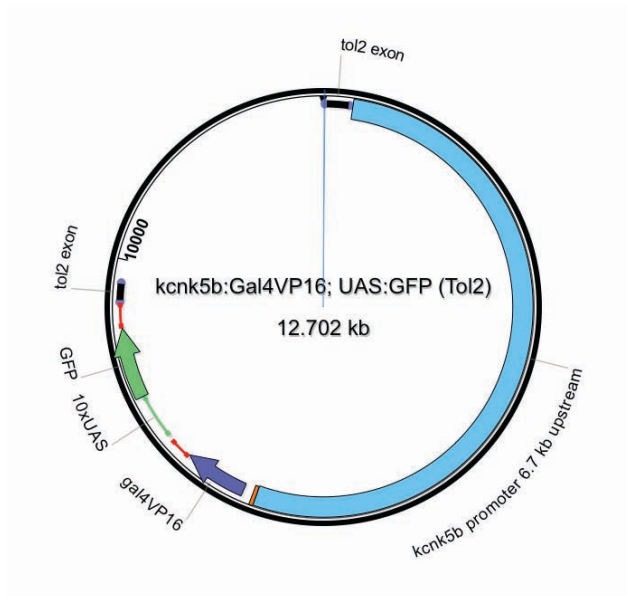


Figure 4.2: Map of 6.7 kb *kcnk5b*: Gal4VP16; UAS:GFP

4.27 *kcnk5b* 6.7 kb reporter construct

A 6.7 kb long upstream sequence of *kcnk5b* was amplified from BAC CH211-245G15 using OSP-130/131 primer pairs and following conditions:

DNA 50 ng/μl	1.00 μl
10× Buffer for KOD Hot Start DNA Polymerase (Toyobo)	5.00 μl
25 mM MgSO ₄ (Toyobo)	3.00 μl
dNTPs (2 mM each) (Toyobo)	5.00 μl
OSP-130 primer 10 μM	1.5 μl
OSP-131 primer 10 μM	1.5 μl
KOD Hot Start DNA polymerase (Toyobo) (1U/μl)	1.00 μl
ddH ₂ O μl	32.00 μl
Total volume	50 μl

Amplification program:

95°C	2 min	initial denaturation	
95°C	20 s	} 30 cycles	
59°C	10 s		
72°C	3 min		

An aliquot of 1 μl was verified on a 1% agarose gel and the remaining sample was cleaned up with Wizard[®] SV Gel and PCR Clean-Up System and cloned into pGEM[®]-T Easy (Promega) vector as described above. Insert was cut out with EcoRI, processed with NEB Quick Blunting[®] Kit according to the manufacturer's protocol. Plasmid pSi22 (kind gift of Dr. Matthew Harris) was digested with NotI restriction enzyme, treated

with NEB Quick Blunting[®] Kit and subsequently with rAPid Alkaline Phosphatase (Roche) as described. The promoter was then inserted in this vector with NEB Quick Ligase[™] as above.

4.28 *kcnk5b* BAC reporter construct

BAC CH211-245G15 was engineered as described [Busmann and Schulte-Merker, 2011] using P*Si*89 as source for recombinase (pRedET, kind gift of Dr. Jana Krauß). The recombination cassettes were amplified with KOD Hot Start DNA polymerase (Toyobo) as described above. Primer pair OSP-279/280 was used to amplify the *tol2* cassette from P*Si*85 (*itol2* 293, kind gift of Prof. Stefan Schulte-Merker) and OSP-387/388 were used to amplify the Gal4FF cassette from P*Si*102 (kind gift of Prof. Stefan Schulte-Merker).

Table 4.1: G4 primer set

LG	SSLPs
1	Z4593, Z9394, Z5508, Z1705, Z1351, Z9704, Z11464, Z6802, Z1781
2	Z7634, Z4662, Z3430, Z1406, Z6617, Z1703, Z20550
3	Z872, Z8208, Z15457, Z9964, Z11227, Z3725, Z20058, Z6019
4	Z1525, Z9920, Z21636, Z7490, Z984
5	Z15414, Z11496, Z6727, Z10456, Z1390, Z3804, Z14143, Z4299, Z1202
6	Z740, Z13275, Z880, Z6624, Z10183, Z5294, Z13614, Z7666, Z4297, Z1680
7	Z3273, Z10785, Z1206, Z4706, Z1182, Z1059, Z8156, Z1239, Z13880, Z13936, Z5563
8	Z1634, Z1068, Z4323, Z13412, Z21115, Z789, Z10929, Z3526
9	Z1777, Z6268, Z4673, Z5080, Z1805, Z20031, Z10789, Z4577

Table 4.1: G4 primer set (continued)

LG	SSLPs
10	Z9199, Z6410, Z8146, Z13632, Z1145, Z9701, Z3260
11	Z10919, Z3362, Z13411, Z1393, Z3527, Z1590
12	Z1778, Z21911, Z1473, Z4188, Z1358
13	Z1531, Z5643, Z6104, Z13611, Z5395, Z1627, Z7102, Z6657, Z1826, Z6007
14	Z1523, Z5436, Z1536, Z5435, Z4203, Z22107, Z1226, Z3984, Z1801
15	Z6312, Z6712, Z21982, Z4396, Z11320, Z13230, Z13822, Z7381, Z5223
16	Z3741, Z21155, Z6365, Z10036, Z1215, Z4670
17	Z4268, Z1490, Z22083, Z22674, Z9847, Z1408, Z4053
18	Z1136, Z1144, Z13329, Z8488, Z10008, Z3558, Z9154, Z5321
19	Z4009, Z160, Z3782, Z3816, Z11403, Z6661, Z7926, Z1803

Table 4.1: G4 primer set (continued)

LG	SSLPs
20	Z9334, Z10056, Z11841, Z3964, Z7158, Z3954, Z22041, Z8554, Z4329
21	Z3476, Z1274, Z4492, Z10960, Z4425, Z1497, Z4074
22	Z1148, Z10673, Z9402, Z230, Z10321, Z21243
23	Z8945, Z4003, Z15422, Z4421, Z3157, Z176, Z1773
24	Z5075, Z1584, Z5413, Z23011, Z3399, Z22375, Z5657, Z3901
25	GOF15, Z1378, Z3490, Z5669, Z1462

Table 4.2: List of OSP primers

Code	Name	Company	Sequence
OSP-015	k5P2aaa_for	MWG	CCC TGA CGA CTG TCG CTG CAG CTG ACT ATG TGG CAG GGG C
OSP-016	k5P2aaa_rev	MWG	CCT GCC ACA TAG TCA GCT GCA GCG ACA GTC GTC AGG GTG G
OSP-021	k1-QtoR_for	Sigma	TGC GGG TTG TCT TTA GAA CG
OSP-022	k1-QtoR_rev	Sigma	CGG GGA CTT CAA ATC CAG AG
OSP-057	gPfau-for	MWG	CAG TGG CCT CAA TGT GGT AA
OSP-058	gPfau-rev	MWG	GTC AGG GTG GTG AAG GAG AA

Table 4.2: List of OSP primers (continued)

Code	Name	Company	Sequence
OSP-105	TtoI-for	MWG	ATG GTG CCC TAC AAC GTC TC
OSP-106	TtoI-rev	MWG	GCA GAC AGG ACA ACA GGT CA
OSP-128	kcnh1-cDNA-fl	MWG	CTC TCA GTG GAG CGC ATG AC
OSP-129	kcnh1-cDNA-r1	MWG	CAC AGA TGT CAG AAG TGG TTC CAT
OSP-130	promo kcnk5-r1/r2	Sigma	GGT TTA AAC TTG AGA GAT CAC CAT GAC C
OSP-131	promo kcnk5-fl	Sigma	TCT ACA TTG AAA CAG AAC ACC AGC ATT T
OSP-137	dege kcnh1-c15f1	Sigma	TGG CTA GTG GTG GAC AGY ATW GTG GA

Table 4.2: List of OSP primers (continued)

Code	Name	Company	Sequence
OSP-138	dege kcnh1-c15f1	Sigma	CGG GCT TCC TTC TGC TGK CGG AAR CGC TGG AAG AG
OSP-151	K1-Pla- Dre15-for	Sigma	GCA AAC TGG ACC ACT ACA TCG AAT A
OSP-155	muta-K1- StoA-for	MWG	CAG CTG GCT TTA TAT GCT TGC TGA GGC CAT CGG GAC ACC CTA CCG CTT CAA TGC AAG
OSP-156	muta-K1- StoA-rev	MWG	CAT TGA AGC GGT AGG GTG TCC CGA TGG CCT CAG CAA GCA TAT AAA GCC AGC TGT CCG
OSP-163	poecilid ex10 rev	MWG	CCG TCC GTC GTC GGA GCG ATG TTG CC
OSP-175	genomic kcnh1 NR3-for	Sigma	GCT GAA AGT GGT TCG GCT CT

Table 4.2: List of OSP primers (continued)

Code	Name	Company	Sequence
OSP-176	genomic kcnh1 NR3-rev	Sigma	GTC AGG CTG GTC ATG GTG AA
OSP-185	muta-K1-nr3- for	Sigma	CAA ACT GGA TCA CTA CAT CGA GTA TGA AGC GGC GGT TTT GGT TCT GCT GGT TTG TGT
OSP-186	muta-K1-nr3- rev	Sigma	AAA CCA GCA GAA CCA AAA CCG CCG CTT CAT ACT CGA TGT AGT GAT CCA GTT TGC GAG
OSP-279	pTarBAC2.1- itol2-for	Thermo	GCG TAA GCG GGG CAC ATT TCA TTA CCT CTT TCT CCG CAC CCG ACA TAG ATC CCT GCT CGA GCC GGG CCC AAG TG

Table 4.2: List of OSP primers (continued)

Code	Name	Company	Sequence
OSP-280	pTarBAC2.1-itol2-rev	Thermo	GCG GGG CAT GAC TAT TGG CGC GCC GGA TCG ATC CTT AAT TAA GTC TAC TAT AGG GAT AAC AGG GTA ATA TTA TGA TCC TCT AGA TCA GAT C
OSP-295	ef1a DsRed minitol2	Sigma	TAA TTT AAA TAG ATC TTC GAG CAG GGG GAT CAT CTA ATC A
OSP-297	ef1a pSGEM Kcnk5-f	Sigma	ATT AAT TCG AGC TCG GTA CCC CTC GAG CAG GGG GAT CAT CT
OSP-298	ef1a pSGEM Kcnk5-r	Sigma	GAA CAA GCA AGC TGG GTA CCC CGG CCG TCG AGG AAT TCT TTG
OSP-304	DsRed minitol2	Sigma	CTA GAT GGC CAG ATC TGC CCG GGA CTT GAT TAG GGT GAT GGT TCA CGT AGT G

Table 4.2: List of OSP primers (continued)

Code	Name	Company	Sequence
OSP-313	ef1alpha Pfau AvrII	Sigma	AAA CCT AGG TCG AGC AGG GGG ATC ATC T
OSP-314	ef1alpha Pfau AvrII	Sigma	AAA CCT AGG ATG ACC ATG ATT ACG CCA AGC TAT
OSP-377	FtoY kcnk5b	MWG	CAA GTG CTT GAT GCA TTG CT
OSP-378	FtoY kcnk5b	MWG	GCC AGT TCC TCC TCC TGT TT
OSP-379	kcnk5-1 for	MWG	TGG GAG TGT GGA GTG TGT GT
OSP-382	kcnk5-2 rev	MWG	TTT TTG GTC CAG CTT TGG TC

Table 4.2: List of OSP primers (continued)

Code	Name	Company	Sequence
OSP-387	kcnk5b-HA1-Gal4-fw	Thermo	TGT GTT ACT TCT TGT GTT ATT GAA CAC AAG GAA GGA ATT ACT TCA GTA TTA CCA TGA AGC TAC TGT CTT CTA TCG AAC
OSP-388	kcnk5b-HA2-kanR-rev	Thermo	TGT TTA TAA AAT GTT AAC GTT AGT TTT CCC AAA ACA CAA ATG AAA CAC AAC TTA CTC AGA AGA ACT CGT CAA GAA GGC G

Table 4.3: List of plasmids

Code	Plasmid name	Source	Backbone
PSi01	pSGEM <i>kcnh1a</i> ⁺	Subcloned from PSi15	PSi10
PSi02	pSGEM <i>kcnh1a</i> ^{sgl}	Subcloned from PSi16	PSi10
PSi03	pSGEM <i>kcnh1a</i> ^{slk}	Subcloned from PSi17	PSi10
PSi05	pSGEM <i>kcnk5b</i> ⁺	Subcloned from PSi97	PSi09
PSi06	pSGEM <i>kcnk5b</i> ^{pfau}	Subcloned from PSi98	PSi09
PSi07	pSGEM <i>kcnk5b</i> ^{alf}	Subcloned from PSi99	PSi09
PSi08	pSGEM <i>kcnk5b</i> ^{GFGAAA}	Mutagenesis	PSi05
PSi09	pSGEM+	Prof. Guiscard Seebohm	-
PSi10	pSGEM KS-	Prof. Guiscard Seebohm	-

Table 4.3: List of plasmids (continued)

Code	Plasmid name	Source	Backbone
PSi15	pGEM [®] -T Easy <i>kcnh1a</i> ⁺	cDNA	pGEM [®] -T Easy
PSi16	pGEM [®] -T Easy <i>kcnh1a</i> ^{sgl}	cDNA	pGEM [®] -T Easy
PSi17	pGEM [®] -T Easy <i>kcnh1a</i> ^{sllk}	cDNA	pGEM [®] -T Easy
PSi22	Gal4-UAS::GFP (75a)	Dr. Matthew Harris	-
PSi30	Tol2 green heart vector	Dr. Jana Krauß	pGEM [®] -T Easy
PSi51	pSGEM <i>kcnh1a</i> ^{fgg}	Mutagenesis	PSi01
PSi73	<i>ef1</i> :DsRed loxP GFP	Alessandro Mongera	-
PSi74	pSGEM <i>ef1:kcnk5b</i> ^{pfau}	In-Fusion [®] reaction	PSi06
PSi75	Tol2 vector	Restriction	PSi30
PSi76	Tol2 <i>ef1a</i> :DsRed vector	In-Fusion [®] reaction	PSi75
PSi81	Tol2 <i>ef1a:kcnk5b</i> ^{pfau} ; <i>ef1a</i> :DsRed	Subcloned from PSi74	PSi76

Table 4.3: List of plasmids (continued)

Code	Plasmid name	Source	Backbone
PSi82	Tol2 transposase	Alessandro Mongera	-
PSi85	itol2 293 cassette	Prof. Stefan Schulte-Merker	-
PSi89	pRedET	Dr. Jana Krauß	-
PSi96	Tol2 <i>ef1a:kcnk5b⁺</i> ; <i>ef1a:DsRed</i>	Subcloned from PSi05	PSi81
PSi97	pGEM [®] -T Easy <i>kcnk5b⁺</i>	cDNA	pGEM [®] -T Easy
PSi98	pGEM [®] -T Easy <i>kcnk5b^{pfau}</i>	cDNA	pGEM [®] -T Easy
PSi99	pGEM [®] -T Easy <i>kcnk5b^{alf}</i>	cDNA	pGEM [®] -T Easy
PSi102	Gal4FF	Prof. Stefan Schulte-Merker	-

Contributions

The work described in this thesis was performed at the Max Planck Institute for Developmental Biology in Tübingen in the laboratory of Prof. Dr. Christiane Nüsslein-Volhard under the supervision of Dr. Matthew P. Harris. The mutants *pfau*, *sgl*, *sllk* and *fgg* were isolated by Dr. Matthew P. Harris. The author of this thesis designed and carried out all experiments with the exception of the electrophysiological measurements, which were performed in collaboration with Prof. Dr. Guiscard Seebohm at the Ruhr Universität in Bochum. Dr. Ulrike Henrion measured *kcnk5b* injected oocytes, while Dr. Katja Steinke provided the data for *kcnh1a* electrophysiology. Rough mapping was supported by Ines Gehring from the Mapping Facility of the Max Planck Institute for Developmental Biology and injections of the misexpression constructs were partially performed by Hans Martin Maischein, Nüsslein-Volhard Lab, in order to achieve higher numbers.

Appendix A

Zebrafish *eda* and *edar* Mutants Reveal Conserved and Ancestral Roles of Ectodysplasin Signaling in Vertebrates

Matthew P. Harris*, Nicolas Rohner, Heinz Schwarz, Simon Perathoner, Peter Konstantinidis, Christiane Nüsslein-Volhard

Max Planck Institute for Developmental Biology, Tübingen, Germany

Abstract

The genetic basis of the development and variation of adult form of vertebrates is not well understood. To address this problem, we performed a mutant screen to identify genes essential for the formation of adult skeletal structures of the zebrafish. Here, we describe the phenotypic and molecular characterization of a set of mutants showing loss of adult structures of the dermal skeleton, such as the rays of the fins and the scales, as well as the pharyngeal teeth. The mutations represent adult-viable, loss of function alleles in the *ectodysplasin* (*eda*) and *ectodysplasin receptor* (*edar*) genes. These genes are frequently mutated in the human hereditary disease hypohidrotic ectodermal dysplasia (HED; OMIM 224900, 305100) that affects the development of integumentary appendages such as hair and teeth. We find mutations in zebrafish *edar* that affect similar residues as mutated in human cases of HED and show similar phenotypic consequences. *eda* and *edar* are not required for early zebrafish development, but are rather specific for the development of adult skeletal and dental structures. We find that the defects of the fins and scales are due to the role of Eda signaling in organizing epidermal cells into discrete signaling centers of the scale epidermal placode and fin fold. Our genetic analysis demonstrates dose-sensitive and organ-specific response to alteration in levels of Eda signaling. In addition, we show substantial buffering of the effect of loss of *edar* function in different genetic backgrounds, suggesting canalization of this developmental system. We uncover a previously unknown role of Eda signaling in teleosts and show conservation of the developmental mechanisms involved in the formation and variation of both integumentary appendages and limbs. Lastly, our findings point to the utility of adult genetic screens in the zebrafish in identifying essential developmental processes involved in human disease and in morphological evolution.

Citation: Harris MP, Rohner N, Schwarz H, Perathoner S, Konstantinidis P, et al. (2008) Zebrafish *eda* and *edar* Mutants Reveal Conserved and Ancestral Roles of Ectodysplasin Signaling in Vertebrates. *PLoS Genet* 4(10): e1000206. doi:10.1371/journal.pgen.1000206

Editor: Irma Thesleff, University of Helsinki, Finland

Received: December 28, 2007; **Accepted:** August 22, 2008; **Published:** October 3, 2008

Copyright: © 2008 Harris et al. This is an open-access article distributed under the terms of the Creative Commons Attribution License, which permits unrestricted use, distribution, and reproduction in any medium, provided the original author and source are credited.

Funding: MPH was supported by a Max Planck Postdoctoral Fellowship.

Competing Interests: The authors have declared that no competing interests exist.

* E-mail: matthew.harris@tuebingen.mpg.de

Introduction

The genetic and developmental basis of the formation of organismal shape and form is a long-standing question in biology. The analysis of mutations has been essential in identifying the genes and regulatory networks underlying development. However, while the genetic basis of embryonic development has been extensively studied by systematic mutagenesis screens, we know little of the genes involved in the development of adult morphology. Yet, it is the heritable variation in adult form that natural selection primarily acts on during evolution. In order to understand the basis of variation, we need to know more about the genetic control of the development of adult form: which genes are involved, what are their function, and when are they required in development [1,2]. To identify genes important for development of adult structures, we initiated a large-scale mutagenesis screen in zebrafish and scored for mutants affected in the shape and pattern of adult structures. We isolated only adult viable mutants, therefore we selected for genes that have an increased probability to be involved in morphological change during evolution. Identification of zebrafish genes homologous to human genes associated with disease that arise during postnatal development into adulthood is also likely in this screen.

We focused on mutants that exhibit defects in the dermal skeleton of the adult zebrafish. The dermal skeleton encompasses

the external form of the adult fish. The most prominent dermal skeletal elements are the dermocranium of the skull and lateral bones of the opercular series, the scales, and the fin rays (or lepidotrichia). Additionally, the teeth and gill rakers (bones that support the gills in teleosts) are elements of the dermal skeleton [3,4]. Unlike the ossification process that occurs during endochondral bone development in which organic matrix is deposited by osteoblasts over a chondrogenic scaffold, dermal skeletal elements originate as direct mineralization of a collagenous matrix deposited by dermal fibroblasts. This process occurs in close association with the epidermis. The initiation and patterning of dermal elements are thought to be similar to epidermal appendages (e.g. hairs and feathers) and is controlled by reciprocal signaling between an epithelium and mesenchyme (see [5,6]). Importantly, in zebrafish, as in most teleosts, the majority of dermal skeletal elements are not formed during larval development, rather through juvenile metamorphosis and development of the adult pattern. Those that begin to form in late larval development such as the teeth and gill rakers, do not fully attain their shape and pattern until juvenile metamorphosis.

Variations in the shape of dermal skeletal elements of the fins, scales, cranium, and teeth play a significant role in adaptations of fish populations to new environments (e.g. dermal plate development and stickleback radiation [7]). Additionally, integumentary

Author Summary

A major goal of the study of developmental genetics is to understand the genes and developmental mechanisms underlying the formation of organismal complexity and diversity. Here, we focus on genes controlling postembryonic development and describe mutations in genes of the ectodysplasin (Eda) pathway in regulating the formation of the scales, skull, fins, and teeth. Mutations in genes of this signaling pathway are common in humans with defects in ectodermal structures such as hair, glands, and teeth. We show that the similar phenotypes of loss of Eda signaling in fish and human are due to a conserved early developmental stage in the development of mammalian hair and fish scales; subsequent development of these two structures diverge. Our findings show that the Eda signaling pathway has an ancestral role in regulating the developmental interactions involved in patterning and growth of the dermal skeleton of fish. Recent work has shown that these genes are associated with morphological variation between humans and evolution within fish populations, suggesting that alteration in the function of these genes permits viable morphological change. Our data support the value of forward genetic studies on postembryonic development to reveal the genetic and developmental basis of both human disease and morphological evolution.

appendages, such as hair and feathers, have been essential and defining traits of vertebrate classes. Early vertebrates, the conodonts, ostracoderms and placoderms, possessed a pronounced dermal skeleton, often in the absence of an ossified axial skeleton [8]. Through vertebrate evolution from fish to tetrapods, dermal structures such as lateral bones of the opercular series, scales, dermal plates and fin rays were either reduced or lost. This evolutionary transition was paralleled with the elaboration of the cartilaginous endoskeleton of the limbs and the evolution of specialized keratinized appendages of the integument such as epidermal scales, feathers and hairs. In contrast, the diversity of form in extant bony fishes involves modification in size, shape and number of the scales/dermal plates, fin rays, cranial dermal bones and teeth.

Here, we describe a collection of mutants that have shared defects in the formation of the dermal skeletal elements of the skull, fins, scales and teeth of the adult zebrafish. The mutations disrupt the genes *ectodysplasin (eda)* and *edar* encoding the *eda* receptor. In mammals the EDA signaling pathway is involved in hair and teeth formation [9] and mutations affecting this pathway cause the human hereditary disease hypohidrotic ectodermal dysplasia (HED). Loss of Eda signaling in the zebrafish causes a spectrum of phenotypes corresponding to those described for HED in humans, and therefore the zebrafish mutants may serve as a genetic model of this disease. We describe the requirement of Eda signaling in the zebrafish epidermis for the formation of a structure resembling an epidermal placode seen in the early development of other vertebrate integumentary appendages. The mutations also result in defects of skeletal elements unique to fish and suggest an ancestral role of Eda signaling in the formation and patterning of the dermal skeleton. Lastly, whereas loss of function of Eda signaling causes a severe phenotype, the expressivity of dominant alleles is sensitive to background modifiers that buffer the phenotypic consequences of loss of Eda signaling. Additionally, we find that the response to reduction of Eda signaling is dose sensitive and organ specific. We suggest that such alleles may provide a basis for morphological variation in evolution.

Results

finless and *Nackt* Mutants Exhibit Defects in the Development of the Dermal Skeleton

In a mutagenesis screen for mutations affecting adult zebrafish structures, we identified three mutants that showed nearly identical defects in the formation of scales, lepidotrichia, and shape of the skull of homozygous fish. These mutants fell into two complementation groups. The first is allelic to the *finless* (fls^{ic370f}) mutant that was previously isolated in the background of the Tübingen wild type stock (Tü) on the basis of the loss of fins in adults [10]. We isolated two new alleles of *fls* in the screen and found another in the background of the *TLF* wild type stock. The majority of the *fls* alleles isolated are recessive and have a strong phenotype (see below). However, the fls^{dt31pl} allele is dominant with a partial scale loss phenotype in heterozygotes (Figure 1G, J). One further *fls* allele was isolated in a screen for mutations that failed to complement the fls^{ic370f} mutant (Figure 1M). We named this allele *fang* (fls^{fang}) after its unique dental phenotype in homozygotes of having only one tooth on the fifth ceratobranchial (Figure 1N). The fls^{fang} allele shows no effect on fin development and has a slight increase in the number of scales than the other *fls* alleles isolated.

The second complementation group was comprised of a single gene, which we called *Nackt* (*Nkt*). This allele is dominant causing a slight defect in the patterning and shape of scales as heterozygotes (Figure 2D). The homozygous phenotype is more severe than that of strong *fls* alleles (Figure 2A).

Phenotypic defects of *fls* and *Nkt* mutants become apparent in juvenile fish; as larvae, homozygous *fls* and *Nkt* mutants are visibly unaffected. Homozygous adults are viable, and of normal size. With the exception of the fls^{fang} allele, the lepidotrichia that form during juvenile metamorphosis are defective, leading to fin loss in the adult (Figure 1D, 2A). The dermal bones of the pectoral girdle are present and patterned appropriately in both the *fls* and *Nkt* mutants. By close examination of the visceral skeleton we found that neither the pharyngeal teeth, nor the bony substrates of the gills, the gill rakers, are formed (Figure 1E and F; Figure 2B, C). In addition, scales are largely absent with infrequent formation of inappropriately shaped scales near the dorsal, anal and pectoral fins (Figure 1D, 2A). *Nkt* homozygous fish exhibit more severe defects in the formation of the dermal skeleton than *fls* alleles in the extent of lepidotrichial growth and number of residual scales formed (compare Figure 1D and Figure 2A). The skull of mutants has a normal appearance with all the bones being present, although the size, shape and relative proportion of the various bones differ compared to wild type individuals (Figure S1); no change in cranial shape was apparent in larvae.

Nkt heterozygous fish exhibit a dominant phenotype as they lack several scales on the flank and those present at the flank are elongated dorso-ventrally. The number of teeth and gill rakers is reduced, however lepidotrichia formation and growth of the fins are not affected (Figure 2D–F). The skulls of *Nkt* heterozygotes do not show increased size, but retain altered shape and proportion as seen in homozygotes (Figure S1).

The Topless Allele of *fls* Uncovers Background Specific Modulation of *fls* Expressivity

We isolated a dominant allele of *fls* that exhibits a distinct phenotype in heterozygotes that we named *Topless* (fls^{dt31pl}). Heterozygous fls^{dt31pl} have a reduction in the number of scales, teeth and gill rakers, but show little to no effect on lepidotrichia development (Figure 1G–I). Mutant fls^{dt31pl} fish exhibit the strong *fls* phenotype when homozygous or heterozygous with other *fls*

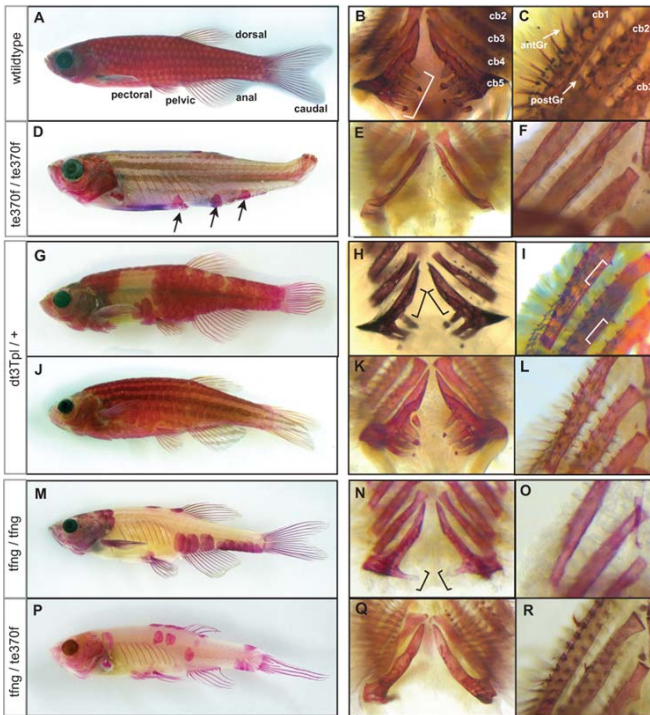


Figure 1. The formation of the adult dermal skeleton and pharyngeal teeth is affected in *fls* mutant zebrafish. A) Alizarin red-stained wild type adult zebrafish shows staining of the scales, fin rays, dermal bones of the skull as well as the pharyngeal teeth along ceratobranchial 5 (bracket, B) and C) gill rakers along both the anterior (antGr) and posterior edge (postGr) of non-teeth bearing ceratobranchials. D) *fls^{te370f}* shows loss of dermal skeletal structures of the fin rays, scales and alteration in the shape of the skull. Additionally, *fls^{te370f}* shows loss of pharyngeal teeth (E) and gill rakers (F). G–I) The Topless allele (*fls^{dt3Tpl}*) shows a dominant effect on scalation and tooth/gill raker formation while not affecting lepidotrichial growth. J–L) Expressivity of *fls^{dt3Tpl}* is sensitive to a modifier in the Tü strain leading to a “weak” *fls^{dt3Tpl}* phenotype; *fls^{dt3Tpl}* homozygotes were phenotypically identical to *fls^{te370f}* (not shown). The fang allele of *fls*, *fls^{tfang}*, isolated in a non-complementation screen with *fls^{te370f}*, shows no effect on fin development while exhibiting partial loss of scales (M), teeth (N), and gill rakers (O). Transallelic *tfang/te370f* zebrafish exhibit an intermediate phenotype between homozygous *fls(te370f)* and *fls(tfang)* (P–R). doi:10.1371/journal.pgen.1000206.g001

alleles. Similar to *Mt₁ fls^{dt3Tpl}* exhibits a dominant effect on skull shape as well (Figure S1).

The expressivity of the dominant *fls^{dt3Tpl}* phenotype depends on the genetic background. Fish heterozygous for *fls^{dt3Tpl}* exhibited either a “strong” or a “weak” phenotype in the Tü background (Figure 1G and J, respectively). The “strong” phenotype shows loss of scales regionally in the midflank, loss of medial pharyngeal teeth along the fifth ceratobranchial and loss of posterior gill rakers of the anterior arches (Figure 1G–I). In contrast, the “weak” phenotype displays only subtle variation in scale patterning and no effect on the teeth or gill rakers could be detected (Figure 1J–L). The segregation pattern of the two phenotypic classes of *fls^{dt3Tpl}* suggests the presence of separate, unlinked, modifier loci in the Tü background affecting the number of scales (Table 1 and data not shown). Additionally, we found that the *fls^{dt3Tpl}* “strong” phenotype was partially suppressed when crossed with the

polymorphic WIK mapping strain indicating the presence of dominant modifier(s) in the WIK line (Table 1). The resulting heterozygous progeny showed reduced scale-loss compared to *fls^{dt3Tpl}* heterozygotes in a Tü background, but had similar defects in scale shape (Table 1). Therefore, dominant modifier loci are present in the WIK strain that buffer the expressivity of the *fls^{dt3Tpl}* dominant phenotype. None of the other *fls* alleles showed any dominance in the Tü, TLF, or WIK strains.

Mutations in *fls* Disrupt the Ectodysplasin Receptor in Zebrafish

We identified the affected loci of the *fls* mutants by positional cloning. The *fls^{te370f}* mutation was linked to SSLP markers on linkage group 9 (LG9). Due to similarity of the *fls* phenotype to ectodermal dysplasia phenotypes in mammals, we mapped several genes of the ectodysplasin pathway to the zebrafish radiation

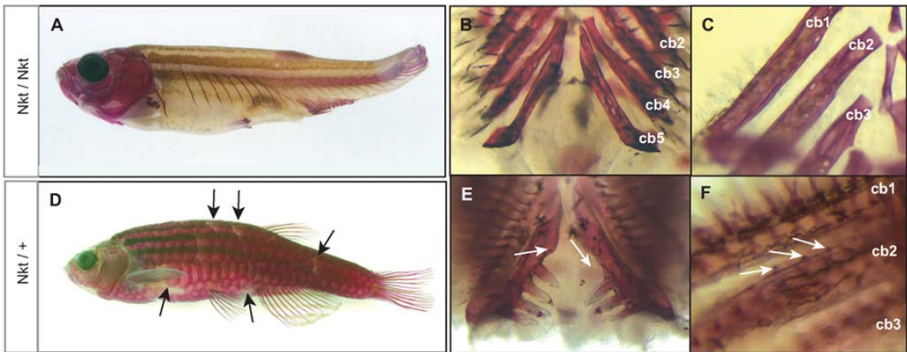


Figure 2. The dominant gene *Nkt* is phenotypically similar, however complements *fls* mutants. *Nkt* homozygotes show complete loss of scales, teeth and gill rakers resembling the *fls* phenotype (A–C). Heterozygous *Nkt* zebrafish show an intermediate phenotype of scale loss and patterning defect (arrows) while no effect on fish development is seen (D). Heterozygous *Nkt* also show a dominant effect on the number of teeth (arrows, E) and gill rakers (F), showing deficiencies along the posterior branchial arches and formation of rudimentary rakers along ceratobranchial 1 and 2 (arrows, F). *Cb1–5*, ceratobranchial bones.
doi:10.1371/journal.pgen.1000206.g002

Table 1. Quantitative effect of *fls* on scale number and shape and the effect of background modifiers in *Danio rerio* strains on *fls*^{Δ3T3pl}.

Phenotype/ Genotype	Scale #/ stl	n fish	Scale DV/AP	n scales
+/+	6.8±0.18	4	1.14±0.15	13
<i>fls</i> ^{Δ3T3pl} / Tü	3.0±0.20 ##	2	1.52±0.29 #	8
<i>fls</i> ^{Δ3T3pl} / Tü; <i>mod</i>	5.6±0.44 #	3	1.4±0.3 #	12
<i>fls</i> ^{Δ3T3pl} / WIK	5.84±0.66 #	9	1.43±0.35 #	32
<i>fls</i> ^{fang} / <i>fls</i> ^{fang}	0.97±0.50 ####	2	1.57±0.18 #	7
<i>fls</i> ^{te370f} / <i>fls</i> ^{te370f}	0.41±0.39 ####	6	1.8±0.64 #	16

The total number of scales on one side of alizarin red stained adults of different genotypes were counted and measured. Counts were normalized for standard length (stl) of individual fish as shape and number of scales in the mutants may vary as a measure of size. Shape characteristics of scales were quantified by measuring three to four scales from set positions across the flank of each fish and comparing the height (dorsal-ventral; DV) to length (anterior-posterior; AP) ratios. Results are presented as sample average and standard deviation around the mean. *mod*, inferred genotype of a modifier in Tü background leading to “weak” phenotype. The numerical symbol (#) indicates significant difference compared to wild type values (students *t*, *p*<0.05). The different number of symbols signifies a significantly different phenotypic classes of scale development (#, ##, ###, ####).
doi:10.1371/journal.pgen.1000206.t001

hybrid map to see if any of these genes were linked to *fls*. The *edar* gene is located on LG9 within the determined linkage interval for *fls* (see Methods). We cloned the full-length wild type cDNA of *edar* and found several polymorphisms in the Tü *edar* cDNA when compared to the WIK mapping strain; these polymorphisms were tightly linked with the *fls* mutation and did not show recombination in 238 meioses (Figure S2).

The *edar* gene encodes a transmembrane protein with similarity to tumor necrosis factor receptor (TNFR). The Edar protein contains a conserved TNFR extracellular ligand binding domain

and a cytoplasmic terminal death domain essential for protein interactions with signaling adaptor complexes. The *fls*^{te370f} mutation is an A to T transversion at a splice acceptor site, resulting in missplicing of the mRNA leading to a frame shift in translation and the generation of a premature stop codon (Figure 3B and Figure S2). This allele is a likely molecular null mutation as only a fragment of the ligand-binding domain is present while the transmembrane and cytoplasmic death domains, which are essential for function of this protein, are both absent. The spontaneous mutation *fls*^{10bp212} was found to have a splicing defect leading to the inclusion of intronic sequence. This is predicted to form a protein with incorrect amino acid sequence after residue 212, at the end of the transmembrane domain leading to a premature termination codon (Figure 3B, Figure S2). The two alleles generated by the ENU mutagen both have missense mutations resulting in amino acid changes in the death domain (*fls*^{Δ3R367W}, R367W^(C→T); *fls*^{Δ3T3pl}, I428F^(A→T)). These mutations were found at identical positions as seen in familial cases of HED in humans (Figure 3B, E; [11,12].

The *fang* Allele Uncovers Dose and Organ Specific Sensitivity to Levels of *Eda* Signaling

The *fang* allele of *fls* was isolated in an allele screen for mutants that failed to complement *fls*^{te370f} (Figure 1P). *fls*^{fang} homozygotes do not show any observable effect on lepidotrichia development yet have a reduction of scales and teeth/rakers as seen in other *fls* alleles (Figure 1M–O). The *fang* allele in *trans* to the *te370f* putative null allele shows an intermediate phenotype affecting lepidotrichial growth and a further reduction of teeth and scales suggesting that the *fang* allele is a hypomorph (Figure 1P–R); *fls*^{fang} heterozygotes do not show any differences compared to wild type. The shape and number of the scales in *fang* is similar to the other homozygous *fls* alleles (Table 1). Analysis of *edar* RNA from homozygous *fls*^{fang} showed the presence of two distinct transcripts with an additional larger isoform than seen in wildtype. Analysis of the sequence of the novel isoform showed the addition of intronic sequence leading to a premature termination codon (Figure 3C). The predicted protein would be similar to the *fls*^{10bp212} allele

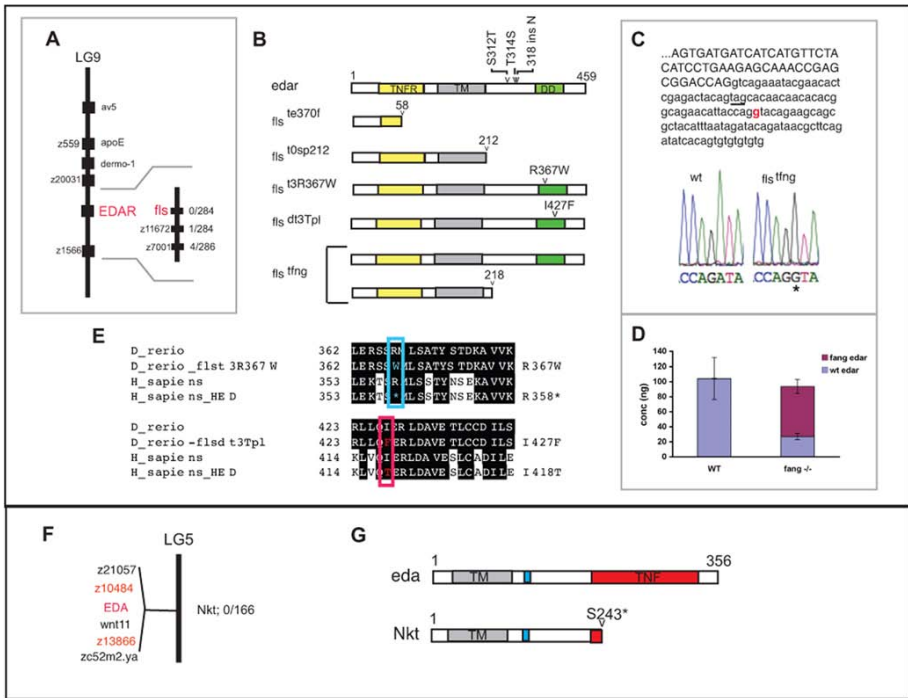


Figure 3. *fls* and *Nkt* are mutations in genes encoding ectodysplasin receptor (*edar*) and its ligand ectodysplasin (*eda*). A) Mapping of *fls* using SSLP markers and placement of the *edar* gene within the candidate region on LG 9 by radiation hybrid mapping. The insert shows genetic linkage of the *fls* gene to local markers on LG 9. The numbers on the right of the insert indicate the number of recombinants seen in identified mutants per the number of meioses tested. B) Schematic of wild type Edar protein and mutant alleles. Polymorphisms seen in the WIK strain are noted above the wild type gene. Mutations that lead to premature termination are represented as truncated proteins showing the predicted residual fragment and position of the identified mutation. C) Analysis of the mutation in *fls*^{tfng}. A unique splice donor site (red) is generated leading to inclusion of additional coding sequence encoding a premature termination codon (underlined). D) Quantitative analysis of different *edar* transcript levels in *fls*^{tfng} homozygotes compared with wildtype. E) Similarity of altered residues in *fls*^{3R367W} and *fls*^{dt3Tpl} with human HED shown in the death domain. The position of the mutated residues in *fls*^{3R367W} (blue box) and in *fls*^{dt3Tpl} (red box) is identical to ones changed in cases of human autosomal dominant HED although the substitution is different. F) Linkage between the *Nkt* allele and *eda* on LG5. G) Schematic of wild type *Eda* protein and position of *Nkt* mutation. Numbers on gene diagrams represent amino acid length. *TNF*, tumor necrosis factor domain; *TNFR*, tumor necrosis factor receptor domain; *TM*, transmembrane domain; *DD*, death domain; the blue box in *Eda* is the furin binding site. doi:10.1371/journal.pgen.1000206.g003

having truncation just after the transmembrane domain at amino acid 218 (Figure 3B and Figure S2). Analysis of the genomic sequence in the mutant revealed that the altered splicing is due to an A to G transition leading to the creation of a new splice donor site in the intron (Figure 3C). Given the presence of both isoforms in homozygous individuals, this novel splice site is used in addition to the normal splice junction. Using quantitative real time PCR we found that the *fang*-specific *edar* transcript represents 74% of the total pool of *edar* transcripts in homozygous mutants (Figure 3D). The dilution of wild type transcripts can explain the observed hypomorphic effect of the allele. From this unique allele of *fls*, it is clear that the phenotypic effect of loss of Eda signaling is dose dependent and that scales and teeth are more sensitive to alterations in the level of Eda signaling than fins.

Ectodysplasin Is Mutated in the *Nacktk* Mutant

EDAR and its orthologue XEDAR recognize specific EDA isoforms that vary by two amino acids [13–16]. The receptor-ligand complex signals through NF- κ B using several adaptor proteins that are generally specific to each receptor. Together, mutations in *Edar* and *Eda* lead to the majority of cases of human HED in which the development of integumentary appendages (hairs, glands and teeth) are affected (OMIM 300451, [17]; OMIM 604095 [18]).

We reasoned that, because of the similarity in phenotype to *fls*, the *Nkt* gene could be *eda*, encoding the ligand for Edar. We isolated the entire coding region for zebrafish *eda* by RACE (Figure S3). The *eda* transcript from the *Nkt* mutant shows a precocious stop codon predicting a truncation of the protein at the beginning

of the TNF domain, which is involved in ligand-receptor binding (S243X^{C-A}); Figure 3G and Figure S3). An analysis of the location of *eda* in the zebrafish radiation hybrid map placed *eda* on LG5. Subsequent linkage analysis of the *Mt* mutation and markers indicated by radiation hybrid analysis demonstrated tight linkage of the mutant to this region (Figure 3F); the S243X mutation was always found in fish with the *Mt* phenotype and served as a consistent genotypic marker.

Role of Ectodysplasin Signaling in Regulating Epithelial Signaling Centers: Scale Placode Formation

In fish, scales are bony elements that develop in the dermis underlying the epidermis. In amniotes, most integumentary organs affected by loss of *Eda* signaling have structural derivatives stemming from the epidermis (e.g. specific keratins of hair, feather and nail, secretory cells of glands). These integumentary organs develop from reciprocal signaling interactions between the basal epidermis and subjacent mesenchyme often controlled by a regional epithelial thickening called the epidermal placode. *Eda* signaling is necessary for the development and patterning of epithelial placodes of many integumentary organs in both the mouse and chick [19–22]. Expression of *Eda* and *Edar* is found predominantly in the basal epidermal cells, but in the case of feathers *Eda* is detected in the subjacent mesenchyme as well [21,22]. Whereas expression of developmental signaling genes such as *sonic hedgehog* (*shh*) in the development of integumentary appendages are comparable between vertebrates [23], evidence for an early developmental role of the epidermis in induction or patterning of the teleost scale is lacking. The formation of an epithelial placode and signaling center in the development of amniote integumentary appendages is associated with histological changes in the basal cells of the epidermis; a similar structure has not been described in fish epidermis [24]. As early teleost scale development is quite different to that of other vertebrate integumentary organs, such as hairs and feathers, we addressed the question whether *Eda* signaling had a similar function in the epidermis of zebrafish during scale formation.

We detected the expression of both *edar* and *eda* in the skin of juvenile fish by whole mount *in situ* analysis (WMISH). The expression of both genes presaged the formation of the initial scale row along the flank just ventral from the midline myoseptum in the caudal peduncle (arrowheads, Figure 4A and C; [24]). During scale formation, the expression of *edar* becomes progressively restricted to the posterior margin (Figure 4B) while *eda* expression persists throughout the scale primordia (Figure 4D). Developmental genes *shh* and *bone morphogenetic protein 2b* (*bmp2b*), whose orthologues are known to be essential for placode development in the mouse and chick, show similar placodal expression as seen with *edar* (Figure 4E and G). Analysis of *shh* and *bmp2b* expression in *fls^{te370f}* indicated the necessity of *edar* function for their expression (Figure 4F and H).

We investigated the development of scale primordia in wild type and mutant *fls^{te370f}* fish by light and transmission electron microscopy. Previous detailed histological work found evidence for raised signaling activity in the epidermis as measured by increased endoplasmic reticulum (ER), and secretory activity of the basal epidermal cells prior to scale formation [23]. However these changes in the basal epidermal cells were not associated regionally with sites of scale formation nor was there any indication of histological changes in basal cell morphology that are associated with placode formation in other vertebrates. To our surprise, in wild type juvenile fish, we discovered the formation of histologically defined, localized assemblies of cells of the basal epidermis that resemble early stages of the formation of hair and feather placodes.

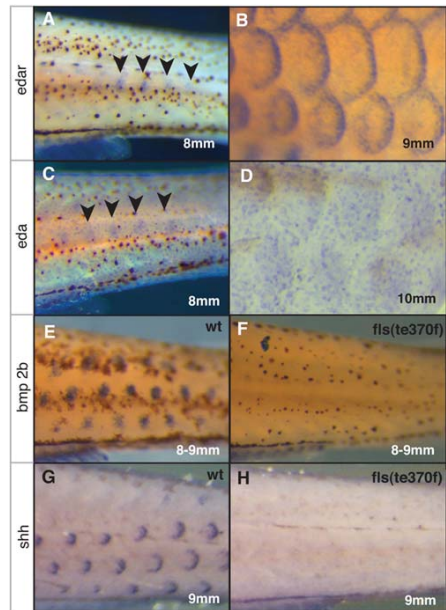


Figure 4. The role of *edar* in expression of developmental patterning genes during early scale development. Expression of *edar* (A, B) and *eda* (C, D) in early forming scales; arrowheads indicate site of expression of initial forming scales. A) *edar* expression above site of scale formation in 8 mm long (approximately 30 dpf juvenile fish) and in larger juveniles (9 mm; 30 dpf). C) *eda* expression during early scale development on the flank (8 mm) and in forming scales of older juvenile fish (10 mm, D). Expression of developmental genes *bmp2b* and *shh* in early scale development in wildtype (E, G) and *fls^{te370f}* (F, H) juveniles (9 mm). doi:10.1371/journal.pgen.1000206.g004

Prior to the development of the scale, the dermis consists of compact collagen layers (stratum compactum) and scattered dermal fibroblasts [24]. The epidermal basal cells have a uniform elongate morphology (black arrows, Figure 5A, D) with high levels of basally located intermediate fibrils (Figure 5G). At the initiation of scale development, there is an accumulation of fibroblasts subjacent to the basal epidermis, associated with a reworking of the collagen strata [24]. We find a specific alteration in the morphology of the basal epidermal cells in wild type juvenile fish that coincides with the initial accumulation of fibroblasts at the sites of scale development (Figure 5B, E). These basal cells become cuboidal and have decreased width, such that they form a unit of closely packed cells (black arrows, Figure 5B, E). This is observed above the localized accumulation of fibroblasts in the dermis (white arrows, Figure 5B, E). In addition, in these placodal-like cells, the ER appears less prominent (data not shown), and hemidesmosomes, the cellular junctions involved in the attachment of the basal epidermal cells to the basal lamina, are almost completely absent (brackets, Figure 5H and I). In contrast, the adjacent lateral epidermal cells show high levels of both ER and hemidesmosomes (data not shown and Figure 5G brackets, respectively).

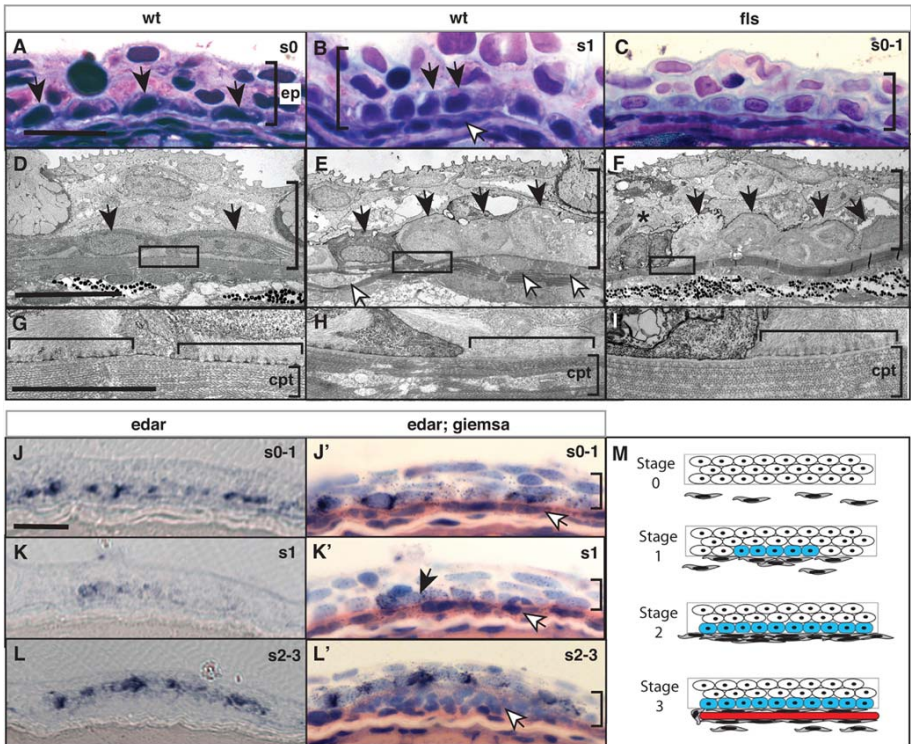


Figure 5. *Eda* signaling regulates the formation of an epidermal placode during scale development. Histological analysis of wild type (A, D, B, E) and *fls*^{ts370f} (C, F, I) integument of 8 mm standard length. In wild type juveniles (B, E), basal epidermal cells (black arrow heads) show a heightened, and cuboidal morphology at sites of scale development as indicated by an accumulation of migrating fibroblast-like cells (white arrowheads). (H) This morphology of the epidermis is associated with a reworking of the collagen layer of the stratum compactum (*cpt*; [24]). This is in contrast to the flattened morphology of basal epidermal cells lateral to those of the scale placode (A, D) and underlying dense stratum compactum (G). In *fls*^{ts370f} this basal epidermal structure is disorganized and cell morphology is disrupted (C, F) including evidence of cell death (asterisk). The lack of reworking of the collagen of the stratum compactum in the *fls*^{ts370f} mutant is associated with retention of hemidesmosomes (horizontal bracket G–I). *edar* is expressed in cells of the wildtype epidermis (J, K, L). Counterstaining of the same sections confirms the expression in basal cells overlying initial accumulating fibroblasts (white arrowheads; J', K', L'). Expression of *edar* is observed prior to organization of the placode and fibroblast aggregation and maintained in cells of the epidermal placode through early scale development (J–L). M) Schematic depicting scale development and *edar* expression. The stages of scale development are modeled using analogous stages as described for hair development [35]; stage 0, nascent epidermis; stage 1, placode specification; stage 2, scale pocket; stage 3, matrix deposition and ossification. Blue, *edar* expression; red, scale formation. *ep*, epidermis; *cpt* stratum compactum. The vertical bracket demarcates the extent of the epidermis in the sections. Measurement bar equals 10 μ m. doi:10.1371/journal.pgen.1000206.g005

In *fls*^{ts370f} juvenile fish, at a corresponding site on the flank as in wild type, we detected the formation of similar aggregations of basal epidermal cells (black arrows, Figure 5C, F). However, unlike the structures found in the wild type zebrafish, the epidermal cells of the placode were disorganized and showed histological evidence of cell death (Figure 5F). As is the case in wild type, the epidermal basal cells in the placode of *fls* display a reduced ER, however hemidesmosomes are present in the same high numbers as in adjacent cells in wildtype (brackets, Figure 5H compared to brackets Fig. 5I). Lateral basal epidermal cells in *fls*^{ts370f}/*edar*

showed elongate morphology similar to those of their wild type siblings (data not shown). The expression of *edar* is seen in the basal cells of forming scale placodes (Figure 5J–L, stages 1–3 Figure 5M) arising during early specification of the scale placode (s1; arrowhead Figure 5K). We were unable to detect *edar* expression in sections due to the weak hybridization signal.

These data support the notion that an epidermal placode is involved in dermal scale formation. Further we find that the epithelial organization and function of the developing scale placode is dependent on *edar*.

Role of Ectodysplasin Signaling in Regulating Epithelial Signaling Centers: Maintenance of the Fin Fold and Establishing Anterior-Posterior Polarity of the Developing Fin

The phenotype of both *Nkt* and *fls* demonstrate that Eda signaling is necessary for fin development. The growth and patterning of lepidotrichia are affected in all fins. Lepidotrichia are specified, however fail to maintain growth and elaboration of the fin rays (Figure 6A–C, H–P). Unpaired fins showed no defects in patterning of the endochondrial bones of the proximal and distal radials (Figure 6K–P); the dorsal pitch of the caudal fin is an

indirect effect of the mutation on swimming without fin rays (amputated fins that fail to regenerate show similar morphology). In *fls* adults, fusions of the distal radials of the pectoral fin are seen at a low penetrance (Figure 6G, data not shown). In *Nkt*, there is an increase in the frequency of patterning and growth defects of the endochondrial components of the fin (Figure 6G). These alterations include the loss of the fourth proximal radial, altered growth patterns of anterior proximal radials 1 and 2, as well as lack of articulation of the distal radials (Figure 6 D–F). *Nkt* causes a strong effect on lepidotrichial growth of both the pectoral and pelvic fins (Figure 6E–F, J). In contrast, a specific effect on the growth of anterior lepidotrichia of the pelvic fin is seen in *fls* where

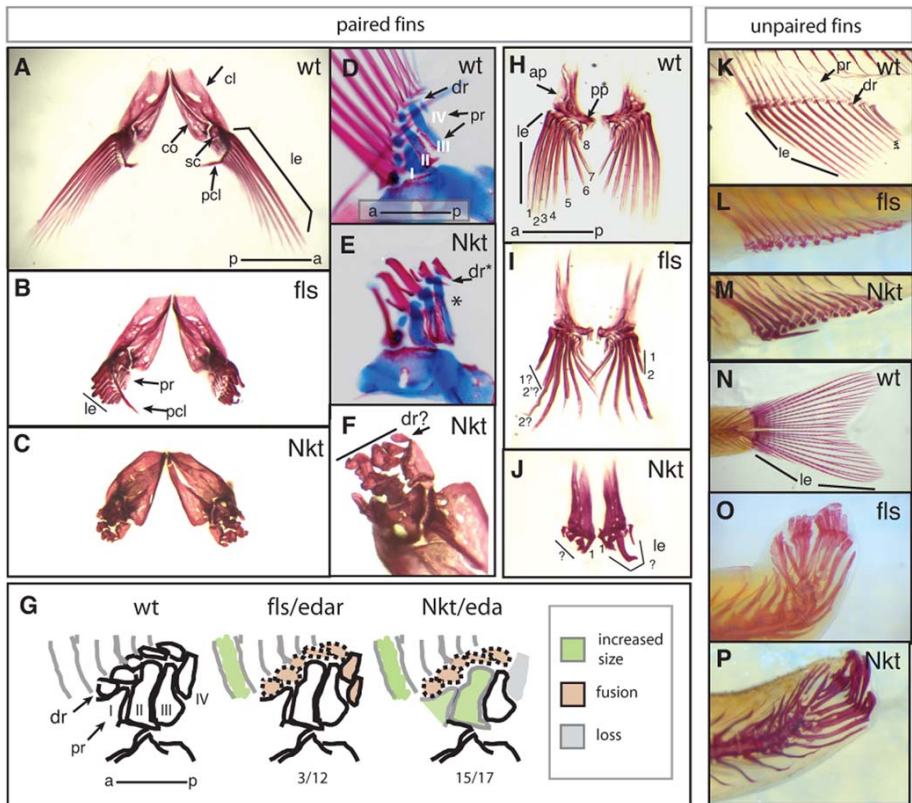


Figure 6. Fin development is defective in *fls* and *Nkt* mutant zebrafish. Alizarin red stained adult zebrafish fins show a drastic effect of *fls*^{6370f} and *Nkt* on development of the lepidotrichial dermal rays of both the paired and unpaired fins. A–C, F) Pectoral fins, anterior-dorsal view; D, E) double staining developing pectoral fins with alcian blue and alizarin red show early patterning of the endochondrial bones of the pectoral fin of size matched wild type and *Nkt* homozygotes (asterisk indicates loss of fourth proximal radial). G) effect of *fls* and *Nkt* mutants on the patterning of the pectoral fin skeleton scored as the number of specimens showing alteration in pattern or form over total analyzed. The identity of the proximal radials is noted (I–IV). H–J) Analysis of pelvic fin development in *fls* and *Nkt* mutants. Numbers denote anterior-posterior identity of the lepidotrichia. K–M) Defects in the formation of the lepidotrichia in adult anal and (N–P) caudal fin of *fls* (L and O) and *Nkt* (M and P). *ap*, ascending process; *cl*, cleithrum; *co*, corticoid; *dr*, distal radial; *sc*, scapula, *le*, lepidotrichia; *pcl*, postcleithrum; *pr*, proximal radial.

doi:10.1371/journal.pgen.1000206.g006

the dermal rays of the anterior (*e.g.* 1,2) are significantly shorter than rays at equivalent positions in wild type (Figure 6I). The asymmetry of lepidotrichial development suggests that, like the proximal endochondrial fin skeleton, the fin rays have a specific regional identity to provide the shape and form of the fin.

Early limb development is driven by a localized organization of epithelial cells at the distal tip of the forming limb, termed the apical ectodermal ridge (AER) [25]. In zebrafish, the AER is involved in larval patterning of the paired fins, while the later stages of fin development are organized by an analogous epidermal formation of the fin fold in both paired and unpaired fins [26,27]. In tetrapod limb development anterior-posterior specification is controlled by posterior mesenchyme expressing *Shh*. The function of this zone of polarizing activity (ZPA) expressing *Shh* is maintained by reciprocal signaling interactions between the ZPA and the AER. This interaction is necessary for proper patterning and growth of the tetrapod limb. In the zebrafish, *shh* and signals from the AER also orchestrate patterning and outgrowth of the early fin buds [28–30]. In addition, genes functioning early in fin development, such as *shh*, play important roles during late fin development regulating growth and branching of lepidotrichia growth [31].

We investigated the regulation of *edar* in mid to late fin development focusing on the development of the paired fins. In

early fin fold stage of pectoral fin development (8 mm), we detected *edar* expression in both the distal margin of the endochondrial radials (black arrowhead, Figure 7A) as well as more distally in the forming lepidotrichial rays (Figure 7A). The expression of *edar* in the fin fold had a posterior bias in wild type fins (Figure 7A, white arrow). The pelvic fin showed similar expression of *edar* in forming lepidotrichial rays (Figure 7E). *shh* and *bmp2b* expression was observed in the forming lepidotrichia of both the pectoral and pelvic fins of wild type juveniles, having a similar distal bias in the leading margin of all rays (Figure 7C, G and I, K, respectively). Expression of all three genes in *fls* was decreased in the anterior portion of the pectoral fins (Figure 7B, D, J). However, residual expression of all three genes was found in the posterior margin of the fin (Figure 7B, D, J arrow). In the pelvic fins, similar loss of anterior expression of *edar* (Figure 7F) and *shh* (Figure 7H) was seen in the *fls* mutant. We did not detect any difference in *bmp2b* expression in the pelvic fins even though obvious morphological differences in the developing rays of the samples could be seen (Figure 7L).

We asked if the alteration of polarity of gene expression in the *fls* mutant was associated with regional cell death. Using acridine orange uptake as an assay for cell death (*e.g.* [32]), we analyzed fins of *fls* and siblings at size matched stages (7–9 mm) for regional

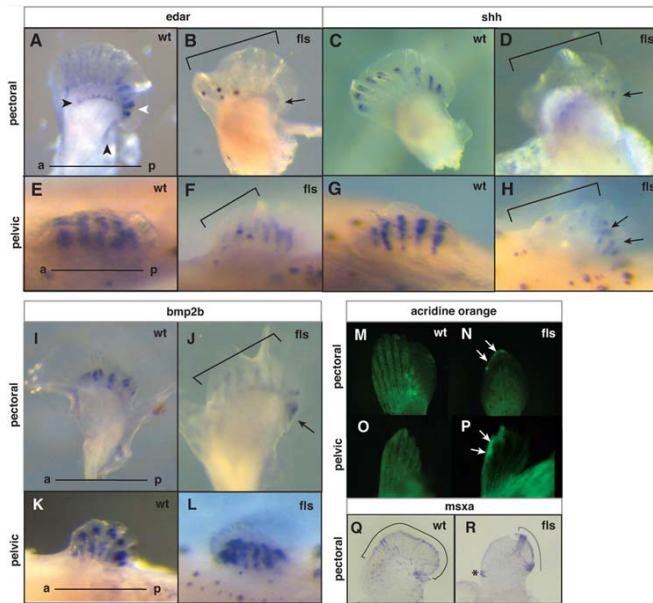


Figure 7. Eda signaling and the maintenance of anterior-posterior pattern in late paired fin development. Analysis of *edar* (A–B, E–F), *shh* (C–D, G–H), and *bmp2b* (I–L) expression in developing pectoral (A–D, –J) and pelvic fins (E–H, K–L) from 8 mm juvenile fish of wild type (A, E, C, G; I, K) and *fls*^{MS204} mutant fish (B, F; D, H; J, L). A–B Arrowheads indicate two distinct patterns of *edar* expression in the pectoral fin: an expression that marks the posterior edge and distal region of the development of the proximal radials (black); and a posterior bias of *edar* expression in the forming lepidotrichia (white). Arrows point out the remaining posterior expression in mutant fins. Brackets in all panels outline anterior deficiencies in gene expression in *fls* mutant fins. M–P, analysis of patterns of cell death in the developing paired fins by retention of acridine orange stain. N, P) Arrows point out anterior distal regions of cell death in both pectoral and pelvic fins from the mutant; (M, N) pectoral fin and (O, P) pelvic fin respectively. Q, R) Expression of *msxa* in wild type and mutant pectoral fins. Region of expression outlined with brackets; asterisk marks an ectopic site of expression. doi:10.1371/journal.pgen.1000206.g007

patterns of cell death. In 7 mm juveniles, we detect a differential retention of acridine orange between *fls* and siblings in the anterior, and anterior-distal margin of the developing pectoral fin (Figure 7M–N). Similarly, in the pelvic fin of 8–9 mm juveniles, retention of the label was seen in the anterior distal margin of the fin (Figure 7O–P). Consistent with these data suggesting asymmetrical loss of the fin fold epidermis, we find that *msxa*, a marker of the distal epithelium, is differentially expressed in the mutant (Figure 7Q and R).

We next analyzed gene expression during late development of the lepidotrichia. The expression of *edar* during late fin development was observed in forming lepidotrichia of all fins with a distal bias in its expression (Figure 8C). The expression in the forming dermal ray was similar in both location and timing to that of *bmp2b* and *shh* (Figure 8A–B, asterisk). In addition, *edar* was found expressed proximally between forming rays and at the distal margin (Figure 8C arrow). We were unable to resolve a clear signal for *eda* in the forming fins using WMISH. The expression of *edar* in the distal lepidotrichial tips suggests a late developmental role of Eda signaling in regulating formation of the lepidotrichia in concert with *shh* and *bmp2b*.

Histological analysis of *fls* mutant fins at an early stage of lepidotrichial formation reveal a general deficiency of the development of the entire mesodermal component of the fin such as cartilage and muscle in both the paired (pectoral fin, Figure 8D, E) and unpaired fins (anal and caudal fins, Figure 8F–G; H–I, respectively). In contrast, the epidermis of the fin is formed and is

similar to that of size matched siblings. However, close inspection of the distal tip of the fins showed disorganization of the epidermis and degeneration of distal epidermal nuclei (insets Figure 8F, J). From these analyses, we hypothesize that loss of *edar*-mediated signaling leads to a defect in mesenchymal cell proliferation, muscle cell migration and defective lepidotrichial growth in the fin that correlates with degenerative defects seen in the distal epidermal fin fold.

Discussion

We used a forward mutagenesis approach in the zebrafish to investigate the developmental mechanisms that underlie changes in adult form. Here, we identified a role of Eda signaling in the development of the dermal skeleton in the adult zebrafish. Mutations in either *Eda* or *Edar* have been shown previously to cause defects in integumentary appendages in several mammalian species. Additionally, Eda signaling genes have been associated with variation in morphology that occurred during the evolution of teleost fishes (*eda*) and in variation of human populations (*Edar*) [33,34]; see below). Thus, through a forward genetic approach, we were successful in identifying genes that are important for the development and variation in adult form. We further show that the ENU generated alleles of *fls*, *t3R357W* and *d3Tpl*, affect similar residues as those mutated in familial cases of HED [11,12,18] supporting the utility of adult zebrafish mutants as models for the investigation of heritable human disease.

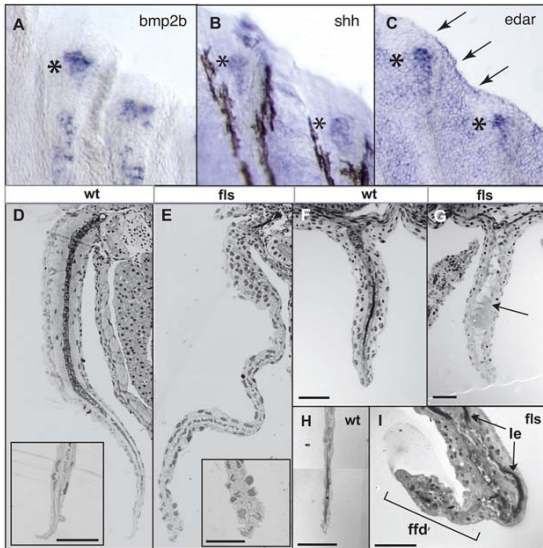


Figure 8. Eda signaling is required for the function of the fin fold during late fin development. Expression of *bmp2b* (A), *shh* (B) and *edar* (C) transcripts in developing juvenile (8 mm, 30 dpf) fin rays of the caudal fin; asterisks indicate regional expression within distal tip of developing ray; arrows in (C), expression in distal epidermis of the fin fold. D–I) Histological analysis of both paired (pectoral, D, E) and unpaired fins (anal F, G; and caudal, H, I) from *fls*^{t3R357W} and wild type siblings. *fls*^{t3R357W} fins showed a general deficiency in the maturation of the muscle and dermis of the fin (arrow G; acellular debris in anal fin of *fls*). Insets (D, E), tip of fin at higher magnification showing degeneration of the nuclei of the epidermis in the mutant fin. *ffd*, fin fold; *le*, lepidotrichia of the fin rays. doi:10.1371/journal.pgen.1000206.g008

Conserved and Ancestral Role of Eda Signaling in Vertebrate Development

We show that Eda signaling is necessary for the development and patterning of the dermal bones of the skull, scales, fin rays as well as teeth of the adult zebrafish. The correlated effect in these zebrafish structures is due to a developmental role of Eda signaling in organizing epithelial cells into signaling centers. In the case of scale development, Eda signaling is necessary for the basal epidermal cells to form a functional placode. Epidermal placodes are involved in the formation of integumentary appendages of other vertebrates such as hair, glands, feathers and teeth. These structures have been shown to act as signaling centers to orchestrate appendage development. We speculate that a primary function of Eda signaling in scale development is to promote cell-cell adhesion within the placode and that the coordinated signaling of the placode induces fibroblast assembly in the underlying dermis, an early step in scale formation.

Schmidt-Ullrich et al. documents the formation of the hair placode and outline a stage series of placode formation in the mouse [35]. They report that the *downless* mouse mutant, which has a mutation that disrupts the mouse *Edar* gene [36], causes arrest of placode formation at a pre-placode stage of development (P0-P1). This stage closely resembles the stage of scale placode formation that is affected in *fls* shown here. In agreement with our findings, Schmidt-Ullrich et al. further note a reduction of cell-to-cell adhesion within the placode and find increased apoptosis in the absence of Edar function. This suggests that there is a conserved developmental role of Edar between dermal scales of fish and mammalian hairs. During normal hair development, the hair placode invaginates to form the hair bulb. By contrast, the post-placodal events of scale formation in fish do not involve morphogenetic changes of the epidermis, rather the accumulation of mesenchymal cells subjacent to the epidermal placodal cells to form the scale pocket. Thus, Eda signaling in mammals and teleosts is conserved in the early phases of placode formation in controlling the functional continuity and signaling of the epidermal placode to orchestrate appendage formation. However, the downstream interpretation of the epithelial-mesenchymal signaling differs beyond this point leading to altered morphogenetic responses and histological differentiation to form diverse appendages such as scales and hair.

In the fin, Eda signaling directs late stages of fin development such as the formation and growth of the dermal rays. The effect of loss of *edar* function on fin development uncovers an intrinsic developmental polarity of the late developing fish fin. This is seen both in the development of the proximal endochondrial bones as well as in the formation of the fin rays. We find that the change in patterning in the mutants is correlated with asymmetrical cell death of the distal marginal fin fold as well as a reduction of *Shh* expression. This finding is similar to the effect of loss of AER function resulting in anterior-distal cell death and reduction of *Shh* activity in tetrapod limbs [37–39]. While there has not been any previous indication of a role of Eda signaling in tetrapod limb development, both the expression of *Edar* and related receptor, *Trop*, have been detected in the AER of mice [40,41].

A second developmental role of Eda signaling in the developing fin is observed in the outgrowth and patterning of the individual lepidotrichial rays evidenced by expression of *edar* in the distal tip of the forming rays and distal epidermis. The expression of *edar* is again associated with that of *shh* and *bmp2b*. The expression of *shh* and *bmp2b* has been shown to be within the basal epidermis overlying the forming lepidotrichia [31]. Given the expression of *edar* during fin development and the defects observed in the distal epidermis in the mutant, it is likely that the function of Eda

signaling is to maintain the growth permissive function of the fin fold through its regulation of a distal signaling center of individual rays. The concomitant expression of *edar*, *shh* and *bmp2b* in both distal lepidotrichia development and during placode specification suggest that they work in concert to mediate the inductive and/or permissive effects of the epidermis – thus organizing signaling centers for the development of the dermal skeleton.

While the nature of the defect in tooth formation or dermal bone patterning of the skull in the *fls* and *Mt* mutants has not been characterized in detail, there is evidence that inductive signaling from the pharyngeal epithelium or cranial epidermis is necessary for appropriate development of both tooth [42] and skull [6], respectively; Eda signaling likely shares a common role in inductive signaling in each of these diverse organs.

Genetic Commonalities of Eda Signaling: From Fish to Man

Mutations in the *EDAR* and *EDA* genes underlie a large percentage of autosomal and X-linked HED in humans, respectively [18,43]. In the case of *EDAR*, both recessive and dominant mutations are associated with the HED phenotype in humans, however dominant mutations are found only within the death domain of the protein. These mutations are believed to act in a dominant negative fashion, although by unknown mechanisms [44]. We see similar dominance of a *fls* allele that affects the death domain of *edar* while all *fls* mutations outside this region do not show a dominant phenotype. Autosomal dominant HED in humans caused by mutation of *EDAR* within the death domain displays a large degree of phenotypic variability [12]. For example, the I418T mutation in human, which affects the same amino acid as *fls*^{d371p} (I327F), shows distinct phenotypic variability depending on genetic background [18]. Interestingly, the *fls*^{d371p} zebrafish mutant displays similar dominance and variation as the human allele affecting the same residue. These findings suggest that the molecular mechanisms of Edar function are similar between fish and humans.

X-linked HED caused by mutations in the human *EDA* gene represents the majority of cases of this disease [43,45]. The zebrafish *Mt* mutation described here is affected in the TNF domain and shows a mild dominant phenotype (S243X). As the *EDA* gene is sex linked in humans the molecular nature of different alleles can not be analyzed since the allele will be hemizygous in males and mosaic in female carriers. The zebrafish *eda* gene is autosomal in the zebrafish. Thus, *Mt* exposes previously unknown dominant function of mutations in this gene since a true heterozygous condition is formed. Hemizygous wildtype condition in humans indicates that the dominance we see in *Eda* is probably not due to haploinsufficiency. Since *EDA* functions as a homotrimeric protein [46], a plausible mechanistic explanation for the observed dominance of *Mt* is that the C-terminal truncation inhibits the function of the wild type protein in binding to Edar.

Eda Signaling and the Development and Variation of Adult Form

Mutations affecting Eda signaling lead to impaired development of integumentary appendages of fish, birds, and man. These changes lead to viable changes in adult morphology. Mutations disrupting Eda signaling have been described for another teleost species. The spontaneous *rs-3* mutant in medaka (*Oryzias latipes*), is shown to have a transposon insertion in the 5' UTR of *edar* resulting in the reduction of scales but no effect on fin or teeth development [47]. The zebrafish mutations described here show a previously undescribed role of Eda signaling in the development of the fins, teeth, as well as dermal bones of the skull – phenotypic

traits observed in human alleles but not reported in the medaka mutant. As the phenotype of the *rs-3* mutant is similar to the *fls^{shans}* allele in the zebrafish, it is likely that the more subtle phenotypes observed in the medaka mutant is due to partial loss of function of *edar* caused by a hypomorphic *rs-3* allele [47].

The graded effects seen in the expressivity of mutations affecting *eda* and *edar* points to a dose sensitive readout of the Eda signaling pathway that affects different organ systems with varied expressivity. In the dominant *fls^{dic31pl}* or *Mt* heterozygotes, the shape and number of scales and teeth as well as patterning of the skull are affected, however there is no change in fin ray development. Similarly, the *fang* allele of *fls* clearly demonstrates this dose sensitivity as functional copies of Edar are titrated by the concomitant use of a new splice site in the mutant leading to the reduction in the amount of wild type transcript made (Figure 3D). This reduction in the amount of *edar* transcripts cause defects in scale and tooth development, however fins are normal. *fang/te37Of*, in which the *fang* allele is in *trans* to a presumed null, further reduces the relative levels of wild type *edar* transcripts leading to further reduction of both teeth as well as fin lepidotrichia. Similar dose sensitive responses to levels of EDA signaling are seen in tooth development of the mouse regulating the number and shape of teeth [48,49]. There are several reports of hypodontia in humans resulting from altered EDA function that do not show other phenotypes such as hypotrachiosis or nail defects [50–52]. Given our findings, it is likely that these particular alleles are hypomorphic and this is sufficient to explain the differential organ sensitivity to levels of EDA signaling during development. These data indicate that control of the level of Eda signaling in post-embryonic development is an essential component for the determination of the number and form of many different organ systems of the adult.

Supporting this finding, we observed significant modification of expressivity of *fls^{dic31pl}* in different genetic backgrounds indicating the existence of genetic modifiers of Eda signaling. This sensitivity of Eda signaling to genetic modifiers occurs in other teleost fish as well. In our analysis of the medaka *rs-3/edar* mutant, we find a high degree of variability in the extent of scale formation (Figure S4) suggesting the existence of background modifiers of Edar function in this species. Additionally, evidence from the stickleback, *Gasterosteus aculeatus*, suggests that genetic variance at the *eda* locus underlies differences in the extent of dermal plate formation in diverged populations of this species [33]. A quantitative trait analysis (QTL) of lateral plate formation in a low-plated form of the stickleback indicates a significant modification of the reduced plate phenotype (*eda* locus) with modifying effects within and between loci affecting plate number and size [53,54]. Interestingly, recent evidence also shows a significant association between the *edar* locus and dermal plate number in sticklebacks in addition to the predominant *eda* locus [55]. Thus variation at these gene loci may act in concert to regulate number of dermal plates/scales.

Thus, while loss of Eda signaling can lead to severe phenotypes, the phenotypic consequences of variation in Eda signaling are graded and canalization of Eda signaling is prevalent. Therefore, buffering of the phenotypic outcome that results from defective Eda signaling could be a common mechanism that permits viable and diverse phenotypes. These viable phenotypic variations then could serve as a basis for selection. The lack of a coding change at the *eda* locus in sticklebacks that is associated with the loss of dermal plates has led to the argument that, in this case, evolution of this trait is due to changes at *cis*-regulatory elements controlling *eda* expression [33]. Our findings on the dose and organ specific sensitivity of Eda signaling in different structures of the zebrafish argues that evolution of this trait could result from a regulation of absolute levels of expression.

Interestingly, recent analysis of single nucleotide polymorphism (SNP) frequency in human populations supports the role of Eda signaling in causing phenotypic variation. Analysis of SNP variation between diverse human populations shows evidence of selection of the *EDAR* locus in East Asian and American populations [56,57]. A defined allelic variant of *EDAR* within these populations leads to a coding change in the death domain of EDAR and is a candidate allele for altered gene function that could have led to the region being fixed in these populations [34]. There is evidence from association data that this allele is associated with thick hair in these populations [58], however the full extent of phenotypes that are affected in these populations that are related to EDA signaling has not been analyzed. It is interesting to note that recent work has identified this allele of *EDAR* as having an enhanced effect on Eda signaling in mouse models containing the altered human residue [59]. Given that variation in the number and shape of integumentary derivatives of the dermal skeleton are a common morphological change in teleost evolution *e.g.* [60], it will be important to further investigate the prevalence and type of genetic changes in Eda signaling genes in cases of natural variation of these adult characters.

Mutagenesis and Allele Designation

Zebrafish mutagenesis was performed following [61] with 5 treatments of 3.3–3.5 mM ethylnitrosourea. Screen design was similar to that described [62]. Allele designation was determined using standard nomenclature with the addition of the molecular lesion or phenotypic description (when appropriate) to the designation. The serial numbers of the mutants found in the ZF models screen are as follows: *fls^{i3R367W}* (#0621); *fls^{dic31pl}* (#1248); *Nkx^{h5S243X}* (#1261). Information on the screen can be found at <http://www.zf-models.org/>. The screen for additional *fls* alleles used mutagenized *TLF* founder males treated similarly as Tü males used in the screen.

Mapping

Rough mapping of F2 progeny against a reference panel of SSLP markers [63] indicated that *fls* was located on linkage group (chromosome) 9 (LG9) with loose linkage to z20031 (61.3cR; Figure 3A). We found *fls* to be closely linked to markers z7001 and z11672. Results from radiation hybrid screening indicated linkage of zebrafish *edar* to markers positioned on LG9 in the region predicted by initial mapping analysis. Analysis of flanking markers and internal polymorphisms in *edar* showed tight linkage of the *fls* mutation to the *edar* gene. Using the defined molecular differences between WIK and Tü strains, we did not find recombination in 238 meioses indicating that the mutation was located less than 0.4 cM away.

Cloning and Sequence Analysis

We isolated the full-length cDNA of zebrafish *edar* and *eda* by reverse transcription (RT) PCR using sequences provided from genomic alignments and subsequent amplification of the cDNA ends by rapid amplification of DNA ends (RAGE). cDNA was generated from RNA from blastemas of amputated caudal fins that had been allowed to regenerate for two days. cDNA sequences of zebrafish *edar* and *eda* genbank accession numbers are EF137867 and EF137866, respectively. Protein alignment of Edar and Eda were generated by ClustalW alignment (<http://www.ebi.ac.uk/clustalw/>) and Box Shade software (http://www.ch.emblnet.org/software/BOX_form.html) using a 0.4 identity threshold. *Edar* and *eda* sequences of other species were obtained from genomic databases at NCBI (<http://www.ncbi.nlm.nih.gov/>), Sanger (<http://www.ensembl.org/index.html>), and Tigr (<http://www.tigr.org/tdb/tgi/>).

Real Time PCR was performed on cDNA obtained from blastemas from two day old caudal fin regenerates. Calculations were made from three biological replicates and three technical replicates according to [64]. Primers were designed for wild type specific transcripts by using sequence from the neighbouring exon borders that are not adjacent to each other in Fang-transcripts. Fang specific primers were designed against the fang specific transcript sequence, which is spliced out in wild type. Crossing points of the control reaction, which were higher than in the water control, were set to the value for water. Normalization was done against the efficiency of primers to β -actin.

Bone Stain and Measurements

Adult bones were stained with alizarin red. Embryos were fixed in formalin (3.7% formaldehyde), briefly dehydrated in 70% ethanol, and placed in 1 g/l alizarin red; 0.5% KOH until bones suitably stained. Fish were destained in 1% KOH until background stain was lost and subsequently cleared in glycerol for analysis. For analysis of forming cartilage, fish were pre-stained in alcian blue from 4–24 hours. The fish were then destained, lightly trypsinized (3 g/l; 37°C) and processed for alizarin red staining.

Skeletal measurements were made using digitizing software from Zeiss using a dissecting microscope. Measurements were made from fixed landmarks on each axis of the skull that did not vary depending on position of the suspensorium: the premaxilla was used for the distal most point on the length (L) axis, while the quadrate-angular joint was used as a ventral landmark for the height (H) axis. Raw measurement values are represented as normalized ratios of the distance along each axis in relation to the position of the center of the eye; values are normalized for standard length of the fish.

Whole Mount In Situ Hybridization and Immunostaining

Probes for whole mount *in situ* hybridization were generated by reverse transcription from cDNA made from regenerating caudal fin tissue. Digoxigenin labeled RNA probes were purified using P-30 micro bio-spin columns before use (BioRad). WMISH protocol was performed as described [65], at 70°C and with the addition of 0.1% CHAPS to hybridization and post hybridization wash buffers. Reactions were stopped in PBS, post-fixed and placed in methanol overnight to reduce non-specific staining.

Acridine orange (Sigma) was used as a marker of apoptosis in developing tissue [32]. Juveniles were immersed in fish water containing 5 μ g/ml acridine orange for 5 minutes and then washed with fish water, anesthetized and post-fixed in formalin to assist visualization of staining.

Statistical Methods

Analysis of cranial measurements were performed using Hotelling's T squared test for two dependent variables. For scale counts and size dimensions, a *t*-statistic for differential means was used to assess significance. Calculations and probability assessment were calculated using Biosoft 200 software (www.biosoft.com) and Excel statistical package.

Electron Microscopy

Specimens of 8–9 mm juvenile fish were fixed with a mixture of 4% formaldehyde in PBS and 1–2.5% glutaraldehyde at room temperature and subsequently placed at 4°C. After post-fixation with 1% osmium tetroxide in 100 mM PBS for 1 h on ice, samples were washed with H₂O, treated with 1% aqueous uranyl acetate for 1 h at 4°C, dehydrated through a graded series of ethanol and embedded in Epon. Ultrathin sections were stained with uranyl

acetate and lead citrate and viewed in a Philips CM10 electron microscope. In addition, toluidine blue stained Epon sections of 0.5 or 3 μ m thickness were prepared for light microscopy.

Supporting Information

Figure S1 *fls* and *Nkt* alter size and proportion of the adult zebrafish skull. In addition to variations in integumentary structures, *fls* and *Nkt* exhibited a distinct change of the shape and size of the adult skull. Measurements of the absolute proportions of the adult skull, normalized for overall growth of the fish as determined by standard length, demonstrate that both *fls* and *Nkt* homozygous mutations result in overall larger skulls of the fish [*fls*^{ec370f/ec370f}, n = 16, T₂ = 23.7, p < 0.001; *Nkt*, n = 10, T₂ = 64.1, p < 0.001; *fls*^{ec370f/dt31pl}, n = 6, T₂ = 22.8, p < 0.005]. The dominant effect of *Nkt* and *fls*^{dt31pl} seen in development of the scale pattern was not observed in the formation of skull size. However, an analysis of changes in the proportional development of the skull by measurements of the relative positioning of the eye within the skull (L1/L2, H1/H2; Panel A) showed a significant and dominant effect of *Nkt*, *fls*^{dt31pl} on the patterning of the skull (Panel C). This effect was seen in *fls*^{ec370f} homozygotes as well and was not specific to particular alleles of *fls*. The alteration in skull size and shape in the mutants does not involve loss of a particular organ structure or specific bone, rather a change in proportions of the developing skull.
Found at: doi:10.1371/journal.pgen.1000206.s001 (3.39 MB TIF)

Figure S2 A comparison of *edar* sequence in representative vertebrates. *edar* alleles *fls*^{dt31pl} and *fls*^{SR367W} positioned above sequence. Sites of splicing defects of *fls*^{ec370f} and *fls*^{09p213} alleles demarcated with * marker. Yellow, TNF domain; Grey, transmembrane domain; Green, death domain; Red, polymorphic sites in WIK mapping strain.
Found at: doi:10.1371/journal.pgen.1000206.s002 (0.04 MB DOC)

Figure S3 A comparison of *eda* sequence of representative vertebrates. Blue, transmembrane domain; Green, furin cleavage site; Yellow, TNF domain; asterisk *Nkt*^{dt5238X} allele; |, deleted residues in alternate spliced form of *Eda-2*.
Found at: doi:10.1371/journal.pgen.1000206.s003 (0.04 MB DOC)

Figure S4 Scale formation and variation in the *rs3/edar* medaka mutant on the *cs-2* background. (A) Alizarin-red stained *rs3* medaka showed substantial scale formation and variation of the extent of scalation. (B) Wild type *cs-2* strain scalation pattern.
Found at: doi:10.1371/journal.pgen.1000206.s004 (5.72 MB TIF)

Acknowledgments

The authors would like to thank Drs. M. Sonawane, K. Siegfried, C. Koehler, M. Levesque, and JY Sire for helpful comments on the manuscript, Dr. M. Hargrave for contributing the *fls*^{09p213} background allele, M. Akimenko for *msxa* cDNA, and Dr. Vu Nguyen for discussions and sharing of results before publication. We are grateful to Dr. Hiroshi Mitani in his gracious offer to provide *medaka/rs-3* mutant for anatomical analysis. In addition, the authors would like to thank the assistance of Dr. Robert Geisler and Ines Gehring for radiation hybrid analysis, Jennifer Zenker for assistance with characterization of the *fls*^{ec370f} mutant, and Brigitte Sailer and Iris Koch for their expertise in histology. Lastly, we would like to thank the assistance and advice of three anonymous reviewers.

Author Contributions

Conceived and designed the experiments: MPH. Performed the experiments: MPH NR HS SP. Analyzed the data: MPH NR HS SP PK. Contributed reagents/materials/analysis tools: MPH NR. Wrote the paper: MPH NR CNV.

References

- Richardson MK (1999) Vertebrate evolution: the developmental origins of adult variation. *Bioessays* 21: 604–613.
- Stern DL (2000) Evolutionary developmental biology and the problem of variation. *Evolution Int J Org Evolution* 54: 1079–1091.
- Sire JY, Hysuysse A (2003) Formation of dermal skeletal and dental tissues in fish: a comparative and evolutionary approach. *Biological Reviews* 78: 219–249.
- Hysuysse A, Sire JY (1998) Evolution of patterns and processes in teeth and tooth-related tissues in non-mammalian vertebrates. *Eur J Oral Sci* 106 Suppl 1: 437–481.
- Coulombre AJ, Coulombre JL (1962) The skeleton of the eye. I. Conjunctival papillae and scleral ossicles. *Dev Biol* 5: 392–401.
- Sil AK, Maceda S, Sano Y, Roop DR, Karim M (2004) IkappaB kinase-alpha acts in the epidermis to control skeletal and craniofacial morphogenesis. *Nature* 428: 660–664.
- Bell MA, Foster SA, eds. *The Evolutionary Biology of the Threespine Stickleback*. Oxford: Oxford University Press, 571 p.
- Donoghue PC, Sansom IJ (2002) Origin and early evolution of vertebrate skeletization. *Microsc Res Tech* 59: 352–372.
- Mikkola ML, Thesleff I (2003) Ectodysplasin signaling in development. *Cytokine Growth Factor Rev* 14: 211–224.
- Haffter P, Odenthal J, Mullins MC, Lin S, Farrell MJ, et al. (1996) Mutations affecting pigmentation and shape of the adult zebrafish. *Dev Genes Evol* 206: 260–276.
- Monreal AW, Ferguson BM, Headon DJ, Street SL, Overbeck PA, et al. (1999) Mutations in the human homologue of mouse *dl* cause autosomal recessive and dominant hypohidrotic ectodermal dysplasia. *Nat Genet* 22: 366–369.
- Lind LK, Sieckens-Blicks C, Lejon K, Schmitt-Egenolf M (2006) EDAR mutation in autosomal dominant hypohidrotic ectodermal dysplasia in two Swedish families. *BMC Med Genet* 7: 80.
- Yan M, Wang LC, Hymowitz SG, Schilbach S, Lee J, et al. (2000) Two-amino acid molecular switch in an epithelial morphogen that regulates binding to two distinct receptors. *Science* 290: 523–527.
- Bayes M, Hartung AJ, Ezer S, Pospa J, Thesleff I, et al. (1998) The anhidrotic ectodermal dysplasia gene (EDA) undergoes alternative splicing and encodes ectodysplasin-A with deletion mutations in collagenous repeats. *Hum Mol Genet* 7: 1661–1669.
- Hymowitz SG, Compaan DM, Yan M, Wallweber HJ, Dixit VM, et al. (2003) The crystal structures of EDA-A1 and EDA-A2: splice variants with distinct receptor specificity. *Structure* 11: 1513–1520.
- Elomaa O, Pulkkinen K, Hanniussu U, Mikkola M, Saarialho-Kere U, et al. (2001) Ectodysplasin is released by proteolytic shedding and binds to the EDAR protein. *Hum Mol Genet* 10: 953–962.
- Kere J, Srivastava AK, Montonen O, Zonana J, Thomas N, et al. (1996) X-linked anhidrotic (hypohidrotic) ectodermal dysplasia is caused by mutation in a novel transmembrane protein. *Nat Genet* 13: 409–416.
- Chassaing N, Bourthoumie S, Cossee M, Calvas P, Vincent MC (2006) Mutations in EDAR account for one-quarter of non-EDA-related hypohidrotic ectodermal dysplasia. *Hum Mutat* 27: 255–259.
- Barsh G (1999) Of ancient tales and hairless tails. *Nat Genet* 22: 315–316.
- Mou C, Jackson B, Schneider P, Overbeck PA, Headon DJ (2006) Generation of the primary hair follicle pattern. *Proc Natl Acad Sci U S A* 103: 9075–9080.
- Houghton L, Lindon C, Morgan BA (2005) The ectodysplasin pathway in feather tract development. *Development* 132: 863–872.
- Drew CF, Lin CM, Jiang TX, Blunt G, Mou C, et al. (2007) The Edar subfamily in feather placode formation. *Dev Biol* 305: 232–245.
- Sire JY, Akimeno MA (2004) Scale development in fish: a review, with description of sonic hedgehog (shh) expression in the zebrafish (*Danio rerio*). *Int J Dev Biol* 48: 233–247.
- Sire JY, Allizard F, Bahiir O, Bourguignon J, Quilhae A (1997) Scale development in zebrafish (*Danio rerio*). *J Anat* 190: 545–561.
- Saunders J (1948) The proximodistal sequence of origin of the parts of the chick wing and the role of the ectoderm. *J Exp Zool* 109: 303–403.
- Grandel H, Schulte-Merker S (1998) The development of the paired fins in the zebrafish (*Danio rerio*). *Mech Dev* 79: 99–120.
- Dane PJ, Tucker JB (1985) Modulation of epidermal cell shaping and extracellular matrix during caudal fin morphogenesis in the zebra fish *Brachydanio rerio*. *J Embryol Exp Morphol* 87: 145–161.
- Akimeno MA, Ekker M (1995) Anterior duplication of the Sonic hedgehog expression pattern in the pectoral fin buds of zebrafish treated with retinoic acid. *Dev Biol* 170: 243–247.
- Schauerte HE, van Eeden EJ, Fricke C, Odenthal J, Strahle U, et al. (1998) Sonic hedgehog is not required for the induction of medial floor plate cells in the zebrafish. *Development* 125: 2983–2993.
- Grandel H, Draper BW, Schulte-Merker S (2000) *dackel* acts in the ectoderm of the zebrafish pectoral fin bud to maintain AER signaling. *Development* 127: 4169–4178.
- Laforest L, Brown CW, Poleo G, Geraudic J, Tada M, et al. (1998) Involvement of the sonic hedgehog, *patched 1* and *bmp2* genes in patterning of the zebrafish dermal fin rays. *Development* 125: 4175–4184.
- Abrams JM, White K, Fessler LI, Steller H (1993) Programmed cell death during *Drosophila* embryogenesis. *Development* 117: 29–43.
- Colosimo PF, Hosemann KE, Balabhadra S, Villarreal G Jr, Dickson M, et al. (2005) Widespread parallel evolution in sticklebacks by repeated fixation of Ectodysplasin alleles. *Science* 307: 1928–1933.
- Sabeti PC, Varilly P, Fry B, Lohmueller J, Hostetter E, et al. (2007) Genome-wide detection and characterization of positive selection in human populations. *Nature* 449: 913–918.
- Schmidt-Ullrich R, Tobin DJ, Lenhard D, Schneider P, Paus R, et al. (2006) NF- κ B transmits EDA A1/EDA-R signalling to activate Shh and cyclin D1 expression, and controls post-initiation hair placode down growth. *Development* 133: 1045–57.
- Headon DJ, Overbeck PA (1999) Involvement of a novel Tnf receptor homologue in hair follicle induction. *Nat Genet* 22: 370–374.
- Delgado I, Dominguez-Frutos E, Schimmang T, Ros MA (2008) The incomplete inactivation of *Igf8* in the limb ectoderm affects the morphogenesis of the anterior autopod through BMP-mediated cell death. *Dev Dyn* 237: 649–658.
- Rowe DA, Cairns JM, Fallon JF (1982) Spatial and temporal patterns of cell death in limb bud mesoderm after apical ectodermal ridge removal. *Dev Biol* 93: 83–91.
- Chiang C, Lättingung Y, Harris MP, Simandl BK, Li Y, et al. (2001) Manifestation of the limb prepattern: limb development in the absence of sonic hedgehog function. *Dev Biol* 236: 421–435.
- Pospa J, Mikkola ML, Mustonen T, Thesleff I (2003) Ectodysplasin, Edar and TNFRSF19 are expressed in complementary and overlapping patterns during mouse embryogenesis. *Gene Expr Patterns* 3: 675–679.
- Tucker AS, Headon DJ, Schneider P, Ferguson BM, Overbeck P, et al. (2000) Edar/Eda interactions regulate enamel knot formation in tooth morphogenesis. *Development* 127: 4691–4700.
- Pospa J, Thesleff I (2003) Mechanisms of ectodermal organogenesis. *Dev Biol* 262: 195–205.
- Vincent MC, Biancalana V, Ginsty D, Mandel JL, Calvas P (2001) Mutational spectrum of the ED1 gene in X-linked hypohidrotic ectodermal dysplasia. *Eur J Hum Genet* 9: 355–363.
- Koppinen P, Pospa J, Laurikkala J, Thesleff I, Mikkola ML (2001) Signaling and subcellular localization of the TNF receptor Edar. *Exp Cell Res* 269: 180–192.
- Paakonon K, Cambiaggi S, Novelli G, Ouzts LV, Penttinen M, et al. (2001) The mutation spectrum of the ED1 gene in X-linked anhidrotic ectodermal dysplasia. *Hum Mutat* 17: 349.
- Ezer S, Bayes M, Elomaa O, Schlessinger D, Kere J (1999) Ectodysplasin is a collagenous trimeric type II membrane protein with a tumor necrosis factor-like domain and co-localizes with cytoskeletal structures at lateral and apical surfaces of cells. *Hum Mol Genet* 8: 2079–2086.
- Kondo S, Kawahara Y, Kondo M, Naruse K, Minami H, et al. (2001) The medaka *rs-3* locus required for scale development encodes ectodysplasin -A receptor. *Curr Biol* 11: 1202–1206.
- Tucker AS, Headon DJ, Courtney JM, Overbeck P, Sharpe PT (2004) The activation level of the TNF family receptor, Edar, determines cup number and tooth number during tooth development. *Dev Biol* 268: 185–194.
- Kangas AT, Evans AR, Thesleff I, Jernvall J (2004) Nonindependence of mammalian dental characters. *Nature* 432: 211–214.
- Li S, Li J, Cheng J, Zhou B, Tong X, et al. (2008) Non-syndromic tooth agenesis in two Chinese families associated with novel missense mutations in the TNF domain of EDA (ectodysplasin A). *PLoS ONE* 3: e2396.
- Tao R, Jin B, Guo SZ, Qing W, Feng GY, et al. (2006) A novel missense mutation of the EDA gene in a Mongolian family with congenital hypodontia. *J Hum Genet* 51: 498–502.
- Tarpey P, Pemberton IJ, Stockton DW, Das P, Nisits V, et al. (2007) A novel Gln358Glu mutation in ectodysplasin A associated with X-linked dominant incisor hypodontia. *Am J Med Genet A* 143: 390–394.
- Piechel CL, Nereug KS, Ohlg KA, Cole BLE, Colosimo PF, et al. (2001) The genetic architecture of divergence between threespine stickleback species. *Nature* 414: 901–905.
- Colosimo PF, Piechel CL, Nereug K, Blackman BK, Shapiro MD, et al. (2004) The genetic architecture of parallel armor plate reduction in threespine sticklebacks. *PLoS Biol* 2: E109.
- Knecht AK, Hosemann KE, Kingsley DM (2007) Constraints on utilization of the EDA-signaling pathway in threespine stickleback evolution. *Evol Dev* 9: 141–154.
- Kimura R, Fujimoto A, Tokunaga K, Ohashi J (2007) A Practical Genome Scan for Population-Specific Strong Selective Sweeps That Have Reached Fixation. *PLoS ONE* 2: e286.
- Williamson SH, Hubisz MJ, Clark AG, Payseur BA, Bustamante CD, et al. (2007) Localizing Recent Adaptive Evolution in the Human Genome. *PLoS Genet* 3: e90.
- Fujimoto A, Kimura R, Ohashi J, Omi K, Yulivulandari R, et al. (2008) A scan for genetic determinants of human hair morphology: EDAR is associated with Asian hair thickness. *Hum Mol Genet* 17: 835–843.
- Mou C, Thomson HA, Willan PM, Clowes C, Harris WE, et al. (2008) Enhanced ectodysplasin-A receptor (EDAR) signaling alters multiple fiber characteristics to produce the East Asian hair form. *Hum Mutat*. *epub*.

60. Stock DW (2007) Zebrafish dentition in comparative context. *J Exp Zool B Mol Dev Evol* 308: 523–549.
61. Pelegri F (2002) Mutagenesis. In: Nueslein-Volhard C, Dahm R, eds. *Zebrafish*. Oxford: Oxford University Press. pp 145–174.
62. Haffter P, Granato M, Brand M, Mullins MC, Hammerschmidt M, et al. (1996) The identification of genes with unique and essential functions in the development of the zebrafish, *Danio rerio*. *Dev* 12: 1–36.
63. Geisler R (2002) Mapping and Cloning. In: Nueslein-Volhard C, Dahm R, eds. *Zebrafish*. Oxford: Oxford University Press. pp 175–212.
64. Pfaffl MW (2001) A new mathematical model for relative quantification in real-time RT-PCR. *Nucleic Acids Res* 29: e45.
65. Shulte-Merker S (2002) Looking at Embryos. In: Nueslein-Volhard C, Dahm R, eds. *Zebrafish*. Oxford: Oxford University Press. pp 39–58.

Appendix B

Enhancing the Efficiency of *N*-Ethyl-*N*-Nitrosourea–Induced Mutagenesis in the Zebrafish

Nicolas Rohner,^{1,2,*} Simon Perathoner,^{1,*} Hans Georg Frohnhofer,¹ and Matthew P. Harris^{1,3}

Abstract

N-Ethyl-*N*-nitrosourea (ENU) treatment is the standard experimental method used for chemical mutagenesis of many vertebrate organisms commonly used in the laboratory. In zebrafish and medaka, the use of a repetitive, sublethal dose of 3–3.5 mM ENU has been shown to give the best balance between mutagenicity and toxicity. However, even at this concentration, a significant proportion of fish die during the treatment. Therefore, large numbers of fish are required to obtain a sufficient number of mutagenized founders at the end of the procedure. Additionally, it is quite common to have high levels of mortality in any particular dosing cycle. This may cause a mutagenesis experiment to suddenly fail after several weeks of work. Here we provide a very simple method for ENU mutagenesis of zebrafish using a subparalytic dose of clove oil as a sedative that drastically reduces the lethality of ENU treatment in fish. This facilitates ENU mutagenesis protocols considerably, facilitates higher dosing, and allows for sensitive strains of fish such as homozygous mutants to be mutagenized for use in genetic studies.

Introduction

THE MUTAGEN *N*-ETHYL-*N*-NITROSOUREA (ENU) is used in the majority of forward genetic screens in vertebrates^{1–4} as well as reverse genetic approaches such as sequencing for induced mutations in particular genes.⁵ This is primarily due to the high efficiency of ENU treatment in causing single base pair substitutions with limited bias in the mutated genomic region. ENU alkylates DNA, which leads to errors during replication and formation of point mutations in the DNA.⁶

ENU mutagenesis is a standard method to generate mutants, which can be used to study development and physiology of zebrafish^{1,7} and medaka.^{8,9} The mutagenesis protocol requires the treatment of fish with doses of ENU that often lead to high lethality during the treatment. The concentration of ENU used in common protocols to mutagenize fish is limited by this toxicity and peaks at 3.3 mM.^{1,10} At this concentration, many fish still die (20%–50%). This lethality makes a large-scale mutagenesis protocol quite arduous, especially as multiple treatments are needed to get sufficient mutagenesis rates. The standard protocol for mutagenesis in zebrafish uses 5–6 independent treatments of ENU (e.g., Ref.¹⁰). Protocols for mutagenizing medaka use a similar concentration of ENU as for zebrafish, however, using fewer doses.⁸ The cause

of lethality arises from shock experienced by fish during washes after ENU treatment rather than ENU toxicity itself (Ref.¹ and personal obs.). This lethality can be dampened by reducing environmental stress of the fish during mutagenesis (such as lighting, temperature, and noise). This observation has led to laboratory-specific tricks to minimize sensory stress to limit adverse effects of the treatment, such as performing the mutagenesis in quiet, isolated areas and only at night. Given the number of replicate treatments needed for a successful mutagenesis and the lethality seen during any one particular treatment, the starting population of fish has to be substantially large at the beginning of the experiment to provide enough mutagenized founders for most studies.

We have recently adapted our mutagenesis protocol to reduce the toxicity observed with ENU by use of a subparalytic dose of clove oil to sedate fish during treatment. With this protocol it is possible to start with lower numbers of fish and have the majority of fish survive the treatments. This amended protocol for mutagenesis of zebrafish supports higher dosing of ENU, less replicate dosing, and most importantly, increased viability and health of the treated fish. Further, we found that addition of clove oil permits efficient mutagenesis on single and double mutants, such as *tra*^{-/-}; *mac*^{-/-} or casper,¹¹ which can be less robust than

¹Department of Genetics, Max-Planck-Institute for Developmental Biology, Tübingen, Germany.

²Department of Genetics, Harvard Medical School, Boston, Massachusetts.

³Department of Genetics, Harvard Medical School, Children's Hospital Boston, Orthopaedic Research, Boston, Massachusetts.

*These two authors contributed equally to this work.

Appendix C

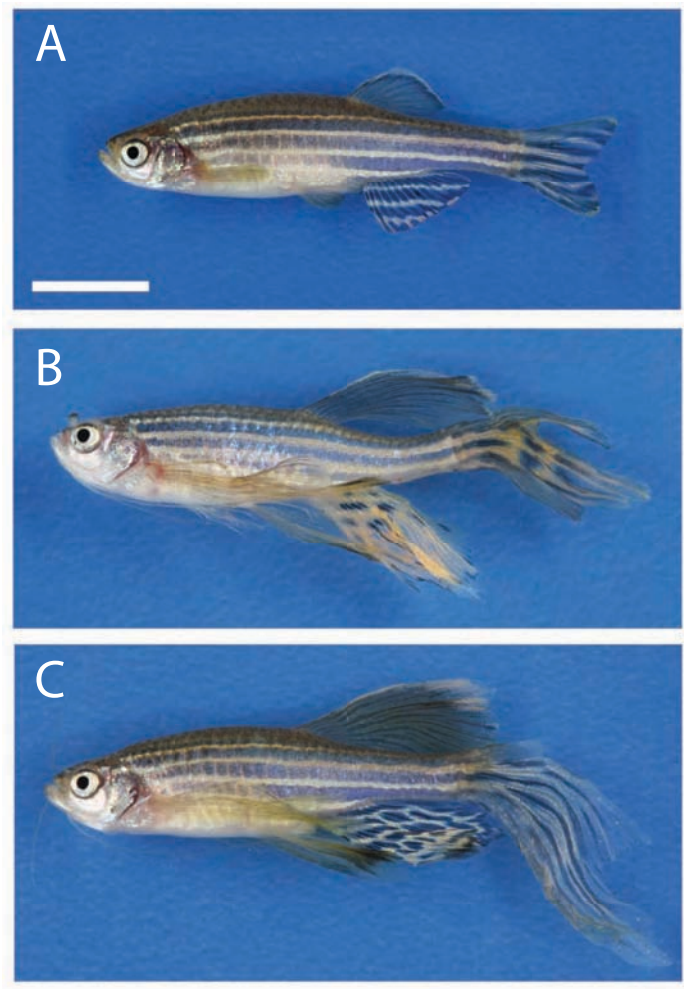


Figure 4.3: Phenotype of homozygous *alf* and *pfau* mutant. (A) wild type, (B) *alf* homozygous, (C) *pfau* homozygous. Scale bar: 10 mm

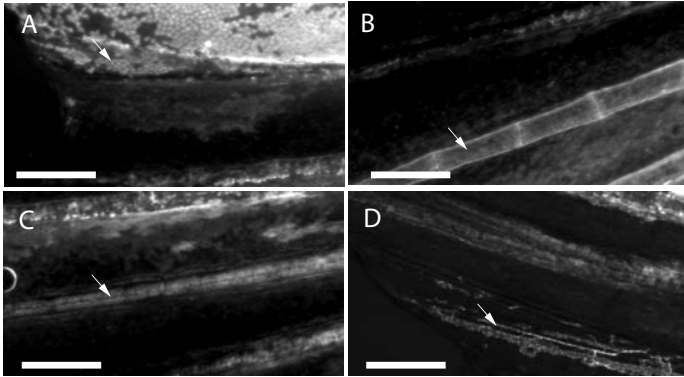


Figure 4.4: DsRed fluorescence was detected in various tissues in fish expressing *ef1a:DsRed;ef1a:kcnk5b^{pfau}* in somatic clones: epidermis (A), osteoblasts (B), fibroblasts (C) and vasculature (D). Arrows point to the respective tissue. Scale bar: 200 μ m

Table 4.4: Genes in the *pfau* mapping interval

Ensembl Gene ID	Gene Description
ENSDARG00000034693	Myb-like SWIRM and MPN domains 1
ENSDARG00000043687	SAYSVFN motif domain containing 1
ENSDARG00000043684	bisphosphate nucleotidase 1
ENSDARG00000043680	YLP motif containing 1
ENSDARG00000092174	si:ch211-59d15.4
ENSDARG00000012390	potassium channel subfamily K member 5
ENSDARG00000001891	synaptotagmin XIVb
ENSDARG00000033742	5'-nucleotidase cytosolic IB b
ENSDARG00000043673	brain-enriched guanylate kinase-associated homolog (rat)
ENSDARG00000043676	Uncharacterized protein
ENSDARG00000002467	retinol dehydrogenase 14b (all-trans/9-cis/11-cis)
ENSDARG00000033201	cysteine-rich protein 2
ENSDARG00000037046	RAD51-like 1 (<i>S. cerevisiae</i>)
ENSDARG00000021443	zinc finger protein 36 C3H type-like 1b
ENSDARG00000009471	nidogen 2b (osteonidogen)
ENSDARG00000037033	prostaglandin E receptor 2b (subtype EP2)
ENSDARG000000091922	si:ch211-13n20.3
ENSDARG000000089556	si:dkey-63j12.4
ENSDARG00000037038	proteasome (prosome macropain) 26S subunit ATPase 6
ENSDARG00000037040	cell growth regulator with ring finger domain 1
ENSDARG00000037042	DDHD domain containing 1

Table 4.4: Genes in the *pfau* mapping interval (continued)

Ensembl Gene ID	Gene Description
ENSDARG00000028354	syntaxin binding protein 6 (amisyn) like
ENSDARG00000070781	connexin 35
ENSDARG00000057911	actin alpha cardiac muscle 1
ENSDARG00000070786	-
ENSDARG00000077840	myeloid ecotropic viral integration site 2.1
ENSDARG00000062849	potassium channel subfamily K member 10a
ENSDARG00000043664	bradykinin receptor B2
ENSDARG00000043665	glutaredoxin 5 homolog (S. cerevisiae)
ENSDARG00000043667	-
ENSDARG00000090850	serine (or cysteine) proteinase inhibitor clade A (alpha-1 antiproteinase member 1 like
ENSDARG00000090286	serine (or cysteine) proteinase inhibitor clade A (alpha-1 antiproteinase member 1
ENSDARG00000070757	si:ch211-155i14.1

Table 4.5: Genes in the *segel* mapping interval

VEGA Gene ID	Gene Description
OTTDARG00000022235	protein phosphatase 1, regulatory (inhibitor) subunit 3Ca
OTTDARG00000035140	ankyrin repeat domain 1a (cardiac muscle)
OTTDARG00000022237	<i>zgc:65997</i>
OTTDARG00000022240	pantothenate kinase 1a
OTTDARG00000035000	solute carrier family 16 (monocarboxylic acid transporters) member 12a
OTTDARG00000035053	interferon-induced protein with tetratricopeptide repeats 2
OTTDARG00000035055	Fas (TNF receptor superfamily, member 6)
OTTDARG00000020224	phosphatase and tensin homolog A
OTTDARG00000028668	3'-phosphoadenosine 5'-phosphosulfate synthase 2a
OTTDARG00000028667	multiple inositol polyphosphate histidine phosphatase, 1a
OTTDARG00000022845	sphingomyelin synthase 1
OTTDARG00000034989	solute carrier family 18 (vesicular monoamine) member 2
OTTDARG00000022843	peroxisome biogenesis factor 13
OTTDARG00000022841	UDP-GlcNAc:betaGal beta-1,3-N-acetylglucosaminyl-transferase 2b
OTTDARG00000020212	orthodenticle homolog 1b
OTTDARG00000028675	malate dehydrogenase 1b, NAD (soluble)

Table 4.5: Genes in the *segel* mapping interval (continued)

VEGA Gene ID	Gene Description
OTTDARG00000022765	UDP-glucose pyrophosphorylase 2b
OTTDARG00000028712	pellino homolog 1b (Drosophila)
OTTDARG00000024808	ATP-binding cassette, sub-family H, member 1
OTTDARG00000024814	aftiphilin b
OTTDARG00000024813	rearranged L-myc fusion
OTTDARG00000024812	dynein, light chain, Tctex-type 1
OTTDARG00000024816	zinc metallopeptidase, STE24 homolog
OTTDARG00000028631	
OTTDARG00000028632	ribosomal protein L13a
OTTDARG00000022764	COMM domain containing 9
OTTDARG00000028711	MORN repeat containing 2
OTTDARG00000028710	zinc finger protein 593
OTTDARG00000028713	selenoprotein N, 1
OTTDARG00000022761	family with sequence similarity 54, member B
OTTDARG00000022762	speedy homolog A (Xenopus laevis)
OTTDARG00000028566	WD repeat domain 43
OTTDARG00000028567	connexin 35.4
OTTDARG00000022763	3-hydroxymethyl-3-methylglutaryl-Coenzyme A lyase (hydroxymethylglutaricaciduria)
OTTDARG00000022719	zinc finger and BTB domain containing 8A
OTTDARG00000022718	UDP-galactose-4-epimerase
OTTDARG00000035141	ceroid-lipofuscinosis, neuronal 8

Table 4.5: Genes in the *segl* mapping interval (continued)

VEGA Gene ID	Gene Description
OTTDARG00000035143	Rho guanine nucleotide exchange factor (GEF) 10
OTTDARG00000035086	poly(A) binding protein, cytoplasmic 4 (inducible form)
OTTDARG00000034081	lymphocyte-specific protein tyrosine kinase
OTTDARG00000034951	serine/arginine repetitive matrix 1
OTTDARG00000035014	chloride intracellular channel 4
OTTDARG00000032842	absent in melanoma 1a
OTTDARG00000032861	reticulon 4 interacting protein 1
OTTDARG00000032859	glutaminyl-tRNA synthase (glutamine-hydrolyzing)-like 1
OTTDARG00000032862	isoleucine-tRNA synthetase 2, mitochondrial
OTTDARG00000035067	protein phosphatase 1, catalytic subunit, beta isoform
OTTDARG00000035017	potassium voltage-gated channel, subfamily H (eag-related), member 1
OTTDARG00000035133	hedgehog acyltransferase
OTTDARG00000028802	mitochondrial ribosomal protein 63
OTTDARG00000028652	tetratricopeptide repeat domain 7B
OTTDARG00000020385	calmodulin 1a
OTTDARG00000020384	progesterone receptor membrane component 2
OTTDARG00000028651	zgc:162232
OTTDARG00000020382	PHD finger protein 17

Table 4.5: Genes in the *segel* mapping interval (continued)

VEGA Gene ID	Gene Description
OTTDARG00000020386	regulator of calcineurin family member 3
OTTDARG00000022822	NIPA-like domain containing 3
OTTDARG00000030448	grainyhead-like 3
OTTDARG00000022824	connector enhancer of kinase suppressor of Ras 1
OTTDARG00000028804	ribosomal protein S6 kinase a, polypeptide 1
OTTDARG00000020387	ArfGAP with SH3 domain, ankyrin repeat and PH domain 3
OTTDARG00000020388	inhibitor of DNA binding 3
OTTDARG00000035069	vestigial like 2b
OTTDARG00000028548	PARK2 co-regulated

***kcnh1a* sequence from poeciliid fish**

P. sphenops cDNA consensus sequence

TGGCTAGTGGTGGACAGTATWGTGGACGTCATCTT
CCTGGTGGACATCGTCTTGAACTTTCACACCACGTT
TGTGGGGCCCGCCGGCGAGGTCATCTCCGACCCCAA
GCTGATCCGCATGAACTACCTGAAGACCTGGTTTGT
GATCGACCTGCTCTCCTGCCTGCCCTACGATGTCAT
CAACGCCTTCGAGAACGTGGACGAGGGAATCAGCAG
TCTGTTTACGCTCTCTTAAGGTTGTCCGGCTCCTCCG
TTTGGGGCCGGGTGCCCCGAAACTGGACCACTACAT
CGAATACGGGGCGGCCGTCTTGGTGCTGCTGGTCTG
TGTTTTTGGACTGGCGGCACACTGGTTGGCCTGCAT
CTGGTATAGCATTGGAGACTACGAGGTGATTGATGA
AGAAACCAACGTTGTCCGCATGGACAGCTGGCTCTA
CATCCTGGCTGAGACGATGGGCAGGCCCTACCGCTT
CAACACCACCGGTTCCGGGAAGTGGGAGGGTGGGC
CCAACAAAGACTCGGTTTACATCACCTCCCTGTACT
TCACCATGACCAGCCTGACCAGCATCGGCTTCGGCA
ACATCGCTCCGACGACGGACGGGGAGAAAATCTTCG
CTGTGGCCATGATGATGATCGGATCCCTTCTTTACG
CCACCATCTTTGGTAAACGTGACAACCATCTTCCAGC
AGATGTATGCCAACACTAATCGCTACCATGAGATGC
TCAACAGTGTCCGGGACTTCCTTAAACTCTATCAGG
TCCCCAAAGGCTTGAGTGAAAGAGTTATGGACTATA
TCGCCTCTACCTGGTCCATGTCACGGGGCATAGACA
CCGAAAAGGTGTTGCAGATTTGTCCAAAGGACATGA
GAGCAGATATTTGTGTTTACCTGAACCGCAAAGTTT
TCAAAGAGCATCCAGCTTTCGACTGGCCAGCGACG
GGTGCTCAGGGCTCTGGCTATGGAGTTTCAGACGA

TCCACTGCGCWCKGGTGACTTgATCTACCACGCCG
GCGAAAGTGTGGACAGCCTGTGTTTTGTGGTGTCTG
GTTCCCTTGGAAAGTCATTCAGGATGATGAGGTGGTGG
CTATTTTAGGTAAAGGAGATGTATTTGGCGACGTTT
TCTGGAAGGAGGTGACTCTGGCTCAGGCCTGCGCCA
ACGTCAGAGCGCTGACCTACTGCGACCTGCACGTCA
TTAAGCGTGACGCCCTGCAGAAGGTCCTGGAGTTCT
ACACGGCGTTCGCCAACCACTTCTCCAGGAACCTGC
TGCTCACTTACAACCTGAGAAAGAGGATTGTCTTCC
GGAAGATCAGCGATGTGAAACGGGAGGAGGAGGAG
AGGCAGCGTTCGCAAAAACGAAGCGCCTCTGAACCTG
CCTCCGGATCACCCGGTACGGAAACTCTTCCAGCGY
TTCCGMCAGCAGAAGGAAGCCCG

P. sphenops protein consensus sequence

WLVVDSIVDVIFLVDIVLNFHTTFVGPAGEVISDPKLIR
MNYLKTWFVIDLLSCLPYDVINAFENVDEGISSLFSSLK
VVRLRLRGRVARKLDHYIEYGAAVLVLLVCVFGLAH
WLACIWYSIGDYEVIDEETNVVRMDSWLYILAETMGRP
YRFNTTGSWKWEGGPNKDSVYITSLYFTMTSLTSIGFG
NIAPTTDGEKIFAVAMMMIGSLLYATIFGNVTTIFQQM
YANTNRYHEMLNSVRDFLKLYQVPKGLSERVMDYIAST
WSMSRGIDTEKVLQICPKDMRADICVHLNRKVFKEHPA
FRLASDGCLRALAMEFQTIHCAPGDLIYHAGESVDSLFC
VVSGSLEVIQDDEVVAILGKGDVFGDVFVWKEVTLAQAC
ANVRALTYCDLHVIKRDALQKVLEFYTAFANHF SRNLL
LTYNLRKRIVFRKISDVKREEEERQRRKNEAPLNLPD
HPVRKLFQRFRQQKEA

P. latipinna cDNA consensus sequence

GTCATCTCCGACCCCAAGCTGATCCGCATGAACTAC
CTGAAGACCTGGTTTGTGATCGACCTGCTCTCCTGC
CTGCCCTAYGATGTCATCAACGCCTTCGAGAACGTG
GACGAGGGRATCAGCAGTCTGTTCAGCTCTCTTAAG
GTTGTCCGGCTCCTCCGTTTGGGCCGGGTGCCCCG
AAACTGGACCACTACATCGAATACGGGGCGGCCGTC
CTGGTGCTGCTGGTCTGTGTTTTTGGACTGGCGGCA
CACTGGTTGGCCTGCATCTGGTATAGCATTGGAGAC
TACGAGGTGATTGATGAAGAAACCAACGTTGTCCGC
ATGGACAGCTGGCTCTACATCCTGGCTGAGGCGATG
GGCAGGCCCTACCGCTTCAACACCACYGGTTCGGGG
AAGTGGGAGGGCGGGCCCAACAAAGACTCGGTTTAC
ATCACCTCCCTGTACTTCACCATGACCAGTCTGACC
AGCATTGGCTTCGGCAACATCGCTCCGACGACGGAC
GGGGAGAAAATCTTCGCTGTGGCCATGATGATGATC
GGATCCCTTCTTTACGCCACCATCTTTGGTAACGTG
ACAACCATCTTCCAGCAGATGTATGCCAACACTAAT
CGTACCATGAGATGCTCAACAGTGTCCGGGACTTC
CTTAAACTCTATCAGGTCCCCAAAGGCTTGAGTGAA
AGAGTTATGGACTATATCGCCTCTACCTGGTCCATG
TCACGGGGCATAGACACCGAAAAGGTGTTGCAGATT
TGTCCAAAGGACRTGAGAGCAGATATTTGTGTTTAC
CTGAACCGCAAAGTTTTCAAAGAGCATCCAGCTTTC
CGACTGGCCAGCGACGGGTGCCTCAGGGCTCTGGCT
ATGGAGTTTCAGACGATCCACTGCGCTCCTGGTGAC
TTGATCTACCACGCYGGCGAAAGTGTGGACAGCCTG
TGTTTTGTGGTGTCTGGTTCCTTGAAGTCATTCAG
GATGATGAGGTGGTGGCTATTTTAGGTAAAGGAGA
TGTATTTGGCGACGTTTTTCTGGAAGGAGGTGACTCT

GGCTCAGGCCTGCGCCAACGTCAGAGCGCTGACCTA
CTGCGACCTGCACGTCATTAAGCGTGACGCCCTGCA
GAAGGTCCTGGAGTTCTACACGGCGTTCGCCAACCA
CTTCTCCAGGAACCTGCTGCTCACTTACAACCTGAG
AAAGAGGATTGTCTTCCGGAAGATCAGCGATGTGAA
ACGGGAGGAGGAGGAG

P. latipinna protein consensus sequence

VISDPKLIRMNYLKTWVVIDLLSCLPYDVINAFENVDEG
ISSLFSSLKVVRLRLGRVARKLDHYIEYGA AVL VLLVC
VFGLAAHWLACIWYSIGDYEVIDEETNVVRMDSWLYIL
AEAMGRPYRFNTTGSWKWEGGPNKDSVYITSLYFTMT
SLTSIGFGNIAPT TDGEKIFAVAMMMIGSLLYATIFGNV
TTIFQQMYANTNRYHEMLNSVRDFLKLYQVPKGLSER
VMDYIASTWSMSRGIDTEKVLQICPKDXRADICVHLNR
KVFKEHPAFRLASDGCLRALAMEFQTIHCAPGDLIYHA
GESVDSLFCVVSGSLEVIQDDEVVAILGKGDVFGDVFV
KEVTLAQACANVRALTYCDLHVIKRDALQKVLEFYTA
FANHFSRNLLLTYNLRKRIVFRKISDVKREEEE

P. velifera cDNA consensus sequence

CACTACATCGAATACGGGGCGGCcGTcCTGGTGCTG
CTGGTCTGTGTTTTTGGACTGGCGGCACACTGGTTG
GCCTGCATCTGGTATAGCATTGGAGACTACGAGGTG
ATTGATGAAGAAACCAACGTTGTCCGCATGGACAGC
TGGCTCTACATCCTGGCTGAGGCGATGGGCAGGCC
TATCGCTTCAACACCACCGGTTCCGGGGAAGTGGGAG
GGCGGGCCCAACAAAGACTCGGTTTACATCACCTCC
CTGTACTTCACCATGACCAGTCTGACCAGCATTGGC
TTCGGCAACATCGCTCCGACGACGGACGGGGAGAAA
ATCTTCGCTGTGGCCATGATGATGATCGGATCCCTT
CTTTACGCCACCATCTTTGGTAAACGTGACAACCC

P. velifera protein consensus sequence

HYIEYGAAVLVLLVCFGLAAHWLACIWYSIGDYEVID
EETNVVRMDSWLYILAEAMGRPYRFNNTTGSWKWEGG
PNKDSVYITSLYFTMTSLTSIGFGNIAPTDDGEKIFAVA
MMMIGSLLYATIFGNVTT

P. latipunctata genomic consensus sequence

GGGgCGCGTCTGGTGCTGCTGGTCTGTGTTTTTGGGA
CTGGCGGCACACTGGTTGGCCTGCATCTG[gtatgtctgca
t...intron...cattattaccctcag]GTATAGCATTGGAGACTA
CGAGGTGATTGATGAAGAAACCAACGTTGTCCGCAT
GGACAGCTGGCTCTACATCCTGGCTGAGACGATGGG
CAGGCCCTACCGCTTCAACACCACCGGTTTCAGGGAA
ATGGGAGGGCGGGCCCAACAAAGACTCGGTTTACAT
CACCTCCCTGTAC

P. latipunctata protein consensus sequence

GARLVLLVCVFGLAAHWLACIWYSIGDYEVIDEETNVV
RMDSWLYILAETMGRPYRFNTTGS GKWEGGPNKDSV
YITSLY

Table 4.6: Alignment of cDNA from *P. velifera* and *P. latipinna*

P. lnn	190	CACTACATCGAATACGGGGCGGCCGTCCTGGTGCTGCTGGTCTGTGTTTTGGACTGGCG	249
P. ve	1	CACTACATCGAATACGGGGCGGCCGTCCTGGTGCTGCTGGTCTGTGTTTTGGACTGGCG	60
P. lnn	250	GCACACTGGTTGGCCTGCATCTGGTATAGCATTGGAGACTACGAGGTGATTGATGAAGAA	309
P. ve	61	GCACACTGGTTGGCCTGCATCTGGTATAGCATTGGAGACTACGAGGTGATTGATGAAGAA	120
P. lnn	310	ACCAACGTTGTCGCGCATGGACAGCTGGCTCTACATCCTGGCTGAGGCGATGGCAGGCC	369
P. ve	121	ACCAACGTTGTCGCGCATGGACAGCTGGCTCTACATCCTGGCTGAGGCGATGGCAGGCC	180
P. lnn	370	TACCGCTTCAACACCACYGGTTCGGGGAAGTGGGAGGGCGGCCAACAAAGACTCGGTT	429
P. ve	181	TATCGCTTCAACACCACCGGTTTCGGGGAAGTGGGAGGGCGGCCAACAAAGACTCGGTT	240
P. lnn	430	TACATCACCTCCCTGTACTTCACCATGACCAGTCTGACCAGCATTGGCTTCGGCAACATC	489
P. ve	241	TACATCACCTCCCTGTACTTCACCATGACCAGTCTGACCAGCATTGGCTTCGGCAACATC	300
P. lnn	490	GTCGACGACGGACGGGAGAAAAATCTTCGCTGTGGCCATGATGATGATCGGATCCCTT	549
P. ve	301	GTCGACGACGGACGGGAGAAAAATCTTCGCTGTGGCCATGATGATGATCGGATCCCTT	360
P. lnn	550	CTTTACGCCACCATCTTTGGTAACGTGACAACC	582
P. ve	361	CTTTACGCCACCATCTTTGGTAACGTGACAACC	393

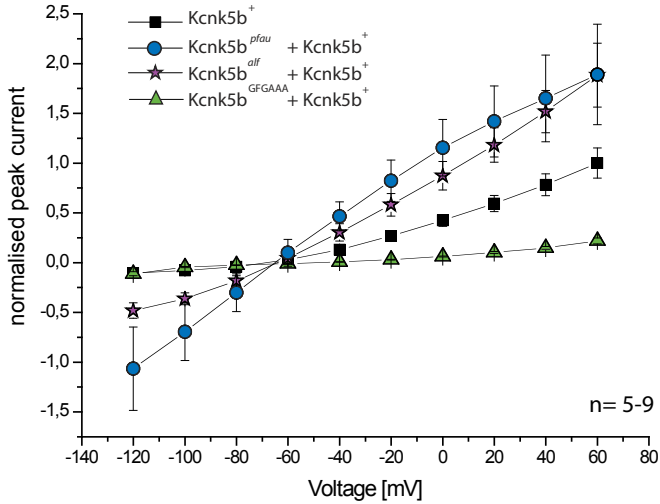


Figure 4.5: Effects of mutated selectivity pore P2 on Kcnk5b conductance. Squares: wild type, purple stars: *alf* + wild type, blue circles: *pfau* + wild type, green triangles: P2 mutant + wild type. Current was normalised to the measurement of wild type current at 60 mV.

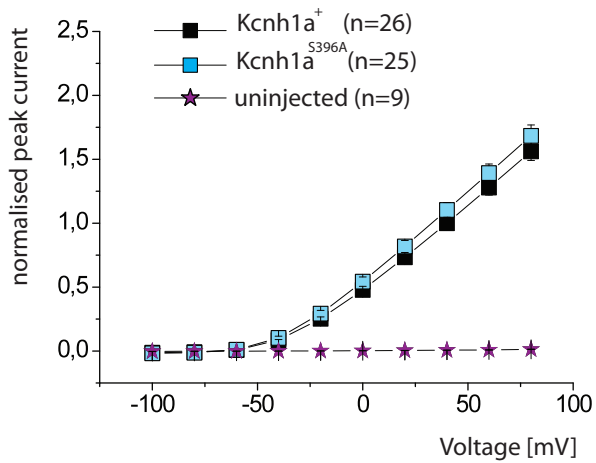


Figure 4.6: Current-voltage relationship of wild type Kcnh1a⁺ (black squares) and Kcnh1a^{S396A} (blue squares), harbouring the sailfin molly specific Ala at position 396 instead of a Ser.



Figure 4.7: Expression of GFP in the caudal fin primordium in a transgenic line driving Gal4/UAS:GFP under a 6.7 kb promoter of *kcnk5b*

Bibliography

- Abe, G., Ide, H., and Tamura, K. (2007). Function of FGF signaling in the developmental process of the median fin fold in zebrafish. *Dev Biol*, 304(1):355–66.
- Abercrombie, W. F. (1936). Studies on cell number and the progression factor in the growth of Japanese beetle larvae (*Popillia japonica* Newman). *Journal of Morphology*, 59(1):91–112.
- Akimenko, M.-A., Marí-Beffa, M., Becerra, J., and Géraudie, J. (2003). Old questions, new tools, and some answers to the mystery of fin regeneration. *Dev Dyn*, 226(2):190–201.
- Alpatov, W. W. (1930). Phenotypical Variation in Body and Cell Size of *Drosophila melanogaster*. *Biological Bulletin*, 58(1):pp. 85–103.
- Alvarez-Baron, C. P., Jonsson, P., Thomas, C., Dryer, S. E., and Williams, C. (2011). The two-pore domain potassium channel KCNK5: induction by estrogen receptor alpha and role in proliferation of breast cancer cells. *Mol Endocrinol*, 25(8):1326–36.
- Azevedo, A. S., Sousa, S., Jacinto, A., and Saude, L. (2012). An amputation resets positional information to a proximal

- identity in the regenerating zebrafish caudal fin. *BMC Dev Biol*, 12(1):24.
- Balk, S. D. (1971). Calcium as a regulator of the proliferation of normal, but not of transformed, chicken fibroblasts in a plasma-containing medium. *Proc Natl Acad Sci U S A*, 68(2):271–5.
- Barman, R. (1991). *A Taxonomic revision of the Indo-Burmese species of Danio Hamilton Buchanan (pisces, Cyprinidae)*. Records of the Zoological Survey of India. Zoological Survey of India.
- Baserga, R. (1985). *The biology of cell reproduction*. Harvard University Press, Cambridge, Mass. .:
- Beane, W. S., Morokuma, J., Adams, D. S., and Levin, M. (2011). A chemical genetics approach reveals H,K-ATPase-mediated membrane voltage is required for planarian head regeneration. *Chem Biol*, 18(1):77–89.
- Becerra, J., Montes, G. S., Bexiga, S. R., and Junqueira, L. C. (1983). Structure of the tail fin in teleosts. *Cell Tissue Res*, 230(1):127–37.
- Beebe, W. (1933). Deep-Sea Stomiatooid Fishes One New Genus and Eight New Species. *Copeia*, 1933(4):pp. 160–175.
- Bird, N. C. and Mabee, P. M. (2003). Developmental morphology of the axial skeleton of the zebrafish, *Danio rerio* (Ostariophysi: Cyprinidae). *Dev Dyn*, 228(3):337–57.

- Blackiston, D. J., McLaughlin, K. A., and Levin, M. (2009). Bioelectric controls of cell proliferation: ion channels, membrane voltage and the cell cycle. *Cell Cycle*, 8(21):3519–28.
- Borowiec, A.-S., Hague, F., Gouilleux-Gruart, V., Lassoued, K., and Ouadid-Ahidouch, H. (2011). Regulation of IGF-1-dependent cyclin D1 and E expression by hEag1 channels in MCF-7 cells: the critical role of hEag1 channels in G1 phase progression. *Biochim Biophys Acta*, 1813(5):723–30.
- Borowiec, A.-S., Hague, F., Harir, N., Guénin, S., Guerineau, F., Gouilleux, F., Roudbaraki, M., Lassoued, K., and Ouadid-Ahidouch, H. (2007). IGF-1 activates hEAG K(+) channels through an Akt-dependent signaling pathway in breast cancer cells: role in cell proliferation. *J Cell Physiol*, 212(3):690–701.
- Bregestovski, P., Medina, I., and Goyda, E. (1992). Regulation of potassium conductance in the cellular membrane at early embryogenesis. *J Physiol Paris*, 86(1-3):109–15.
- Browder, M. H., D’Amico, L. J., and Nijhout, H. F. (2001). The role of low levels of juvenile hormone esterase in the metamorphosis of *Manduca sexta*. *J Insect Sci*, 1:11.
- Brüggemann, A., Stühmer, W., and Pardo, L. A. (1997). Mitosis-promoting factor-mediated suppression of a cloned delayed rectifier potassium channel expressed in *Xenopus* oocytes. *Proc Natl Acad Sci U S A*, 94(2):537–42.
- Bryant, P. J. and Simpson, P. (1984). Intrinsic and Extrinsic Control of Growth in Developing Organs. *The Quarterly Review of Biology*, 59(4):pp. 387–415.

- Burket, C. T., Montgomery, J. E., Thummel, R., Kassen, S. C., LaFave, M. C., Langenau, D. M., Zon, L. I., and Hyde, D. R. (2008). Generation and characterization of transgenic zebrafish lines using different ubiquitous promoters. *Transgenic Res*, 17(2):265–79.
- Bussmann, J. and Schulte-Merker, S. (2011). Rapid BAC selection for tol2-mediated transgenesis in zebrafish. *Development*, 138(19):4327–32.
- Canady, K. S., Ali-Osman, F., and Rubel, E. W. (1990). Extracellular potassium influences DNA and protein syntheses and glial fibrillary acidic protein expression in cultured glial cells. *Glia*, 3(5):368–74.
- Capiod, T. (2011). Cell proliferation, calcium influx and calcium channels. *Biochimie*, 93(12):2075 – 2079. The Calcium signal: a universal carrier to code, decode and transduce information.
- Chiu, S. Y. and Wilson, G. F. (1989). The role of potassium channels in Schwann cell proliferation in Wallerian degeneration of explant rabbit sciatic nerves. *J Physiol*, 408:199–222.
- Cidad, P., Jiménez-Pérez, L., García-Arribas, D., Miguel-Velado, E., Tajada, S., Ruiz-McDavitt, C., López-López, J. R., and Pérez-García, M. T. (2012). Kv1.3 channels can modulate cell proliferation during phenotypic switch by an ion-flux independent mechanism. *Arterioscler Thromb Vasc Biol*, 32(5):1299–307.
- Clark, R. B., Kondo, C., Belke, D. D., and Giles, W. R. (2011). Two-pore domain K⁺ channels regulate membrane potential

- of isolated human articular chondrocytes. *J Physiol*, 589(Pt 21):5071–89.
- Cole, K. S. and Moore, J. W. (1960). Ionic current measurements in the squid giant axon membrane. *J Gen Physiol*, 44:123–67.
- Cone, Jr, C. D. (1969). Electroosmotic interactions accompanying mitosis initiation in sarcoma cells in vitro. *Trans N Y Acad Sci*, 31(4):404–27.
- Conlon, I. and Raff, M. (1999). Size Control in Animal Development. *Cell*, 96(2):235 – 244.
- Cubbage, C. C. and Mabee, P. M. (1996). Development of the Cranium and Paired Fins in the Zebrafish *Danio rerio* (Ostariophysi, Cyprinidae). *Journal of Morphology*, 229:121–160.
- Deutsch, C., Slater, L., and Goldstein, P. (1982). Volume regulation of human peripheral blood lymphocytes and stimulated proliferation of volume-adapted cells. *Biochim Biophys Acta*, 721(3):262–7.
- Di Giusto, G., Flamenco, P., Rivarola, V., Fernández, J., Melamud, L., Ford, P., and Capurro, C. (2012). Aquaporin 2-increased renal cell proliferation is associated with cell volume regulation. *J Cell Biochem*.
- Downie, B. R., Sánchez, A., Knötgen, H., Contreras-Jurado, C., Gymnopoulos, M., Weber, C., Stühmer, W., and Pardo, L. A. (2008). Eag1 expression interferes with hypoxia homeostasis and induces angiogenesis in tumors. *J Biol Chem*, 283(52):36234–40.

- Driever, W., Solnica-Krezel, L., Schier, A. F., Neuhauss, S. C., Malicki, J., Stemple, D. L., Stainier, D. Y., Zwartkruis, F., Abdelilah, S., Rangini, Z., Belak, J., and Boggs, C. (1996). A genetic screen for mutations affecting embryogenesis in zebrafish. *Development*, 123:37–46.
- Dubois, J. M. and Rouzaille-Dubois, B. (1993). Role of potassium channels in mitogenesis. *Prog Biophys Mol Biol*, 59(1):1–21.
- Dufourcq, P., Roussigné, M., Blader, P., Rosa, F., Peyrieras, N., and Vríz, S. (2006). Mechano-sensory organ regeneration in adults: the zebrafish lateral line as a model. *Mol Cell Neurosci*, 33(2):180–7.
- Dupertuis, S. M. (1941). Actual growth of young cartilage transplants in rabbits: Experimental studies. *Archives of Surgery*, 43:32–63.
- Eicher, E. M. and Beamer, W. G. (1976). Inherited ateliotic dwarfism in mice. Characteristics of the mutation, little, on chromosome 6. *J Hered*, 67(2):87–91.
- Enyedi, P. and Czirják, G. (2010). Molecular background of leak K⁺ currents: two-pore domain potassium channels. *Physiol Rev*, 90(2):559–605.
- Erdogan, A., Schaefer, C. A., Schaefer, M., Luedders, D. W., Stockhausen, F., Abdallah, Y., Schaefer, C., Most, A. K., Tillmanns, H., Piper, H. M., and Kuhlmann, C. R. W. (2005). Margatoxin inhibits VEGF-induced hyperpolarization, proliferation and nitric oxide production of human endothelial cells. *J Vasc Res*, 42(5):368–76.

- Eugster, E. A. and Pescovitz, O. H. (1999). Gigantism. *J Clin Endocrinol Metab*, 84(12):4379–84.
- Fankhauser, G. (1952). Nucleo-Cytoplasmic Relations in Amphibian Development. *International Review of Cytology*, 1:165 – 193.
- Filipski, E., King, V. M., Li, X., Granda, T. G., Mormont, M.-C., Liu, X., Claustrat, B., Hastings, M. H., and Lévi, F. (2002). Host circadian clock as a control point in tumor progression. *J Natl Cancer Inst*, 94(9):690–7.
- Fink, S. V. and Fink, W. L. (1981). Interrelationships of the ostariophysan fishes (Teleostei). *Zoological Journal of the Linnean Society*, 72(4):297–353.
- Fischer, S., Draper, B. W., and Neumann, C. J. (2003). The zebrafish *fgf24* mutant identifies an additional level of Fgf signaling involved in vertebrate forelimb initiation. *Development*, 130(15):3515–24.
- Fisher, S., Jagadeeswaran, P., and Halpern, M. E. (2003). Radiographic analysis of zebrafish skeletal defects. *Dev Biol*, 264(1):64–76.
- Fleisch, V. C., Fraser, B., and Allison, W. T. (2011). Investigating regeneration and functional integration of CNS neurons: Lessons from zebrafish genetics and other fish species. *Biochimica et Biophysica Acta (BBA) - Molecular Basis of Disease*, 1812(3):364 – 380. <ce:title>Including the Special Section: Zebrafish Models of Neurological Diseases</ce:title>.

- Flemming, A. J., Shen, Z. Z., Cunha, A., Emmons, S. W., and Leroi, A. M. (2000). Somatic polyploidization and cellular proliferation drive body size evolution in nematodes. *Proc Natl Acad Sci U S A*, 97(10):5285–90.
- Fox, H. (1999). Barbels and barbel-like tentacular structures in sub-mammalian vertebrates: a review. *Hydrobiologia*, 403:153–193.
- Freitas, R., Zhang, G., and Cohn, M. J. (2006). Evidence that mechanisms of fin development evolved in the midline of early vertebrates. *Nature*, 442(7106):1033–7.
- Garcia-Bellido, A. (1965). Larvalentwicklung transplantierter Organe von *Drosophila melanogaster* im Adultmilieu. *Journal of Insect Physiology*, 11(8):1071 – 1078.
- Geisler, R., Rauch, G.-J., Geiger-Rudolph, S., Albrecht, A., van Bebber, F., Berger, A., Busch-Nentwich, E., Dahm, R., Dekens, M. P. S., Dooley, C., Elli, A. F., Gehring, I., Geiger, H., Geisler, M., Glaser, S., Holley, S., Huber, M., Kerr, A., Kirn, A., Knirsch, M., Konantz, M., Kuchler, A. M., Maderspacher, F., Neuhauss, S. C., Nicolson, T., Ober, E. A., Praeg, E., Ray, R., Rentzsch, B., Rick, J. M., Rief, E., Schauerte, H. E., Schepp, C. P., Schönberger, U., Schonthaler, H. B., Seiler, C., Sidi, S., Söllner, C., Wehner, A., Weiler, C., and Nüsslein-Volhard, C. (2007). Large-scale mapping of mutations affecting zebrafish development. *BMC Genomics*, 8:11.
- Georgieva, V., Patzner, R. A., and Adam, H. (1979). Transmissions- und rasterelektronen-mikroskopische Untersuchung an den Sinnesknospen der Tentakeln von *Myxine glutinosa* L. (Cyclostomata). *Zoologica Scripta*, 8(1-4):61–67.

- Géraudie, J., Monnot, M. J., Brulfert, A., and Ferretti, P. (1995). Caudal fin regeneration in wild type and long-fin mutant zebrafish is affected by retinoic acid. *Int J Dev Biol*, 39(2):373–81.
- Gerhard, G. S., Kauffman, E. J., Wang, X., Stewart, R., Moore, J. L., Kasales, C. J., Demidenko, E., and Cheng, K. C. (2002). Life spans and senescent phenotypes in two strains of Zebrafish (*Danio rerio*). *Exp Gerontol*, 37(8-9):1055–68.
- Goldsmith, M. I., Fisher, S., Waterman, R., and Johnson, S. L. (2003). Saltatory control of isometric growth in the zebrafish caudal fin is disrupted in long fin and rapunzel mutants. *Dev Biol*, 259(2):303–17.
- Goldstein, S. A., Bockenhauer, D., O’Kelly, I., and Zilberberg, N. (2001). Potassium leak channels and the KCNK family of two-P-domain subunits. *Nat Rev Neurosci*, 2(3):175–84.
- González, D., Gómez-Hernández, J. M., and Barrio, L. C. (2007). Molecular basis of voltage dependence of connexin channels: an integrative appraisal. *Prog Biophys Mol Biol*, 94(1-2):66–106.
- Grandel, H. and Schulte-Merker, S. (1998). The development of the paired fins in the zebrafish (*Danio rerio*). *Mech Dev*, 79(1-2):99–120.
- Gumm, J. M., Snekser, J. L., and Iovine, M. K. (2009). Fin-mutant female zebrafish (*Danio rerio*) exhibit differences in association preferences for male fin length. *Behav Processes*, 80(1):35–8.

- Gurdon, J. B., Lane, C. D., Woodland, H. R., and Marbaix, G. (1971). Use of Frog Eggs and Oocytes for the Study of Messenger RNA and its Translation in Living Cells. *Nature*, 233(5316):177–182.
- Hadzhiev, Y., Lele, Z., Schindler, S., Wilson, S. W., Ahlberg, P., Strähle, U., and Müller, F. (2007). Hedgehog signaling patterns the outgrowth of unpaired skeletal appendages in zebrafish. *BMC Dev Biol*, 7:75.
- Haffter, P., Granato, M., Brand, M., Mullins, M. C., Hammer-schmidt, M., Kane, D. A., Odenthal, J., van Eeden, F. J., Jiang, Y. J., Heisenberg, C. P., Kelsh, R. N., Furutani-Seiki, M., Vogelsang, E., Beuchle, D., Schach, U., Fabian, C., and Nüsslein-Volhard, C. (1996). The identification of genes with unique and essential functions in the development of the zebrafish, *Danio rerio*. *Development*, 123:1–36.
- Haffter, P. and Nüsslein-Volhard, C. (1996). Large scale genetics in a small vertebrate, the zebrafish. *Int. J. Dev. Biol.*, 40:221–227.
- Halder, G. and Johnson, R. L. (2011). Hippo signaling: growth control and beyond. *Development*, 138(1):9–22.
- Hansen, A., Reutter, K., and Zeiske, E. (2002). Taste bud development in the zebrafish, *Danio rerio*. *Dev Dyn*, 223(4):483–96.
- Hansen, J. and Stevens, R. G. (2012). Case-control study of shift-work and breast cancer risk in Danish nurses: impact of shift systems. *Eur J Cancer*, 48(11):1722–9.
- Harris, M. P., Rohner, N., Schwarz, H., Perathoner, S., Konstantinidis, P., and Nüsslein-Volhard, C. (2008). Zebrafish

- eda and edar mutants reveal conserved and ancestral roles of ectodysplasin signaling in vertebrates. *PLoS Genet*, 4(10):e1000206.
- Haverstick, D. M., Heady, T. N., Macdonald, T. L., and Gray, L. S. (2000). Inhibition of human prostate cancer proliferation in vitro and in a mouse model by a compound synthesized to block Ca²⁺ entry. *Cancer Res*, 60(4):1002–8.
- Hegle, A. P., Marble, D. D., and Wilson, G. F. (2006). A voltage-driven switch for ion-independent signaling by ether-à-go-go K⁺ channels. *Proc Natl Acad Sci U S A*, 103(8):2886–91.
- Hervé, J.-C. and Derangeon, M. (2012). Gap-junction-mediated cell-to-cell communication. *Cell Tissue Res*.
- Higashijima, S., Okamoto, H., Ueno, N., Hotta, Y., and Eguchi, G. (1997). High-frequency generation of transgenic zebrafish which reliably express GFP in whole muscles or the whole body by using promoters of zebrafish origin. *Dev Biol*, 192(2):289–99.
- Hildebrand, A., Remmert, M., Biegert, A., and Söding, J. (2009). Fast and accurate automatic structure prediction with HHpred. *Proteins*, 77 Suppl 9:128–32.
- Hoffmann, E. K. (2011). Ion channels involved in cell volume regulation: effects on migration, proliferation, and programmed cell death in non adherent EAT cells and adherent ELA cells. *Cell Physiol Biochem*, 28(6):1061–78.
- Howes, G. J. (1991). Systematics and biogeography: An overview. In Winfield, I. J. and Nelson, J. S., editors, *Cyp-*

rind fishes: systematics, biology and exploitation., pages 1–33.
Chapman and Hall, London.

- Huang, C.-c., Wang, T.-C., Lin, B.-H., Wang, Y.-W., Johnson, S. L., and Yu, J. (2009). Collagen IX is required for the integrity of collagen II fibrils and the regulation of vascular plexus formation in zebrafish caudal fins. *Dev Biol*, 332(2):360–70.
- Iovine, M. K., Higgins, E. P., Hindes, A., Coblitz, B., and Johnson, S. L. (2005). Mutations in connexin43 (GJA1) perturb bone growth in zebrafish fins. *Dev Biol*, 278(1):208–19.
- Iovine, M. K. and Johnson, S. L. (2000). Genetic analysis of isometric growth control mechanisms in the zebrafish caudal Fin. *Genetics*, 155(3):1321–9.
- Jiang, Y., Ruta, V., Chen, J., Lee, A., and MacKinnon, R. (2003). The principle of gating charge movement in a voltage-dependent K⁺ channel. *Nature*, 423(6935):42–48.
- Jopling, C., Sleep, E., Raya, M., Martí, M., Raya, A., and Izpisua Belmonte, J. C. (2010). Zebrafish heart regeneration occurs by cardiomyocyte dedifferentiation and proliferation. *Nature*, 464(7288):606–9.
- Kahl, C. R. and Means, A. R. (2003). Regulation of Cell Cycle Progression by Calcium/Calmodulin-Dependent Pathways. *Endocrine Reviews*, 24(6):719–736.
- Kaplan, J. G. and Owens, T. (1980). Activation of lymphocytes of man and mouse: monovalent cation fluxes. *Ann N Y Acad Sci*, 339:191–200.

- Kelkar, D. A. and Chattopadhyay, A. (2006). Membrane interfacial localization of aromatic amino acids and membrane protein function. *J Biosci*, 31(3):297–302.
- Kendall Jr., A. W., Ahlstrom, E. H., and Moser, H. G. (1984). *Ontogeny and Systematics of Fishes*, volume 1, chapter Early life history stages of fishes and their characters, pages 11–22. American Society of Ichthyologists and Herpetologists.
- Kim, S., Li, Q., Dang, C. V., and Lee, L. A. (2000). Induction of ribosomal genes and hepatocyte hypertrophy by adenovirus-mediated expression of c-Myc in vivo. *Proc Natl Acad Sci U S A*, 97(21):11198–202.
- Kimmel, C. B., Ballard, W. W., Kimmel, S. R., Ullmann, B., and Schilling, T. F. (1995). Stages of embryonic development of the zebrafish. *Dev Dyn*, 203(3):253–310.
- King, D. B. (1969). Effect of hypophysectomy of young cockerels, with particular reference to body growth, liver weight, and liver glycogen level. *Gen Comp Endocrinol*, 12(2):242–55.
- Kirkegaard, S. S., Lambert, I. H., Gammeltoft, S., and Hoffmann, E. K. (2010). Activation of the TASK-2 channel after cell swelling is dependent on tyrosine phosphorylation. *Am J Physiol Cell Physiol*, 299(4):C844–53.
- Kiyokawa, H., Kineman, R. D., Manova-Todorova, K. O., Soares, V. C., Hoffman, E. S., Ono, M., Khanam, D., Hayday, A. C., Frohman, L. A., and Koff, A. (1996). Enhanced growth of mice lacking the cyclin-dependent kinase inhibitor function of p27(Kip1). *Cell*, 85(5):721–32.

- Klausen, T. K., Preisler, S., Pedersen, S. F., and Hoffmann, E. K. (2010). Monovalent ions control proliferation of Ehrlich Lettre ascites cells. *Am J Physiol Cell Physiol*, 299(3):C714–25.
- Kusano, K., Miledi, R., and Stinnakre, J. (1982). Cholinergic and catecholaminergic receptors in the *Xenopus* oocyte membrane. *J Physiol*, 328:143–70.
- Lambie, E. J. (2002). Cell proliferation and growth in *C. elegans*. *Bioessays*, 24(1):38–53.
- Lang, F., Busch, G. L., Ritter, M., Völkl, H., Waldegger, S., Gulbins, E., and Häussinger, D. (1998). Functional significance of cell volume regulatory mechanisms. *Physiol Rev*, 78(1):247–306.
- Langeland, J. and Kimmel, C. B. (1997). *Embryology: Constructing the Organism.*, chapter The embryology of fish., pages 383–407. Sinauer Associates, Sunderland, MA.
- Lawrence, A. M., Goldfine, I. D., and Kirsteins, L. (1970). Growth hormone dynamics in acromegaly. *J Clin Endocrinol Metab*, 31(3):239–47.
- LeClair, E. E. and Topczewski, J. (2010). Development and regeneration of the zebrafish maxillary barbel: a novel study system for vertebrate tissue growth and repair. *PLoS One*, 5(1):e8737.
- Lee, K.-P., Lee, J.-H., Kim, T.-S., Kim, T.-H., Park, H.-D., Byun, J.-S., Kim, M.-C., Jeong, W.-I., Calvisi, D. F., Kim, J.-M., and Lim, D.-S. (2010). The Hippo-Salvador pathway

- restrains hepatic oval cell proliferation, liver size, and liver tumorigenesis. *Proc Natl Acad Sci U S A*, 107(18):8248–53.
- Lee, S. C., Price, M., Prystowsky, M. B., and Deutsch, C. (1988). Volume response of quiescent and interleukin 2-stimulated T-lymphocytes to hypotonicity. *Am J Physiol*, 254(2 Pt 1):C286–96.
- Lee, Y., Grill, S., Sanchez, A., Murphy-Ryan, M., and Poss, K. D. (2005). Fgf signaling instructs position-dependent growth rate during zebrafish fin regeneration. *Development*, 132(23):5173–83.
- Lesage, F. and Lazdunski, M. (2000). Molecular and functional properties of two-pore-domain potassium channels. *Am J Physiol Renal Physiol*, 279(5):F793–801.
- Lin, C. S., Boltz, R. C., Blake, J. T., Nguyen, M., Talento, A., Fischer, P. A., Springer, M. S., Sigal, N. H., Slaughter, R. S., and Garcia, M. L. (1993). Voltage-gated potassium channels regulate calcium-dependent pathways involved in human T lymphocyte activation. *The Journal of Experimental Medicine*, 177(3):637–645.
- Liu, P., Carvalho, C. M. B., Hastings, P. J., and Lupski, J. R. (2012). Mechanisms for recurrent and complex human genomic rearrangements. *Curr Opin Genet Dev*, 22(3):211–20.
- Makarenkova, H. and Patel, K. (1999). Gap junction signalling mediated through connexin-43 is required for chick limb development. *Dev Biol*, 207(2):380–92.

- Mari-Beffa, M., Mateos, I., Palmqvist, P., and Becerra, J. (1996). Cell to cell interactions during teleosts fin regeneration. *Int J Dev Biol*, Suppl 1:179S–180S.
- Mari-Beffa, M. and Murciano, C. (2010). Dermoskeleton morphogenesis in zebrafish fins. *Dev Dyn*, 239(11):2779–94.
- McCabe, J., French, V., and Partridge, L. (1997). Joint regulation of cell size and cell number in the wing blade of *Drosophila melanogaster*. *Genet Res*, 69(1):61–8.
- Metcalf, D. (1963). The autonomous behaviour of normal thymus grafts. *Aust J Exp Biol Med Sci*, 41:SUPPL437–47.
- Metcalf, D. (1964). Restricted growth capacity of multiple spleen grafts. *Transplantation*, 2:387–92.
- Miledi, R. and Parker, I. (1984). Chloride current induced by injection of calcium into *Xenopus* oocytes. *J Physiol*, 357:173–83.
- Millership, J. E., Devor, D. C., Hamilton, K. L., Balut, C. M., Bruce, J. I. E., and Fearon, I. M. (2011). Calcium-activated K⁺ channels increase cell proliferation independent of K⁺ conductance. *Am J Physiol Cell Physiol*, 300(4):C792–802.
- Montagne, J., Stewart, M. J., Stocker, H., Hafen, E., Kozma, S. C., and Thomas, G. (1999). *Drosophila* S6 kinase: a regulator of cell size. *Science*, 285(5436):2126–9.
- Moore, A., Mark, T., Hogan, A., Topczewski, J., and Leclair, E. E. (2012). Peripheral axons of the adult zebrafish maxillary barbel extensively remyelinate during sensory appendage regeneration. *J Comp Neurol*.

- Morata, G. and Ripoll, P. (1975). Minutes: mutants of *Drosophila* autonomously affecting cell division rate. *Dev Biol*, 42(2):211–21.
- Morton, M. J., Abohamed, A., Sivaprasadarao, A., and Hunter, M. (2005). pH sensing in the two-pore domain K⁺ channel, TASK2. *Proc Natl Acad Sci U S A*, 102(44):16102–6.
- Mu, D., Chen, L., Zhang, X., See, L.-H., Koch, C. M., Yen, C., Tong, J. J., Spiegel, L., Nguyen, K. C. Q., Servoss, A., Peng, Y., Pei, L., Marks, J. R., Lowe, S., Hoey, T., Jan, L. Y., McCombie, W. R., Wigler, M. H., and Powers, S. (2003). Genomic amplification and oncogenic properties of the KCNK9 potassium channel gene. *Cancer Cell*, 3(3):297–302.
- Müller, F., Chang, B., Albert, S., Fischer, N., Tora, L., and Strähle, U. (1999). Intronic enhancers control expression of zebrafish sonic hedgehog in floor plate and notochord. *Development*, 126(10):2103–16.
- Munn, A. J. and Dawson, T. J. (2003). How important is milk for near-weaned red kangaroos (*Macropus rufus*) fed different forages? *J Comp Physiol B*, 173(2):141–8.
- Murciano, C., Pérez-Claros, J., Smith, A., Avaron, F., Fernández, T. D., Durán, I., Ruiz-Sánchez, J., García, F., Becerra, J., Akimenko, M.-A., and Marí-Beffa, M. (2007). Position dependence of hemiray morphogenesis during tail fin regeneration in *Danio rerio*. *Dev Biol*, 312(1):272–83.

- Nabrit, M. (1929). The role of the fin rays in the regeneration in the tail-fins of fishes. (In fundulus and goldfish.). *Biological Bulletin*, 60(4):235–266.
- Nasevicius, A. and Ekker, S. C. (2000). Effective targeted gene 'knockdown' in zebrafish. *Nat Genet*, 26(2):216–20.
- Nechiporuk, A. and Keating, M. T. (2002). A proliferation gradient between proximal and msxb-expressing distal blastema directs zebrafish fin regeneration. *Development*, 129(11):2607–17.
- Neumann, C. J., Grandel, H., Gaffield, W., Schulte-Merker, S., and Nüsslein-Volhard, C. (1999). Transient establishment of anteroposterior polarity in the zebrafish pectoral fin bud in the absence of sonic hedgehog activity. *Development*, 126(21):4817–26.
- Niemeyer, M. I., Cid, L. P., Barros, L. F., and Sepúlveda, F. V. (2001). Modulation of the two-pore domain acid-sensitive K⁺ channel TASK-2 (KCNK5) by changes in cell volume. *J Biol Chem*, 276(46):43166–74.
- Nijhout, H. F. and Emlen, D. J. (1998). Competition among body parts in the development and evolution of insect morphology. *Proc Natl Acad Sci U S A*, 95(7):3685–9.
- Nilius, B. (2001). Chloride channels go cell cycling. *J Physiol*, 532(Pt 3):581.
- Nilius, B. and Droogmans, G. (1994). A role for K⁺ channels in cell proliferation. *News Physiol Sci*, 9:105–110.

- Nüsslein-Volhard, C. and Dahm, R. (2002). *Zebrafish: a practical approach*, volume no. 261. Oxford University Press, Oxford, 1st ed edition.
- Orr, C. W., Yoshikawa-Fukada, M., and Ebert, J. D. (1972). Potassium: effect on DNA synthesis and multiplication of baby-hamster kidney cells: (cell cycle-membrane potential-synchronization-transformation). *Proc Natl Acad Sci U S A*, 69(1):243–7.
- Oviedo, N. J., Morokuma, J., Walentek, P., Kema, I. P., Gu, M. B., Ahn, J.-M., Hwang, J. S., Gojobori, T., and Levin, M. (2010). Long-range neural and gap junction protein-mediated cues control polarity during planarian regeneration. *Dev Biol*, 339(1):188–99.
- Owen, N. E. and Villereal, M. L. (1985). Role of Ca²⁺ in serum-stimulated Na⁺ influx in normal and transformed cells. *Am J Physiol*, 248(3 Pt 1):C288–95.
- Parichy, D. M., Elizondo, M. R., Mills, M. G., Gordon, T. N., and Engeszer, R. E. (2009). Normal table of postembryonic zebrafish development: staging by externally visible anatomy of the living fish. *Dev Dyn*, 238(12):2975–3015.
- Pei, L., Wisner, O., Slavin, A., Mu, D., Powers, S., Jan, L. Y., and Hoey, T. (2003). Oncogenic potential of TASK3 (Kcnk9) depends on K⁺ channel function. *Proc Natl Acad Sci U S A*, 100(13):7803–7.
- Poleo, G., Brown, C. W., Laforest, L., and Akimenko, M. A. (2001). Cell proliferation and movement during early fin regeneration in zebrafish. *Dev Dyn*, 221(4):380–90.

- Pollard, H. B. (1894). The „ÄûCirrhostomial" Origin of the Head in Vertebrates. *Anatomischer Anzeiger*, 9:349–359.
- Polyak, K., Kato, J. Y., Solomon, M. J., Sherr, C. J., Massague, J., Roberts, J. M., and Koff, A. (1994). p27Kip1, a cyclin-Cdk inhibitor, links transforming growth factor-beta and contact inhibition to cell cycle arrest. *Genes Dev*, 8(1):9–22.
- Poss, K. D., Keating, M. T., and Nechiporuk, A. (2003). Tales of regeneration in zebrafish. *Dev Dyn*, 226(2):202–10.
- Prasad, M. K., Reed, X., Gorkin, D. U., Cronin, J. C., McAdow, A. R., Chain, K., Hodonsky, C. J., Jones, E. A., Svaren, J., Antonellis, A., Johnson, S. L., Loftus, S. K., Pavan, W. J., and McCallion, A. S. (2011). SOX10 directly modulates ERBB3 transcription via an intronic neural crest enhancer. *BMC Dev Biol*, 11:40.
- Ptacek (1998). Interspecific mate choice in sailfin and shortfin species of mollies. *Anim Behav*, 56(5):1145–1154.
- Rauch, G.-J., Granato, M., and Haffter, P. (1997). A polymorphic zebrafish line for genetic mapping using SSLPs on high-percentage agarose gels. *Technical Tips Online*, 2(1):148–150.
- Richardson, M. K. and Wright, G. M. (2003). Developmental transformations in a normal series of embryos of the sea lamprey *Petromyzon marinus* (linnaeus). *Journal of Morphology*, 257(3):348–363.
- Richter, T. A., Dvoryanchikov, G. A., Chaudhari, N., and Roper, S. D. (2004). Acid-sensitive two-pore domain po-

- tassium (K2P) channels in mouse taste buds. *J Neurophysiol*, 92(3):1928–36.
- Rimoin, D. L., Merimee, T. J., and Mc Kusick, V. A. (1966). Growth-hormone deficiency in man: an isolated, recessively inherited defect. *Science*, 152(3729):1635–7.
- Rivkees, S. A., Bode, H. H., and Crawford, J. D. (1988). Long-Term Growth in Juvenile Acquired Hypothyroidism:. *New England Journal of Medicine*, 318(10):599–602.
- Robertson, F. W. (1959). Studies in Quantitative Inheritance. Xii. Cell Size and Number in Relation to Genetic and Environmental Variation of Body Size in *Drosophila*. *Genetics*, 44(5):869–96.
- Rohner, N., Perathoner, S., Frohnhöfer, H. G., and Harris, M. P. (2011). Enhancing the efficiency of N-ethyl-N-nitrosourea-induced mutagenesis in the zebrafish. *Zebrafish*, 8(3):119–23.
- Rolland-Lagan, A.-G., Paquette, M., Tweedle, V., and Akiemenko, M.-A. (2012). Morphogen-based simulation model of ray growth and joint patterning during fin development and regeneration. *Development*, 139(6):1188–97.
- Rosenthal, G. G. and Evans, C. S. (1998). Female preference for swords in *Xiphophorus helleri* reflects a bias for large apparent size. *Proc Natl Acad Sci U S A*, 95(8):4431–6.
- Rouzaire-Dubois, B. and Dubois, J. M. (1998). K⁺ channel block-induced mammalian neuroblastoma cell swelling: a possible mechanism to influence proliferation. *J Physiol*, 510 (Pt 1):93–102.

- Rouzaire-Dubois, B. and Dubois, J. M. (2004). Calcium-dependent proliferation of NG108-15 neuroblastoma cells. *Gen Physiol Biophys*, 23(2):231–9.
- Rouzaire-Dubois, B., Milandri, J. B., Bostel, S., and Dubois, J. M. (2000). Control of cell proliferation by cell volume alterations in rat C6 glioma cells. *Pflugers Arch*, 440(6):881–8.
- Runnels, L. W., Yue, L., and Clapham, D. E. (2001). TRP-PLIK, a bifunctional protein with kinase and ion channel activities. *Science*, 291(5506):1043–7.
- Santamaría, J. A. and Becerra, J. (1991). Tail fin regeneration in teleosts: cell-extracellular matrix interaction in blastemal differentiation. *J Anat*, 176:9–21.
- Santarius, T., Bignell, G. R., Greenman, C. D., Widaa, S., Chen, L., Mahoney, C. L., Butler, A., Edkins, S., Waris, S., Thornalley, P. J., Futreal, P. A., and Stratton, M. R. (2010). GLO1-A novel amplified gene in human cancer. *Genes Chromosomes Cancer*, 49(8):711–25.
- Sarzi-Puttini, P., Atzeni, F., Schölmerich, J., Cutolo, M., and Straub, R. H. (2006). Anti-TNF antibody treatment improves glucocorticoid induced insulin-like growth factor 1 (IGF1) resistance without influencing myoglobin and IGF1 binding proteins 1 and 3. *Ann Rheum Dis*, 65(3):301–5.
- Sato, M. (1937). Histological observations on the barbels of fishes. *Science Reports of the Tohoku Imperial University, Sendai, Japan (Fourth Series, Biology)*, 4(12).

- Schliess, F., Schreiber, R., and Häussinger, D. (1995). Activation of extracellular signal-regulated kinases Erk-1 and Erk-2 by cell swelling in H4IIE hepatoma cells. *Biochem J*, 309 (Pt 1):13–7.
- Schulte, C. J., Allen, C., England, S. J., Juárez-Morales, J. L., and Lewis, K. E. (2011). *Evx1* is required for joint formation in zebrafish fin dermoskeleton. *Dev Dyn*, 240(5):1240–8.
- Shafiei, M., Moczek, A. P., and Nijhout, H. F. (2001). Food availability controls the onset of metamorphosis in the dung beetle *Onthophagus taurus* (Coleoptera: Scarabaeidae). *Physiological Entomology*, 26(2):173–180.
- Shimoda, N., Knapik, E. W., Ziniti, J., Sim, C., Yamada, E., Kaplan, S., Jackson, D., de Sauvage, F., Jacob, H., and Fishman, M. C. (1999). Zebrafish genetic map with 2000 microsatellite markers. *Genomics*, 58(3):219–32.
- Sims, Jr, K., Eble, D. M., and Iovine, M. K. (2009). Connexin43 regulates joint location in zebrafish fins. *Dev Biol*, 327(2):410–8.
- Smith, A., Zhang, J., Guay, D., Quint, E., Johnson, A., and Akimenko, M. A. (2008). Gene expression analysis on sections of zebrafish regenerating fins reveals limitations in the whole-mount in situ hybridization method. *Dev Dyn*, 237(2):417–25.
- Stengel, R., Rivera-Milla, E., Sahoo, N., Ebert, C., Bollig, F., Heinemann, S. H., Schonherr, R., and Englert, C. (2012). *Kcnh1* voltage-gated potassium channels are essential for early zebrafish development. *J Biol Chem*.

- Stevenson, R. D., Hill, M. F., and Bryant, P. J. (1995). Organ and cell allometry in Hawaiian *Drosophila*: how to make a big fly. *Proc Biol Sci*, 259(1355):105–10.
- Strutz-Seebohm, N., Gutcher, I., Decher, N., Steinmeyer, K., Lang, F., and Seebohm, G. (2007). Comparison of potent Kv1.5 potassium channel inhibitors reveals the molecular basis for blocking kinetics and binding mode. *Cell Physiol Biochem*, 20(6):791–800.
- Sun, X. X., Hodge, J. J. L., Zhou, Y., Nguyen, M., and Griffith, L. C. (2004). The eag potassium channel binds and locally activates calcium/calmodulin-dependent protein kinase II. *J Biol Chem*, 279(11):10206–14.
- Sundström, E., Komisarczuk, A. Z., Jiang, L., Golovko, A., Navratilova, P., Rinkwitz, S., Becker, T. S., and Andersson, L. (2012). Identification of a melanocyte-specific, microphthalmia-associated transcription factor-dependent regulatory element in the intronic duplication causing hair greying and melanoma in horses. *Pigment Cell Melanoma Res*, 25(1):28–36.
- Szászi, K., Buday, L., and Kapus, A. (1997). Shrinkage-induced protein tyrosine phosphorylation in Chinese hamster ovary cells. *J Biol Chem*, 272(26):16670–8.
- Tanaka, S. K. (1973). Suction Feeding by the Nurse Shark. *Copeia*, 1973(3):pp. 606–608.
- Taylor, J. M. and Simpson, R. U. (1992). Inhibition of cancer cell growth by calcium channel antagonists in the athymic mouse. *Cancer Res*, 52(9):2413–8.

- Teissier, G. (1939). Biométrie de la cellule. *Tabulae biologicae*, 19:1–64.
- Trager, W. (1935). The relation of cell size to growth in insect larvae. *Journal of Experimental Zoology*, 71(3):489–508.
- Tresnake, I. (1981). The long-finned zebra Danio. *Tropical Fish Hobby.*, 29:43–56.
- Tu, S. and Johnson, S. L. (2011). Fate restriction in the growing and regenerating zebrafish fin. *Dev Cell*, 20(5):725–32.
- Tumaneng, K., Russell, R. C., and Guan, K.-L. (2012). Organ size control by Hippo and TOR pathways. *Curr Biol*, 22(9):R368–79.
- Twitty, V. (1940). Size-controlling Factors. *Growth*, 4:109–120.
- Twitty, V. C. and Schwind, J. L. (1931). The growth of eyes and limbs transplanted heteroplastically between two species of *Amblystoma*. *Journal of Experimental Zoology*, 59(1):61–86.
- Udan, R. S., Kango-Singh, M., Nolo, R., Tao, C., and Halder, G. (2003). Hippo promotes proliferation arrest and apoptosis in the Salvador/Warts pathway. *Nat Cell Biol*, 5(10):914–20.
- Van Coppenolle, F., Skryma, R., Ouadid-Ahidouch, H., Slo-mianny, C., Roudbaraki, M., Delcourt, P., Dewailly, E., Humez, S., Crépin, A., Gourdou, I., Djiane, J., Bonnal, J.-L., Mauroy, B., and Prevarskaya, N. (2004). Prolactin stimulates cell proliferation through a long form of prolactin receptor and K⁺ channel activation. *Biochem J*, 377(Pt 3):569–78.

- van Eeden, F. J., Granato, M., Schach, U., Brand, M., Furutani-Seiki, M., Haffter, P., Hammerschmidt, M., Heisenberg, C. P., Jiang, Y. J., Kane, D. A., Kelsh, R. N., Mullins, M. C., Odenthal, J., Warga, R. M., and Nüsslein-Volhard, C. (1996). Genetic analysis of fin formation in the zebrafish, *Danio rerio*. *Development*, 123:255–62.
- Voloshyna, I., Besana, A., Castillo, M., Matos, T., Weinstein, I. B., Mansukhani, M., Robinson, R. B., Cordon-Cardo, C., and Feinmark, S. J. (2008). TREK-1 is a novel molecular target in prostate cancer. *Cancer Res*, 68(4):1197–203.
- Weigmann, K., Cohen, S. M., and Lehner, C. F. (1997). Cell cycle progression, growth and patterning in imaginal discs despite inhibition of cell division after inactivation of *Drosophila* Cdc2 kinase. *Development*, 124(18):3555–63.
- Whitaker, M. (2006). Calcium microdomains and cell cycle control. *Cell Calcium*, 40(5–6):585 – 592. <ce:title>Calcium microdomains and the fine control of cell function</ce:title>.
- White, J. A., Boffa, M. B., Jones, B., and Petkovich, M. (1994). A zebrafish retinoic acid receptor expressed in the regenerating caudal fin. *Development*, 120(7):1861–72.
- Williams, G. R. (2009). Actions of thyroid hormones in bone. *Endokrynol Pol*, 60(5):380–8.
- Wonderlin, W. F., Woodfork, K. A., and Strobl, J. S. (1995). Changes in membrane potential during the progression of MCF-7 human mammary tumor cells through the cell cycle. *J Cell Physiol*, 165(1):177–85.

- Wood, A. and Thorogood, P. (1984). An analysis of in vivo cell migration during teleost fin morphogenesis. *J Cell Sci*, 66:205–22.
- Wood, P. A., Du-Quiton, J., You, S., and Hrushesky, W. J. M. (2006). Circadian clock coordinates cancer cell cycle progression, thymidylate synthase, and 5-fluorouracil therapeutic index. *Mol Cancer Ther*, 5(8):2023–33.
- Xu, B., Wilson, B. A., and Lu, L. (1996). Induction of human myeloblastic ML-1 cell G1 arrest by suppression of K⁺ channel activity. *Am J Physiol*, 271(6 Pt 1):C2037–44.
- Yano, T. and Tamura, K. (2012). The making of differences between fins and limbs. *Journal of Anatomy*, pages no–no.
- Yoshinari, N. and Kawakami, A. (2011). Mature and juvenile tissue models of regeneration in small fish species. *Biol Bull*, 221(1):62–78.
- Zardoya, R. and Doadrio, I. (1999). Molecular evidence on the evolutionary and biogeographical patterns of European cyprinids. *J Mol Evol*, 49(2):227–37.
- Zeng, H., Fei, H., and Levitan, I. B. (2004). The slowpoke channel binding protein Slob from *Drosophila melanogaster* exhibits regulatable protein kinase activity. *Neurosci Lett*, 365(1):33–8.
- Zhang, J., Wagh, P., Guay, D., Sanchez-Pulido, L., Padhi, B. K., Korzh, V., Andrade-Navarro, M. A., and Akimenko, M.-A. (2010). Loss of fish actinotrichia proteins and the fin-to-limb transition. *Nature*, 466(7303):234–7.

Zheng, L., Baumann, U., and Reymond, J.-L. (2004). An efficient one-step site-directed and site-saturation mutagenesis protocol. *Nucleic Acids Res*, 32(14):e115.

Zhu, L., Yang, H., Zuo, W., Yang, L., Zhang, H., Ye, W., Mao, J., Chen, L., and Wang, L. (2012). Differential expression and roles of volume-activated chloride channels in control of growth of normal and cancerous nasopharyngeal epithelial cells. *Biochem Pharmacol*, 83(3):324–34.